University of Potsdam

Cumulative Dissertation

Using spaceborne radar platforms to enhance the homogeneity of weather radar calibration

---

by

Irene Crisologo

Supervisors:
Maik Heistermann, Ph.D.
Prof. Dr. Axel Bronstert

for the degree of
doctor rerum naturalium (Dr. rer. nat.)
in Geoecology
Institute of Environmental Science and Geography
Faculty of Science

April 2019

Published online at the
Institutional Repository of the University of Potsdam:
https://doi.org/10.25932/publishup-44570
https://nbn-resolving.org/urn:nbn:de:kobv:517-opus4-445704

Using spaceborne radar platforms to enhance the homogeneity of weather radar calibration

by Irene Crisologo

Supervisor:	*Affiliation:*
Maik Heistermann, Ph.D. (*Reviewer*)	*University of Potsdam*
Co-Supervisor:	
Prof. Dr. Axel Bronstert (*Reviewer*)	*University of Potsdam*
Mentor:	
Prof. Oliver Korup, Ph.D.	*University of Potsdam*

Assessment Committee:

Prof. Oliver Korup, Ph.D. *(Chair)*	*University of Potsdam*
Prof. Dr. Bodo Bookhagen	*University of Potsdam*
Prof. Dr. Annegret Thieken	*University of Potsdam*
Prof. Dr. Remko Uijlenhoet (*Reviewer*)	*Wageningen University and Research, Netherlands*

Publication-based dissertation submitted in fulfilment of the requirements for the degree of Doctor of Philosophy under the discipline of Geoecology in the Institute of Environmental Science and Geography Faculty of Science at the University of Potsdam.

Declaration of Authorship

I, Irene Crisologo, declare that this thesis titled, "Using spaceborne radar platforms to enhance the homogeneity of weather radar calibration " and the work presented in it are my own. I confirm that:

- This work was done wholly or mainly while in candidature for a research degree at the University of Potsdam.
- Where any part of this dissertation has previously been submitted for a degree or any other qualification at the University of Potsdam, or any other institution, this has been clearly stated.
- Where I have consulted the published work of others, this is always clearly attributed.
- Where I have quoted from the work of others, the source is always given. With the exception of such quotations, this thesis is entirely my own work.
- I have acknowledged all main sources of help.
- Where the thesis is based on work done by myself jointly with others, I have made clear exactly what was done by others and what I have contributed myself.

Signature:

Date:

"*Sometimes attaining the deepest familiarity with a question is our best substitute for actually having the answer.*"

Brian Greene

Abstract

Accurate weather observations are the keystone to many quantitative applications, such as precipitation monitoring and nowcasting, hydrological modelling and forecasting, climate studies, as well as understanding precipitation-driven natural hazards (i.e. floods, landslides, debris flow). Weather radars have been an increasingly popular tool since the 1940s to provide high spatial and temporal resolution precipitation data at the mesoscale, bridging the gap between synoptic and point scale observations. Yet, many institutions still struggle to tap the potential of the large archives of reflectivity, as there is still much to understand about factors that contribute to measurement errors, one of which is calibration. Calibration represents a substantial source of uncertainty in quantitative precipitation estimation (QPE). A miscalibration of a few dBZ can easily deteriorate the accuracy of precipitation estimates by an order of magnitude. Instances where rain cells carrying torrential rains are misidentified by the radar as moderate rain could mean the difference between a timely warning and a devastating flood.

Since 2012, the Philippine Atmospheric, Geophysical, and Astronomical Services Administration (PAGASA) has been expanding the country's ground radar network. We had a first look into the dataset from one of the longest running radars (the Subic radar) after devastating week-long torrential rains and thunderstorms in August 2012 caused by the annual southwest-monsoon and enhanced by the north-passing Typhoon Haikui. The analysis of the rainfall spatial distribution revealed the added value of radar-based QPE in comparison to interpolated rain gauge observations. However, when compared with local gauge measurements, severe miscalibration of the Subic radar was found. As a consequence, the radar-based QPE would have underestimated the rainfall amount by up to 60% if they had not been adjusted by rain gauge observations—a technique that is not only affected by other uncertainties, but which is also not feasible in other regions of the country with very sparse rain gauge coverage.

Relative calibration techniques, or the assessment of bias from the reflectivity of two radars, has been steadily gaining popularity. Previous studies have demonstrated that reflectivity observations from the Tropical Rainfall Measuring Mission (TRMM) and its successor, the Global Precipitation Measurement (GPM), are accurate enough to serve as a calibration reference for ground radars over low-to-mid-latitudes ($\pm$ 35 deg for TRMM; $\pm$ 65 deg for GPM). Comparing spaceborne radars (SR) and ground radars (GR) requires cautious consideration of differences in measurement geometry and instrument specifications, as well as temporal coincidence. For this purpose, we implement a 3-D volume matching method developed by Schwaller and Morris (2011) and extended by Warren et al. (2018) to 5 years worth of observations from the Subic radar. In this method, only the volumetric intersections of the SR and GR beams are considered.

Calibration bias affects reflectivity observations homogeneously across the entire radar domain. Yet, other sources of systematic measurement errors are highly heterogeneous in space, and can either enhance or balance the bias introduced by miscalibration. In order to account for such heterogeneous errors, and thus isolate the calibration bias, we assign a quality index to each matching SR–GR volume, and thus compute the GR calibration bias as a quality-weighted average of reflectivity differences in any sample of matching SR–GR volumes. We exemplify the idea of quality-weighted averaging by using beam blockage fraction (BBF) as a quality variable. Quality-weighted averaging is able to increase the consistency of SR and

GR observations by decreasing the standard deviation of the SR–GR differences, and thus increasing the precision of the bias estimates.

To extend this framework further, the SR–GR quality-weighted bias estimation is applied to the neighboring Tagaytay radar, but this time focusing on path-integrated attenuation (PIA) as the source of uncertainty. Tagaytay is a C-band radar operating at a lower wavelength and is therefore more affected by attenuation. Applying the same method used for the Subic radar, a time series of calibration bias is also established for the Tagaytay radar.

Tagaytay radar sits at a higher altitude than the Subic radar and is surrounded by a gentler terrain, so beam blockage is negligible, especially in the overlapping region. Conversely, Subic radar is largely affected by beam blockage in the overlapping region, but being an S-Band radar, attenuation is considered negligible. This coincidentally independent uncertainty contributions of each radar in the region of overlap provides an ideal environment to experiment with the different scenarios of quality filtering when comparing reflectivities from the two ground radars. The standard deviation of the GR–GR differences already decreases if we consider either BBF or PIA to compute the quality index and thus the weights. However, combining them multiplicatively resulted in the largest decrease in standard deviation, suggesting that taking both factors into account increases the consistency between the matched samples.

The overlap between the two radars and the instances of the SR passing over the two radars at the same time allows for verification of the SR–GR quality-weighted bias estimation method. In this regard, the consistency between the two ground radars is analyzed before and after bias correction is applied. For cases when all three radars are coincident during a significant rainfall event, the correction of GR reflectivities with calibration bias estimates from SR overpasses dramatically improves the consistency between the two ground radars which have shown incoherent observations before correction. We also show that for cases where adequate SR coverage is unavailable, interpolating the calibration biases using a moving average can be used to correct the GR observations for any point in time to some extent. By using the interpolated biases to correct GR observations, we demonstrate that bias correction reduces the absolute value of the mean difference in most cases, and therefore improves the consistency between the two ground radars.

This thesis demonstrates that in general, taking into account systematic sources of uncertainty that are heterogeneous in space (e.g. BBF) and time (e.g. PIA) allows for a more consistent estimation of calibration bias, a homogeneous quantity. The bias still exhibits an unexpected variability in time, which hints that there are still other sources of errors that remain unexplored. Nevertheless, the increase in consistency between SR and GR as well as between the two ground radars, suggests that considering BBF and PIA in a weighted-averaging approach is a step in the right direction.

Despite the ample room for improvement, the approach that combines volume matching between radars (either SR–GR or GR–GR) and quality-weighted comparison is readily available for application or further scrutiny. As a step towards reproducibility and transparency in atmospheric science, the 3D matching procedure and the analysis workflows as well as sample data are made available in public repositories. Open-source software such as Python and wradlib are used for all radar data processing in this thesis. This approach towards open science provides both research institutions and weather services with a valuable tool that can be applied to radar calibration, from monitoring to a posteriori correction of archived data.

Zusammenfassung

Die zuverlässige Messung des Niederschlags ist Grundlage für eine Vielzahl quantitativer Anwendungen. Bei der Analyse und Vorhersage von Naturgefahren wie Sturzfluten oder Hangrutschungen ist dabei die räumliche Trennschärfe der Niederschlagsmessung besonders wichtig, da hier oft kleinräumige Starkniederschläge auslösend sind. Seit dem 2. Weltkrieg gewinnen Niederschlagsradare an Bedeutung für die flächenhafte Erfassung des Niederschlags in hoher raumzeitlicher Auflösung. Und seit Ende des 20. Jahrhunderts investieren Wetterdienste zunehmend in die Archivierung dieser Beobachtungen. Die quantitative Auswertung solcher Archive gestaltet sich jedoch aufgrund unterschiedlicher Fehlerquellen als schwierig. Eine Fehlerquelle ist die Kalibrierung der Radarsysteme, die entlang der sog. "*receiver chain*" eine Beziehung zwischen der primären Beobachtungsvariable (der zurückgestreuten Strahlungsleistung) und der Zielvariable (des Radarreflektivitätsfaktors, kurz Reflektivität) herstellt. Die Reflektivität wiederum steht über mehrere Größenordnungen hinweg in Beziehung zur Niederschlagsintensität, so dass bereits kleine relative Fehler in der Kalibrierung große Fehler in der quantitativen Niederschlagsschätzung zur Folge haben können. Doch wie kann eine mangelhafte Kalibrierung nachträglich korrigiert werden?

Diese Arbeit beantwortet diese Frage am Beispiel des kürzlich installierten Radarnetzwerks der Philippinen. In einer initialen Fallstudie nutzen wir das S-Band-Radar nahe Subic, welches die Metropolregion Manila abdeckt, zur Analyse eines außergewöhnlich ergiebigen Niederschlagsereignisses im Jahr 2012: Es zeigt sich, dass die radargestützte Niederschlagsschätzung um rund 60% unter den Messungen von Niederschlagsschreibern liegt. Kann die Hypothese einer mangelhaften Kalibrierung bestätigt werden, indem die Beobachtungen des Subic-Radars mit den Messungen exzellent kalibrierter, satellitengestützter Radarsysteme verglichen werden? Kann die satellitengestützte Referenz ggf. sogar für eine nachträgliche Kalibrierung genutzt werden? Funktioniert eine solche Methode auch für das benachbarte C-Band-Radar nahe Tagaytay? Können wir die Zuverlässigkeit einer nachträglichen Kalibrierung erhöhen, indem wir andere systematische Fehlerquellen in den Radarmessungen identifizieren?

Zur Beantwortung dieser Fragen vergleicht diese Arbeit die Beobachtungen bodengestützter Niederschlagsradare (GR) mit satellitengestützten Niederschlagsradaren (SR) der *Tropical Rainfall Measuring Mission* (TRMM) und ihrem Nachfolger, der *Global Precipitation Measurement* (GPM) Mission. Dazu wird eine Methode weiterentwickelt, welche den dreidimensionalen Überlappungsbereich der Samplingvolumina des jeweiligen Instruments—GR und SR—berücksichtigt. Desweiteren wird jedem dieser Überlappungsbereiche ein Wert für die Datenqualität zugewiesen, basierend auf zwei Unsicherheitsquellen: dem Anteil der Abschattung (engl. *beam blockage fraction*, BBF) und der pfadintegrierten Dämpfung (engl. *path-integrated attenuation*, PIA). Die BBF zeigt, welcher Anteil des Radarstrahls von der Geländeoberfläche blockiert wird (je höher, desto niedriger die Qualität). PIA quantifiziert den Energieverlust des Signals, wenn es intensiven Niederschlag passiert (je höher, desto niedriger die Qualität). Entsprechend wird der Bias (also der Kalibrierungsfaktor) als das qualitätsgewichtete Mittel der Differenzen zwischen den GR- und SR-Reflektivitäten (ausgedrückt auf der logarithmischen Dezibelskala) berechnet.

Diese Arbeit zeigt, dass beide Radare, Subic und Tagaytay, gerade in den frühen Jahren stark von mangelhafter Kalibrierung betroffen waren. Der Vergleich mit satellitengestützten Messungen erlaubt es uns, diesen Fehler nachträglich zu schätzen und zu korrigieren. Die Zuverlässigkeit dieser Schätzung wird durch die Berücksichtigung anderer systematischer Fehler im Rahmen der Qualitätsgewichtung deutlich erhöht. Dies konnte auch dadurch bestätigt werden, dass nach Korrektur der Kalibierung die Signale im Überlappungsbereich der beiden bodengestützten Radare deutlich konsistenter wurden. Eine Interpolation des Fehlers in der Zeit war erfolgreich, so dass die Radarbeobachtungen auch für solche Tage korrigiert werden können, an denen keine satellitengestützten Beobachtungen verfügbar sind.

Acknowledgements

I would like to extend my sincere gratitude to the people who have been instrumental in this PhD journey.

To Maik, my main supervisor, for his unwavering trust and support, for sharing his sense of humor when I have lost mine. It was through his guidance that I learned about radars and decided to pursue it further, six years and counting.

To Axel, for support in all forms, for believing in me from the start and for the encouragement throughout the PhD.

To the institutions that supported me—to RTG NatRiskChange for adopting me as an associate PhD student and providing the environment for collaboration and learning; to DAAD for the financial support; and to the Geoecology staff (namely Andi, Daniel, and Sabine) for all the help in the administrative and technical things, and for the many thoughtful things in between.

To Mr. Jun Austria and PAGASA, for providing the data and technical support needed to carry out this research study.

To my PhD colleagues, who I consider friends and family. The "old" ones—Sebastian, Dadi, Ugur, Jonas, Tobi, Georg, Erwin, for the cordial camaraderie and constructive collaboration. The "new" ones as well—Ina, Melli, Matthias, Joscha, Kata—for introducing our Monday evening activity that helps relieve the stress of the later part of the PhD. To my working group—Arthur, Georgy, and Lisei—for the fruitful discussions about work and non-work subjects.

To Arlena, for the life-enriching moments inside and outside the office.

To my Potsdam Filipino family, for being my home away from home.

To my family, who despite the distance, extended their support and believed in me.

Contents

List of Figures

Chapter 1

Introduction

During the second world war, when radio engineers noticed that aircrafts were interfering with communication signals of the US Navy, they came up with a brilliant idea of using pulses of radio waves for target detection (Rinehart, 1991), and thus RADAR (**Ra**dio **D**etection and **R**anging) was born. As the technology of radars developed, the resolution and detection capabilities also improved, leading to better detection of aircrafts. When military radar operators realized that the large patches of unknown echoes "cluttering" their observations were, in fact, meteorological in origin, meteorology personnel took notice, and a whole new application of radars emerged.

How weather radars work

A weather radar transmits a signal along a path called the *radar beam*, and the antenna rotates at a constant elevation angle to complete one *sweep* or *elevation scan*. The antenna makes a series of sweeps at increasing elevation angles, producing a set of nesting conical surfaces of three-dimensional data called a *volume scan*. When the radar beams encounter a backscattering target (e.g. rain drops, hail, snow, birds), some of the energy is scattered back to the radar receiver, and is then interpreted as the quantity *reflectivity factor*. This process is summarized by the radar equation (Hong and Gourley, 2015):

$$P_r = \frac{z}{r^2}\left(\frac{P_t g^2 \theta \phi h}{\lambda^2}\right)\left(\frac{\pi^3}{1024\ln(2)}\right)|K|^2 l \quad (1.1)$$

where the non-numeric parameters can be classified into three categories:

Derived quantities

$P_r =$ power received by radar (watts)
$r =$ range or distance to target (m)
$z =$ radar reflectivity factor (mm^6/m^3)

Radar constants

$P_t =$ power transmitted by radar (watts)
$g =$ antenna gain
$\theta =$ horizontal beam width (radians)
$\phi =$ vertical beam width (radians)
$h =$ pulse length (m)
$\lambda =$ wavelength of radar pulse (m)

Assumed values

$|K|^2 =$ dielectric constant for radar targets (usually set at 0.93 for liquid water)
$l =$ loss factor for beam attenuation (assumed to be 1 for if attenuation is unknown)

The equation can be simplified by combining the numeric values, the assumed values, and the radar-specific variables into a single constant c_1, and solve for z, such that:

$$z = c_1 P_r r^2 \quad (1.2)$$

The constant c_1 depends on a specific radar and its configuration, such that the reflectivity factor z is calculated based on the two parameters measured by the radar: the amount of power return (P_r) and the range (r). This reflectivity factor is a function of the distribution of the rainfall drop sizes within a unit volume of air measured. The reflectivity factor is derived as:

$$z = \sum_{vol} D^6 = D_1^6 + D_2^6 + D_3^6 + \ldots + D_N^6 \quad (1.3)$$

where D is the drop diameter in mm. The reflectivity factor can take on values across several orders of magnitudes (from 0.001 mm^6/m^3 for fog to 36,000,000 mm^6/m^3 for baseball-sized hail). To compress the range of magnitudes to a more comprehensible scale, the reflectivity factor is typically converted to decibels of reflectivity (dBZ) or simply Z, given by:

$$Z = 10\log_{10}\left(\frac{z}{mm^6/m^3}\right) \quad (1.4)$$

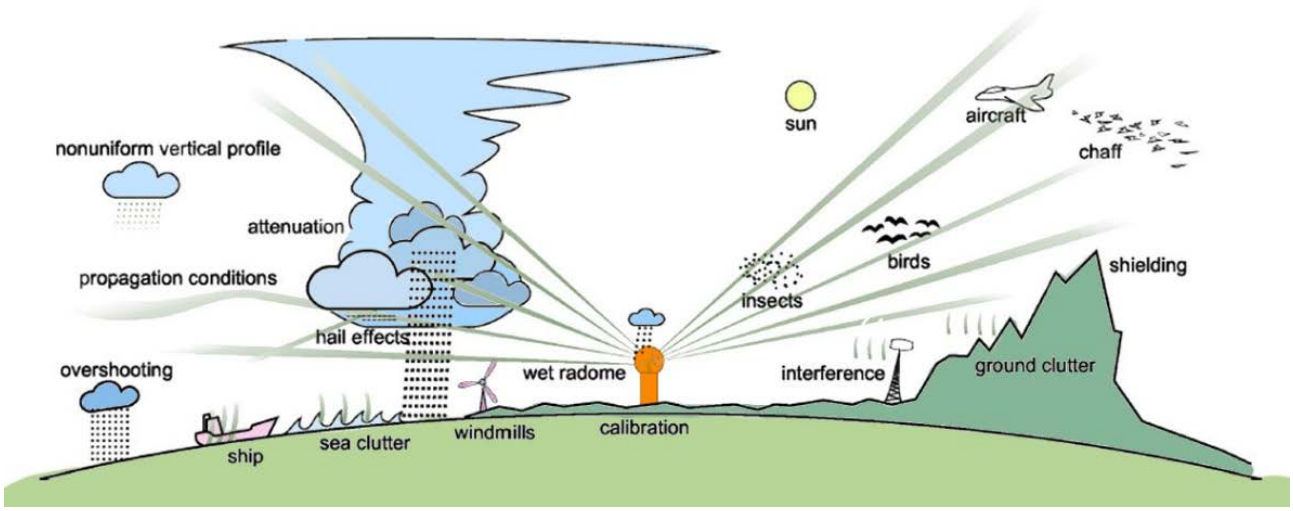

Figure 1.1: Sources of uncertainty in weather radar measurements (Peura et al., 2006)

Rain rate is also derived from drop-size distribution, such that we can relate reflectivity (Z) and rain-rate (R) into a so-called Z–R relation of the form:

$$Z = A \cdot R^b \tag{1.5}$$

where A and b are empirically derived constants. This bridge between the radar reflectivity measured aloft and the estimated rain-rate allows us to actively observe and monitor rainfall from distances far from the station (as far as 250 km) even before it hits the ground.

The good and the bad

Weather radars bridged the gap between the synoptic scale observations of weather systems and the point scale human observations at weather stations (Fabry, 2015). They allow for an understanding of atmospheric processes at the mesoscale, such as internal cyclone structures; the evolution of cyclones and tornadoes; the conversion from ice to water in the atmosphere; and cloud microphysics, among many other things. Fabry highlights the importance of weather radar applications by the following:

1. Weather radars can predict the type, timing, location, and amount of precipitation, which are the most important components of weather forecasts (Lazo et al., 2009);
2. They can detect hazardous weather conditions, such as hail, severe thunderstorms, and tornadoes; and
3. Weather radar data is available in real-time, enabling access to spatiotemporally high resolution weather information.

As with any instrument, however, weather radars are not infallible to errors. Figure 1.1 illustrates the different factors that could affect the integrity of radar measurements (Peura et al., 2006). Villarini and Krajewski (2010) classified these error sources into nine categories: radar miscalibration; radar signal attenuation by rain; ground clutter and anomalous propagation; beam blockage; variability of the rainfall-rainrate (Z–R) relation; range effects; vertical variability of the precipitation system; vertical air motion and precipitation drift; and temporal sampling errors.

Radar (mis)calibration contributes the most to the deterioration of rainfall estimation accuracy (Houze et al., 2004). This is no surprise, as the exponential nature of the Z–R relationship means that a slight change in reflectivity could mean a big change in the estimated rain-rate. The standard Marshall-Palmer Z–R relationship can be used to demonstrate how the rain-rate estimates from reflectivity change depending on varying degrees of calibration biases (Figure 1.2). The effects of calibration bias are minimal at the lower range reflectivities. However, even a 1 dB change in bias could mean a difference of 25 mm/hr for the higher

reflectivity ranges, which usually means intense rainfall, even though 1 dB accuracy is already considered well-calibrated. A seemingly small 3 dB underestimation could already mean that a 100 mm/hr rain—which could trigger landslides and/or flash floods—would have been measured as only 65 mm/hr. Such inaccuracies at the higher end of the reflectivity range could be disastrous. In the case of flood forecasting, for example, rainfall estimation errors could further accumulate throughout hydrologic and flood models, deeming event prediction no longer reliable.

Calibration

Calibrating weather radars became routine soon after the discovery of its meteorological use. In 1951, the Weather Radar Group at the Massachusetts Institute of Technology discovered disparities between radar estimates and gauge measurements, which led them to research radar calibration (Atlas, 2002). Traditional attempts at radar calibration made use of standard targets with known backscattering properties, such as BB gun pellets fired into radar beams; metalized ping pong balls dropped from light aircraft; or metalized spheres suspended from balloons or helicopters. While such physical methods work well for single-radar calibration and monitoring, they however pose challenges for networks of tens or hundreds of radars. Auxiliary instruments for calibration, such as radar profilers and disdrometers, measure drop size distribution at the same time as the radar. The corresponding reflectivities from the drop size distribution measured by the disdrometers and the reflectivity measured by the radar are then compared for consistency (Joss et al., 1968; Ulbrich and Lee, 1999). However, since radars measure precipitation aloft while disdrometers measure drop size distribution on the ground, the sample volumes between those two instruments can differ by as much as eight orders (Droegemeier et al., 2000). The height difference between these sample volumes mean that external factors such as wind and temperature can change the microphysical characteristics of the droplets that reach the disdrometer, e.g. drop size change through fusion/breakup, change of state through melting.

Relative calibration (defined as the assessment of reflectivity bias between two radars) has been gaining popularity, in particular the comparison with spaceborne precipitation radars (SR) (such as the precipitation radar on-board the Tropical Rainfall Measuring Mission (TRMM; 1007-2014; Kummerow et al. (1998)) and Global Precipitation Measurement (GPM; 2014-present; (Hou et al., 2013)). The precipitation radars on-board these satellite platforms are calibrated to within 1 dBZ (Kawanishi et al., 2000; Takahashi et al., 2003; Furukawa et al., 2015; Toyoshima et al., 2015), and hence they are accurate enough to serve as a reference for relative calibration. The measured reflectivities from the on-board spaceborne precipitation radars are matched with the ground radar measurements, where the reflectivities (the primary measured quantity) are compared (Warren et al., 2018) or the estimated rainfall from both instruments (Kirstetter et al., 2012; Speirs et al., 2017; Joss et al., 2006; Amitai et al., 2009; Gabella et al., 2017; Petracca et al., 2018) for the same event in areas of overlap for calibration. In addition, a major advantage of relative calibration in contrast to absolute calibration (i.e. minimizing the bias in measured power between an external reference noise source and the radar at hand) is that they can be carried out *a posteriori*, and this be applied to historical data. The large spatial coverage of spaceborne radars enables the calibration of multiple radars in a large network against a single, stable reference (Hong and Gourley, 2015), making them particularly helpful for countries like the Philippines with a sparse rain-gauge network.

The need for (calibrated) radars in the Philippines

With over 20 typhoons passing through or near the country annually, there are months when rainy days outnumber dry days. Although people are accustomed to frequent thunderstorms, typhoons, and monsoons, they are still caught by surprise by extreme rainfall events. Tropical Storm Ketsana (locally named as *Ondoy*) passed through the northern island of Luzon in September 2009, which brought rainfall that exceeded the country's forty-year meteorological record (Abon et al., 2011). TS Ketsana dumped 350 mm rainfall within six hours, which reached 450 mm after twelve hours in Metropolitan Manila. This unusual amount of rain within a short time period resulted in catastrophic flooding in several cities in the metropolitan area and much of Southern Luzon, leading to an estimated PhP 11 Billion (USD 211 Million) in damages and 464 casualties (Abon et al., 2011).

As a response to the need for better disaster awareness, prevention, and mitigation, a disaster risk reduction program (Project NOAH: Nationwide Operational Assessment of Hazards, Lagmay et al. (2017)) was established in July 2012. Within the framework of this

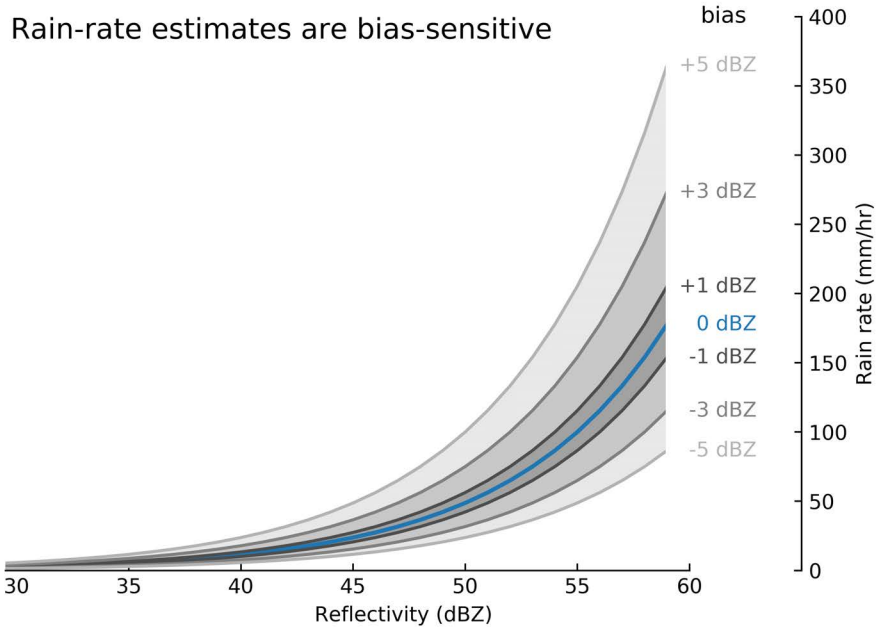

Figure 1.2: Reflectivity vs rain-rate estimates for different calibration biases. The base Z–R relationship (in blue) shows the standard Marshall-Palmer Z–R relationship ($Z = 200R^{1.6}$). Z–R scenarios for different degrees of calibration biases are shown in dark gray (± 1 dBZ), medium gray (± 3 dBZ), and light gray (± 5 dbZ).

project, radar data was visualized and released to a public domain in (near) real-time, that people can access anytime and anywhere. This newly established platform was put to the test a month later, when Metro Manila and the surrounding areas were struck by sustained torrential rainfall brought by the southwest monsoon, which went on for several days. The southwest monsoon (named after the origin of the winds) is a regular natural weather phenomenon that brings significant rainfall from June to September in the Asian subcontinent, lasting for several days or weeks at a time (Lagmay et al., 2015). At the same time, Typhoon Haikui was passing north of the Philippines, where its southern portion already carrying winds in the northeast direction enhanced the winds of the southwest monsoon. This typhoon pulled in more warm air and precipitation from the West Philippine Sea towards the western coast of the country, which led to the event named as *Habagat of August 2012*.

This event, coupled with the recent access to the radar data due to Project NOAH, led to a collaboration with the University of Potsdam. Together, we had a first look at the extent of the rainfall distribution in high resolution through the Subic radar, discussed more in detail in Chapter 2 of this thesis. Apart from the key findings of Chapter 2 about the rainfall distribution, we also learned that the Subic radar estimates are highly underestimating by as much as a third of the rain gauge recordings, for reasons unclear to the authors at the time of writing. This was the first time we were confronted with the idea that the Philippine radars might be experiencing calibration issues. Following these developments, the work carried out in Chapters 3 and 4 allowed for further investigation of the radar biases. With more years of data, a study on the calibration of the Philippine radars can be conducted.

The Philippine Atmospheric, Geophysical, and Astronomical Services Administration (PAGASA) established and began expanding the country's radar network in 2012. There are 15 operational ground weather radars as of April 2019. This thesis focuses on investigating calibration biases of the two longest-running weather radars of the PAGASA radar network: the Subic and Tagaytay radars (Figure 1.3), which are about 100 km apart and overlap Metro Manila, the country's most populated region.

The approach

This thesis attempts to thread the relative calibration approach together with the concept of data quality. Radar calibration ensures homogeneity in radar networks where comparable measurements of precipitation are essential in the overlapping regions of two or more weather radars. When combining two or more

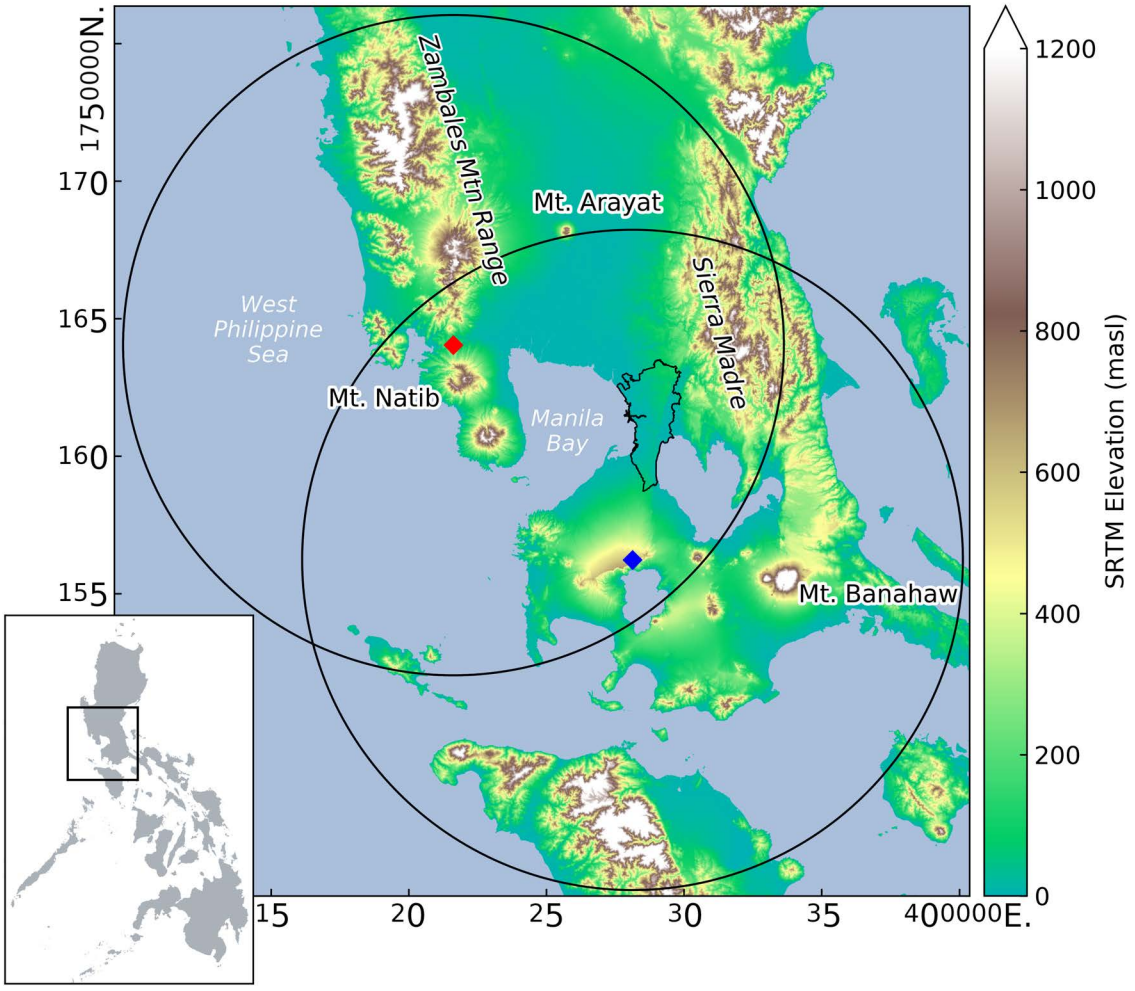

Figure 1.3: Subic (red diamond) and Tagaytay (blue diamond) radars and their coverage. The underlying DEM shows the complex topography surrounding the radars. In both coverages lies Metropolitan Manila (in black outline), the country's capital and most populated city.

overlapping radar sweeps to produce a composite image, often the basis for selection is data quality.

Data quality is defined in Michelson et al. (2005) as the *"attribute of the data which is inverse to uncertainties and errors, i.e. error-free data with few uncertainties are of high quality while data with errors or large uncertainties are of low quality"*. A Quality Index metric classifies the data quality within an interval of 0 to 1, where 0 represents poor quality and 1 represents excellent quality. Quality indices are typically used in combining data from multiple radars to create a composite image over larger regions (e.g. radar composites for a specific catchment, or for an entire country). For bias calibration purposes, quality indices can be used as weights in a weighted-averaging approach for calibration.

In particular, this thesis looks at two factors affecting data quality—beam blockage and path-integrated attenuation:

1. **Beam Blockage**: When the topography surrounding a radar interferes with the path of the radar beam, it may partially or completely hinder the radar's ability to detect the precipitation further along the beam. Such topographic barriers may lead to a weaker backscattered signal. Flat regions within the radar coverage are assigned high data quality. Data quality quickly drops when the radar is blind due to the topographic barriers. This source of uncertainty is considered static, as the obstacles (such as mountains, buildings, or other permanent structures) do not change from scan to scan.

2. **Path-integrated attenuation**: At wavelengths shorter than 10 cm (such as C-band radars), the

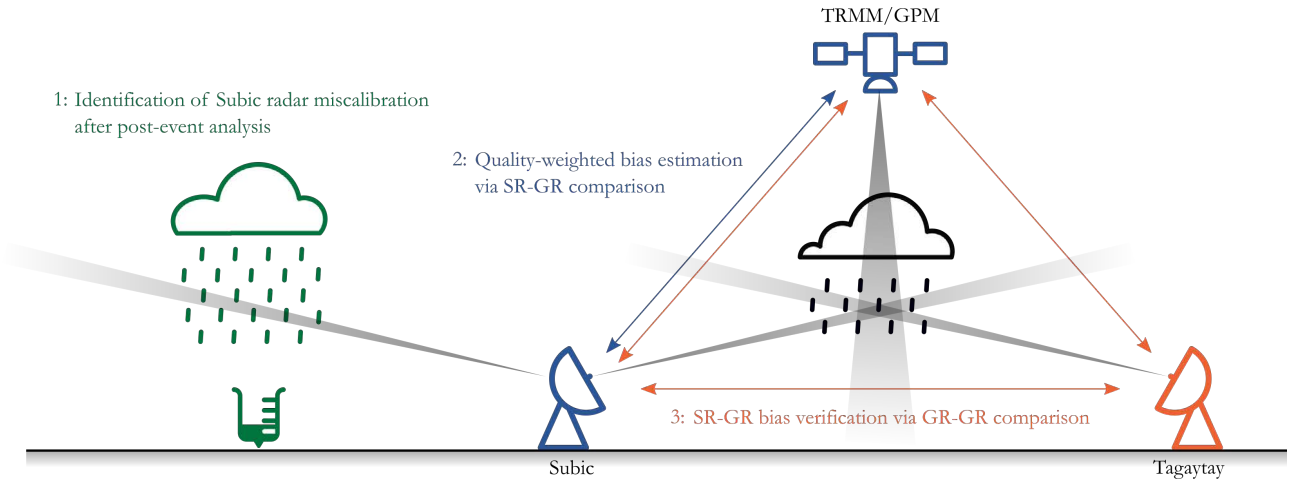

Figure 1.4: Schematic diagram of the research flow and structure

radar signal becomes weaker as it passes through rainfall. The magnitude of attenuation is proportional to rain intensity, making it highly variable in space and time. The effects accumulate along the radar beam (hence the term path-integrated). This source of uncertainty is dynamic, as it depends on the rain intensity and therefore changes with every scan.

Determining calibration bias through comparison with spaceborne radars and integrating a quality-weighted approach brings together different threads of the field. Calibration estimation and correction attempts to address systematic errors that are homogeneous over the entire radar domain, whereas factoring in quality allows other sources of systematic errors that are heterogeneous in space to be addressed separately. It is always worthwhile to question the data quality and the reliability, when determining the calibration bias of the ground radar with respect to the spaceborne radar. Poor data quality used in such a comparison may lead to errors in bias estimation, resulting in inaccurate bias correction.

Research questions and structure

The research questions and the corresponding answers in this thesis were developed in succession. The findings of Chapter 2 (Paper 1) gave rise to the second research question (Chapter 3; Paper 2), whose findings prompted the third research question (Chapter 4; Paper 3). The thesis story starts from the identification of the Subic radar miscalibration, to the quality-weighted calibration bias estimation through SR–GR comparison, and eventually the verification of the method through GR-GR comparison. Figure 1.4 gives an overview of the flow and the structure of the thesis.

The use of radar in operations and research worldwide has been going on for decades. For the Philippines, the radar network has only been collecting and archiving data since 2012. The frequency of typhoons and other convective systems that define the country's weather provides plenty of research potential in terms of understanding the underlying processes, as well as understanding the spatiotemporal distribution of rainfall. To explore the potential role of weather radars in understanding extreme weather in the Philippines, the first research question asks:

RQ1: Can we use recently-acquired weather radar data to reconstruct the enhanced southwest monsoon event of 2012? What additional information can radars provide that are not offered by the rain gauges to explore the spatial distribution of rainfall?

The question is answered in the first chapter, where we made an initial attempt at examining the rainfall distribution for the *Habagat 2012* rainfall event. This was a four-day event of continuous torrential precipitation, brought by southwest monsoon and enhanced further by a typhoon. Twenty-five (25) rain gauges captured the intensity of the event with a maximum accumulated rainfall of 1000 mm. When comparing radar estimates with actual gauge readings, we found that the radar underestimates rainfall by as much as 60%. We adjusted the radar estimates based on the rain gauge values and then produced a gauge-adjusted rainfall map over the

Subic radar coverage. We learned from the rainfall distribution map that Manila already received 1000 mm of accumulated rain over the course of four days, whereas most of the accumulated rainfall (~1200 mm) fell over Manila Bay, which was impossible for the rain gauges to capture.

We observed from Chapter 2 that the Subic radar underestimates rainfall compared to the rain gauges, and that rain gauges are unable to adequately capture the spatial distribution of rainfall. Hence there is a need for another source to calibrate the weather radar data. We peered into the possibility of calibration of the Subic radar via spaceborne radars, following the study of Warren et al. (2018) and the method of Schwaller and Morris (2011). In addition, we wanted to explore the added value of considering data quality in comparing the two instruments, which leads to the second research question:

RQ2: Are SR and GR observations consistent enough to allow for calibration bias estimates? Can we increase the level of consistency by introducing a formal framework for data quality (in terms of measurement quality)?

The second chapter looks at the underestimation of the Subic radar discovered in Chapter 1, and suggests a method to adjust the radar estimates in a more systematic manner. The rain gauge density within radar coverage is insufficient to create a reliable basis for adjustment, although it is a common practice as discussed in Chapter 2. Moreover, using gauges for calibration requires the additional step of converting reflectivity to rain rate, which could introduce another layer of uncertainty. In this chapter, we instead turn towards spaceborne radars. We compare the reflectivity measurements of the spaceborne radars with the reflectivity measurements of the ground radars by taking the values only at the volumes where the beams from the two radars intersect adapting the geometry matching method (Schwaller and Morris, 2011). In addition, we quantify the effect of beam blockage caused by the terrain. We are able to estimate the fraction of the beam being blocked by the terrain and assign a quality index between 0 (bad quality) and 1 (good quality) by modeling the beam blockage map based on a digital elevation model (DEM). We then estimate the bias between SR and GR using the quality index as weights by taking a weighted mean of the differences of the reflectivities from the two instruments. We look at how the comparison of the two radars can be improved (i.e. reduction of the standard deviation) when the data quality based on beam blockage is considered in calibration bias estimation.

Another question is whether the SR–GR calibration method also works for a C-Band radar with a different dominating quality factor (e.g. path-integrated attenuation. The Subic S-Band radar from Chapters 2 and 3 overlaps with the Tagaytay C-Band radar, which sets up the possibility for a three-way comparison between SR (TRMM/GPM), GR (Subic) and GR (Tagaytay), whenever all three datasets intersect in time and space. With this, we ask:

RQ3: Can we validate the SR–GR calibration approach by comparing the consistency of two overlapping ground radars before and after bias correction? And can we interpolate the calculated biases to produce a time series of bias estimates and use it to correct historical data for periods when there are no available SR overpasses?

Chapter 4 extends the quality-weighting framework by introducing path-integrated attenuation as the basis for data quality. The calculation for PIA is done on the Tagaytay radar, a C-band radar overlapping the Subic radar. The Tagaytay radar was also found to suffer from rainfall underestimation compared to rain gauges (Crisologo et al., 2014). C-Band radars are more prone to attenuation, hence the need to consider this source of uncertainty in estimating the calibration bias. In this chapter, we also assess the ability to estimate GR calibration bias from SR overpasses by comparing the reflectivities between Subic and Tagaytay radars before and after bias correction.

Towards open science

Open source software plays a big role in this thesis. All processing steps, from reading the data to creating visualizations were done using wradlib, which was in turn built in Python. *wradlib* (short for weather radar library) is an open-source library for weather radar data processing. Codes in the form of Jupyter notebooks starting from Chapter 3 were published online through Github, along with sample data, to allow for a transparent view of how the results came to be, and provide a starting point for interested parties who might want to give the procedures a try. The computational procedures are also thoroughly described in the article texts as suggested by Irving (2016), which supports the steps towards reproducibility and transparency in atmospheric sciences.

Contribution to Publications

The scientific papers that merge the core of the thesis is as follows:

Paper I / Chapter 2

Heistermann, Maik, Irene Crisologo, Catherine C. Abon, Bernard Alan Racoma, Stephan Jacobi, Nathaniel T. Servando, Carlos Primo C. David, and Axel Bronstert. 2013. "Brief Communication 'Using the New Philippine Radar Network to Reconstruct the Habagat of August 2012 Monsoon Event around Metropolitan Manila.'" Nat. Hazards Earth Syst. Sci. 13 (3): 653–57. https://doi.org/10.5194/nhess-13-653-2013.

MH conceptualized the study, together with IC and CCA; NTS and CPCD provided the radar data; MH wrote the software code, and MH and IC carried out the analysis. MH prepared the manuscript, with contributions from all co-authors.

Paper II / Chapter 3

Crisologo, Irene, Robert A. Warren, Kai Mühlbauer, and Maik Heistermann. 2018. "Enhancing the Consistency of Spaceborne and Ground-Based Radar Comparisons by Using Beam Blockage Fraction as a Quality Filter." Atmospheric Measurement Techniques 11 (9): 5223–36. https://doi.org/10.5194/amt-11-5223-2018.

IC and MH conceptualized the study. KM, MH, RW, and IC formulated the 3D-matching code based on previous work of RW. IC carried out the analyses; IC and MH the interpretation of results. IC and MH, with contributions from all authors, prepared the manuscript.

Paper III / Chapter 4

Crisologo, Irene and Maik Heistermann: Using ground radar overlaps to verify the retrieval of calibration bias estimates from spaceborne platforms, Atmos. Meas. Tech., submitted.

IC and MH conceptualized the study and formulated the code for 3D-matching of GRs. IC prepared the scripts for 3-way comparison and carried out the analysis. IC and MH interpreted the results and prepared the manuscript.

Chapter 2

Brief communication: Using the new Philippine radar network to reconstruct the Habagat of August 2012 monsoon event around Metropolitan Manila

This chapter is published as:

Heistermann, M., I. Crisologo, C. C. Abon, B. A. Racoma, S. Jacobi, N. T. Servando, C. P. C. David, and A. Bronstert. 2013. "Brief Communication 'Using the New Philippine Radar Network to Reconstruct the Habagat of August 2012 Monsoon Event around Metropolitan Manila.'" Nat. Hazards Earth Syst. Sci. 13 (3): 653–57. https://doi.org/10.5194/nhess-13-653-2013.

Abstract

From 6 to 9 August 2012, intense rainfall hit the northern Philippines, causing massive floods in Metropolitan Manila and nearby regions. Local rain gauges recorded almost 1000 mm within this period. However, the recently installed Philippine network of weather radars suggests that Metropolitan Manila might have escaped a potentially bigger flood just by a whisker, since the centre of mass of accumulated rainfall was located over Manila Bay. A shift of this centre by no more than 20 km could have resulted in a flood disaster far worse than what occurred during Typhoon Ketsana in September 2009.

2.1 Introduction

From 6 to 9 August 2012, a period of intense rainfall hit Luzon, the northern main island of the Philippines. In particular, it affected Metropolitan Manila, a region of about 640 km^2 and home to a population of about 12 million people. The torrential event resulted from a remarkably strong and sustained movement of the southwest monsoon, locally known as *Habagat*. The extraordinary development of the *Habagat* was caused by the cyclonic circulation of Typhoon *Saola* (local name *Gener*) from 1 to 3 August and was further enhanced by Typhoon *Haikui*, both passing north of the Philippines. This mechanism was already discussed by Cayanan et al. (2011). In the following, we will refer to this event as the *Habagat of August 2012*.

The event caused the heaviest damage in Metropolitan Manila since Typhoon Ketsana hit the area in September 2009 (Abon et al., 2011). The *Habagat of August 2012* particularly affected the Marikina River basin, the largest river system in Manila. Rain gauges in Metropolitan Manila recorded anywhere from 500 to 1100 mm of rain from 6 to 9 August. A total of 109 people have been confirmed dead. Over four million people were affected by the flood (NDRRMC, 2012).

Despite these numbers and despite the tragic and massive impacts of this flood event, the present study suggests that Metropolitan Manila might have escaped a bigger disaster just by a few kilometres. This analysis was made possible by using the recently established network of Doppler radars of the Philippine Atmospheric, Geophysical, and Astronomical Services Administration (PAGASA) and other meteorological data provided through the country's Project NOAH (Nationwide Operational Assessment of Hazards). The *Habagat of August 2012* was the first major rainfall event after the implementation of this project.

In this paper, we will present a first reconstruction of the rainfall event. It is the very first time such an analysis is shown for the Philippines, and it illustrates the immense potential for flood risk mitigation in the Philippines.

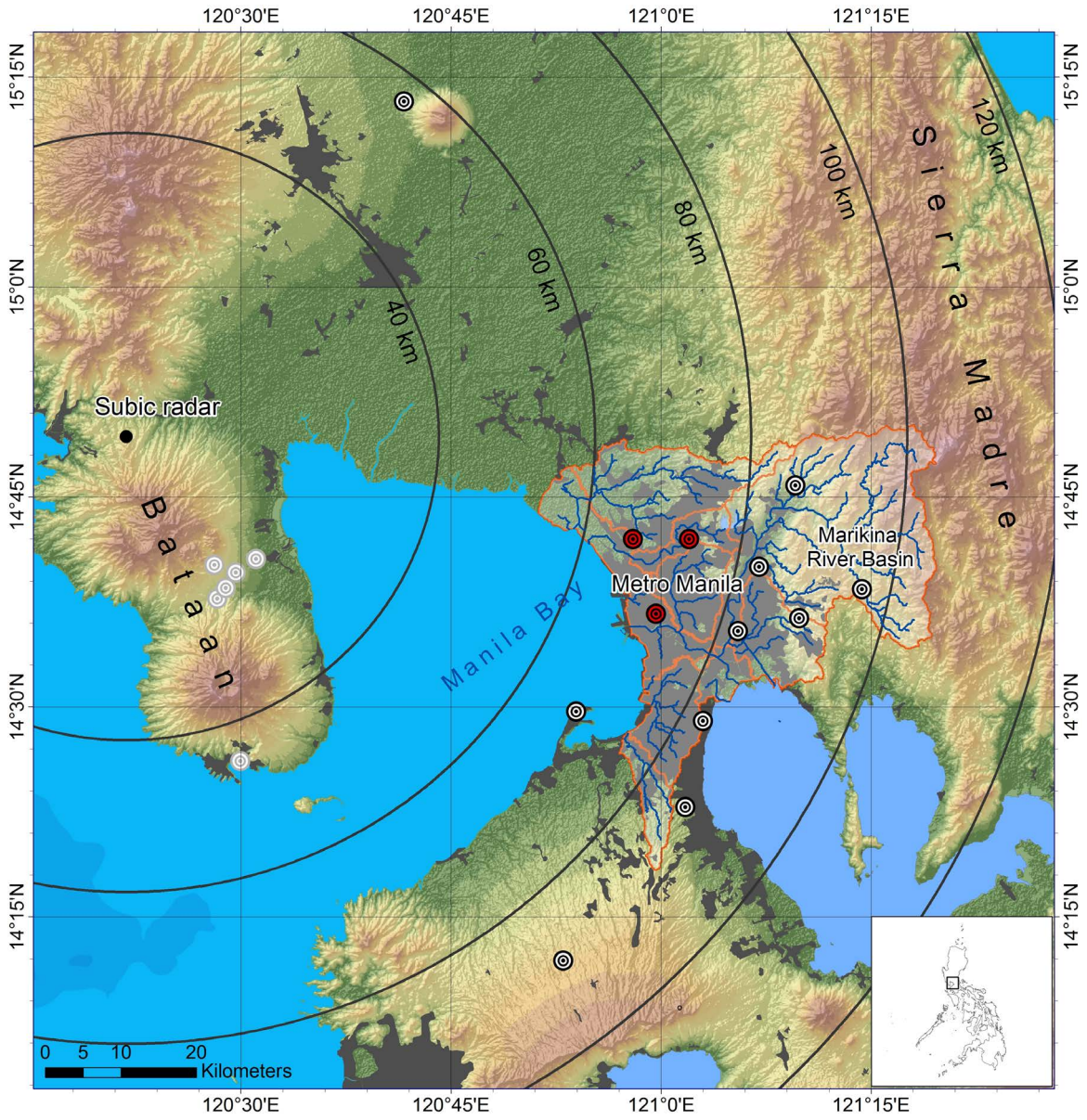

Figure 2.1: Geographical overview of the area, including Subic radar, different radar range radii as orientation, and the NOAH rain gauges (small circles). The red circles are the gauges shown in Figure 2.2. The gauges with grey circles have been ignored in this study, because the entire Bataan Peninsula is affected by massive beam shielding. Urban areas (including Metropolitan Manila) are shown in grey. Major rivers (blue lines) draining to Metropolitan Manila are shown together with their drainage basins (orange borders).

2.2 Radar data and data processing

Figure 2.1 shows a map of the area around Manila Bay. Radar coverage is provided by a Doppler S-band radar based near the city of Subic. The radar device is located at 500 m a.s.l. and has a nominal range of 120 km, a range resolution of 500 m, and an angular resolution of 1°. Radar sweeps are repeated at an interval of 9 min and at 14 elevation angles (0.5°, 1.5°, 2.4°, 3.4°, 4.3°, 5.3°, 6.2°, 7.5°, 8.7°, 10°, 12°, 14°, 16.7°, and 19.5°).

In addition, 25 rain gauges were used as ground reference. The rain gauge recordings were obtained from automatic rain gauges (ARGs) and automatic weather stations (AWSs) under Project NOAH; all instruments have a temporal resolution of 15 min.

For radar data processing, the *wradlib* software (Heistermann et al., 2013b) was used. *wradlib* is an open source library for weather radar processing and allows for the most important steps of radar-based

quantitative precipitation estimation (QPE). The reconstruction of rainfall depths from 6 to 9 August included all available radar sweep angles and was based on a four-step procedure (see library reference on `http://wradlib.bitbucket.org` for further details):

1. **Clutter detection**: clutter is generally referred to as nonmeteorological echo, mainly ground echo. Clutter was identified by applying the algorithm of Gabella and Notarpietro (2002) to the rainfall accumulation map. Pixels flagged as clutter were filled by using nearest neighbour interpolation.

2. **Conversion from reflectivity (in dBZ) to rainfall rate (in mm/hr)**: for this purpose, we used the Z–R relation which is applied by the United States national weather service NOAA for tropical cyclones ($Z = 250 \cdot R^{1.2}$). According to Moser et al. (2010), the use of this tropical Z–R relation could be shown to reduce the underestimation of rainfall rates in tropical cyclones as compared to standard Z–R relationships.

3. **Gridding**: based on the data from all available elevation angles, a constant altitude plan position indicator (Pseudo-CAPPI) was created for an altitude of 2000 m a.s.l. by using three-dimensional inverse distance weighting. The CAPPI approach was used in order to increase the comparability of estimated rainfall at different distances from the radar—an important precondition for the following step of gauge adjustment.

4. **Gauge adjustment**: the radar-based rainfall estimate accumulated over the entire event was adjusted by rain gauge observations using the simple, but robust mean field bias (MFB) approach Goudenhoofdt and Delobbe (2009); Heistermann and Kneis (2011). A correction factor was computed from the mean ratio between rain gauge observations and the radar observations in the direct vicinity of the gauge locations. Basically, this procedure is equivalent to an ex-post adjustment of the coefficient a in the Z–R relationship.

2.3 Event reconstruction

Figure 2.2 shows the rainfall dynamics in the area of Metropolitan Manila over a period of four days, based on rain gauge recordings. The main portion of rainfall accumulated rather continuously between noon of 6 August and the evening of 7 August. However, significant periods of intermittent, but intense rainfall followed until the early morning of 9 August. Keeping in mind that the distance between the gauges is only around 10 km (Figure 2.1), and that the accumulation period lasted four days, the differences between the rainfall accumulations are quite remarkable. As will be seen later (in Figure 2.4), this heterogeneity is consistent with the distribution of rainfall inferred from the radar.

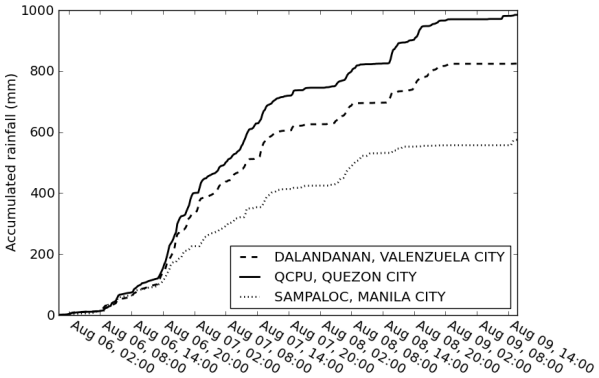

Figure 2.2: Cumulative rainfall from 6 to 9 August for three rain gauges in Metropolitan Manila. Refer to Fig. 2.1 for the position of the rain gauges. The distances between the three gauges are about 10 km.

According to Fig. 2.3, three marked convective cells poured rain around Manila Bay, the largest of them extending from the centre of Manila Bay eastwards over Metropolitan Manila. Over the entire period of three days, the position of these cells remained quite persistent. This persistence—together with the high average rainfall intensities—explains the extreme local rainfall accumulations. Figure 2.3 also illustrates the mean vertical structure of rainfall between the evening of August 6 and the early morning of 7 August. The convective structures exhibit a marked decrease in rainfall intensity above an altitude of 5 to 6 km, which is typical for shallow convection. This vertical structure is also representative of the duration of the entire event.

However, the unadjusted radar-based rainfall accumulation from 6 August (08:00 UTC) to 9 August (20:00 UTC) exhibits a significant underestimation if compared to the rain gauge recordings. While the radar estimates between 300 and 400 mm around Quezon City, rain gauges recorded up to 1000 mm. At the moment, the reasons for this level of underestimation remain unclear. Hardware calibration issues might as well play a role as effects of the vertical profile of reflectivity, which were not yet analysed in the course of this analysis. Beyond this general underestimation, the

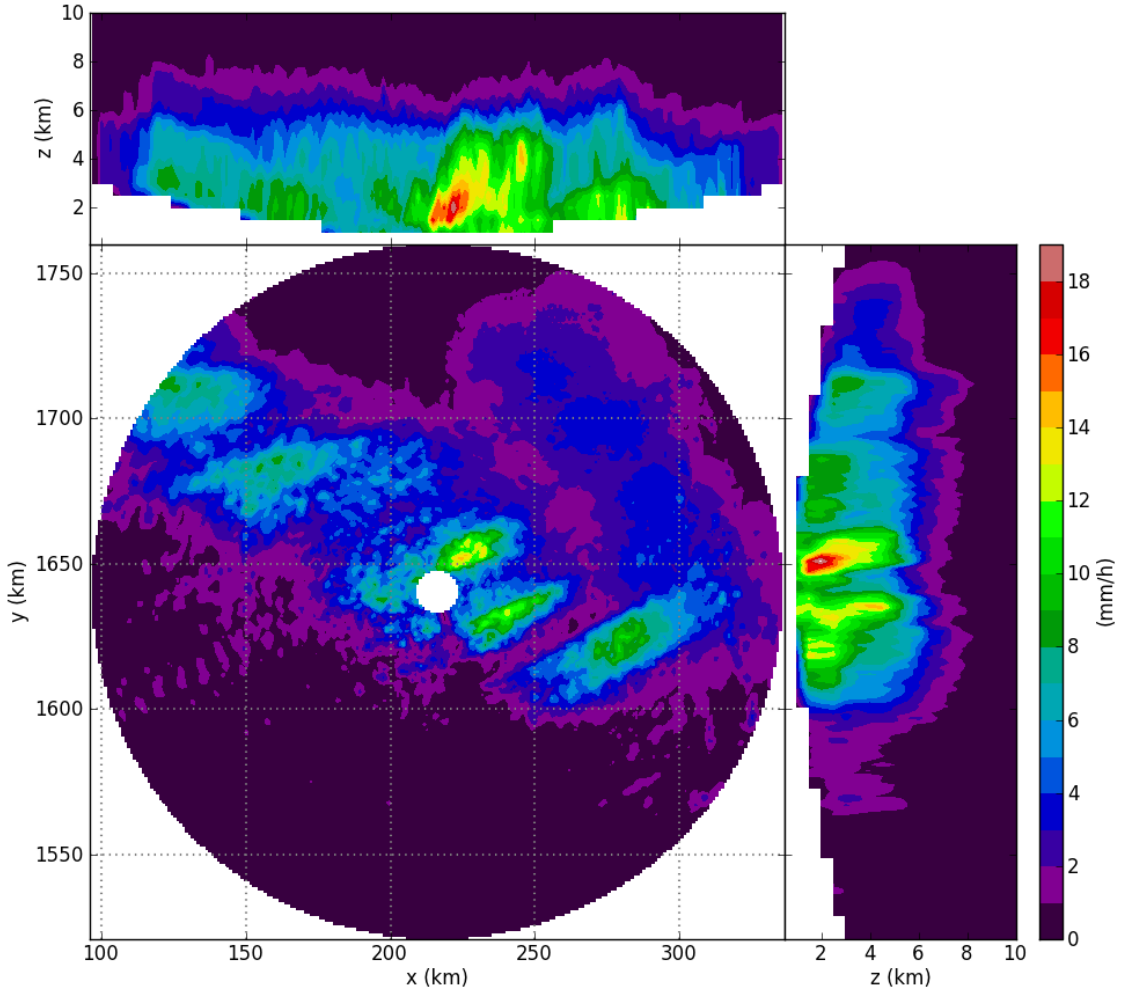

Figure 2.3: Mean rainfall intensity in the night from 6 August (20:00 UTC) until 7 August (08:00 UTC) as seen by the Subic S-band radar. The central figure shows a CAPPI at 3000 m altitude (for the rainfall estimation, we used the Pseudo-CAPPI at 2000 m; see Sect. 2.2). The marginal plots show the vertical distribution of intensity maxima along the x- and y-axis, respectively. In the area around Manila Bay, three marked cells appear. For these cells, the rainfall intensity exhibits a marked decrease above an altitude of 5 to 6 km, indicating rather shallow convection.

Subic radar shows massive beam shielding in the southern sectors, which is caused by Mount Natib, a volcano and caldera complex located in the province of Bataan. Other sectors of the Subic radar are affected by partial beam shielding due to a set of mountain peaks in the northern vicinity of the radar.

In order to correct for the substantial underestimation, rain gauge recordings were used to adjust the rainfall estimated by the radar at an altitude of 2000 m (using the mean field bias adjustment approach). This procedure reduced the crossvalidation RMSE of the event-scale rainfall accumulation by more than half. The resulting rainfall distribution is shown in Figure 2.4. This figure gives an impressive view on the amount of rain that actually came down around Metropolitan Manila. Obviously, the actual "epicentre" of the event was situated rather over the Manila Bay than over Metropolitan Manila itself.

Due to its size and shape, the Marikina River basin (see Figure 2.1)—as it did in September 2009—most strongly contributed to the flooding of Metropolitan

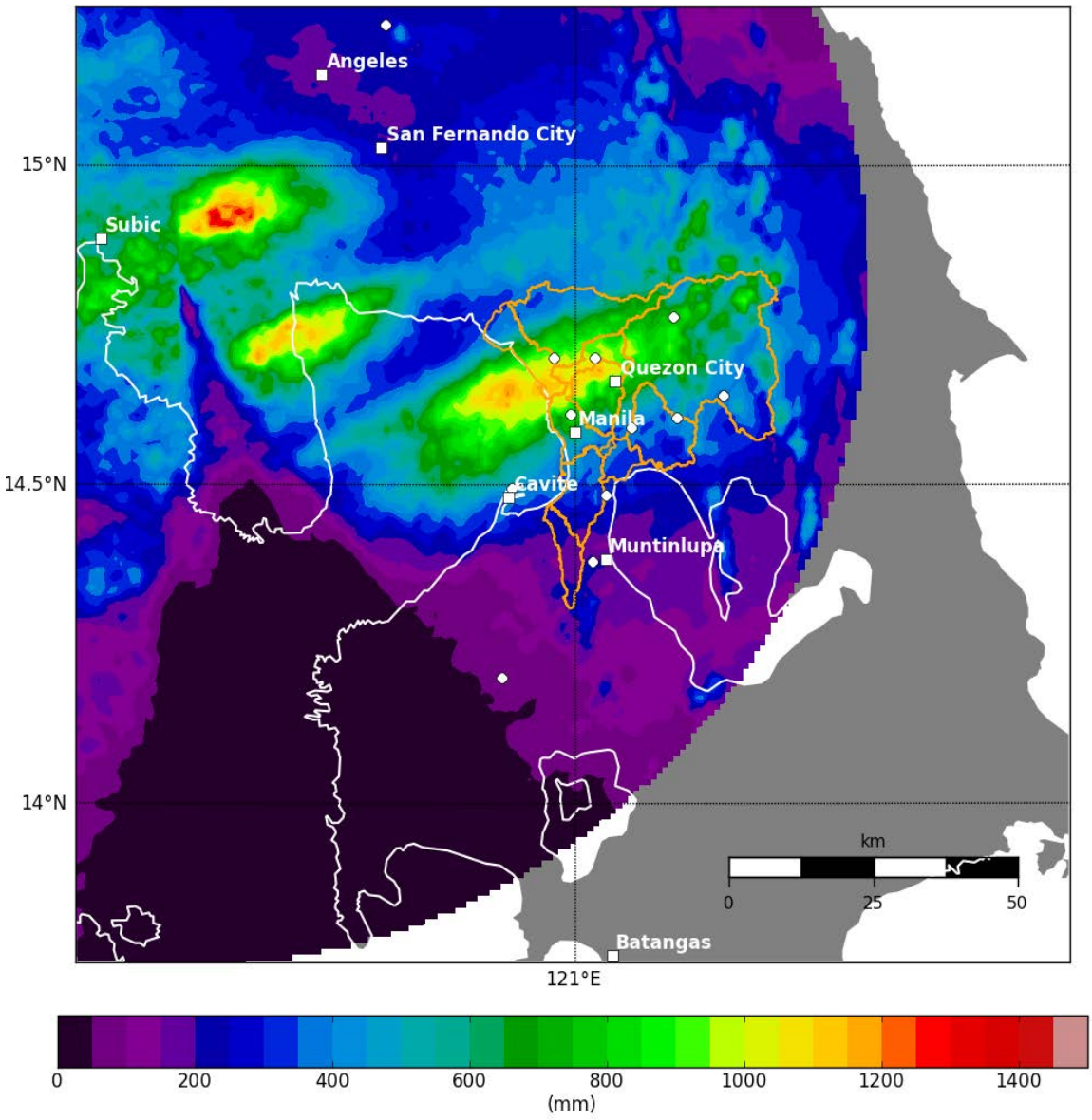

Figure 2.4: Gauge-adjusted radar-based rainfall estimation; accumulation period from 6 August (00:80 UTC) to 9 August (20:00 UTC). Basins draining to Metropolitan Manila are shown in orange, coastlines in white. Major cities are shown as white squares, while rain gages are represented as white circles. Note that the corresponding rainfall field obtained from the interpolation of rain gauge observations is available as Supplement.

Manila during the *Habagat of August 2012*. According to the gauge-adjusted radar rainfall estimates, the areal mean rainfall depth for the Marikina River basin amounted to 570 mm. In contrast, the areal rainfall average would add up to 440 mm (more than 20% less) if we only interpolated the rain gauge observations (by inverse distance weighting.

If we now assumed a scenario in which the rainfall field had been shifted eastward by no more than 20 km, the areal rainfall average in the Marikina River basin would have increased by almost 30%. Since the catchment had already been saturated before the onset of the main event, almost all of the additional rain would have been directly transformed to runoff. A very rough, but illustrative calculation demonstrates the potential implications: according to the extreme value statistic for the Marikina River, a 500 m^3/s increase in peak discharge at stream flow gauge Sto. Nino approximately corresponds to a 2.5-fold increase in the return period (DPWH-JICA, 2003). For the *Habagat of August 2012* event, the peak discharge at gauge Sto. Nino was estimated to be around 3000 m^3/s, corresponding to a return period of about 50 years. Assuming that every additional raindrop had been effective rainfall and assuming linear runoff concentration, the "20 km-shift" scenario would have resulted in a peak discharge of about

3900 m^3/s—or a return period of more than 200 years. The return period of the flood event related to Typhoon Ketsana in September 2009 was estimated to be 150 years (Tabios III, 2009).

2.4 Conclusions

The local rain gauge recordings in Quezon City already indicate the magnitude of the *Habagat of August 2012* event. However, the rain gauge data alone could not provide a complete picture of what happened around Metropolitan Manila from 6 to 9 August.

Only the combination of the Subic S-band radar and the dense rain gauge network around Metropolitan Manila reveals that a significant portion of the heavy rainfall was dropped right over the shorelines of Manila Bay. Assuming a scenario in which the rainfall field was shifted eastwards by no more than 20 km, the peak discharge of the Marikina River would have increased by almost 30%, potentially resulting into a return period well beyond the 150 yr of Typhoon Ketsana in September 2009. It appears that—despite the terrible harm and damage that was caused by this flood event—the *Habagat of August 2012* was no more than a glimpse of the disaster that Metropolitan Manila missed by no more than 20 km.

Nonetheless, a lot of open questions remain to be answered, particularly concerning the underestimation of rainfall by the radar, the potential effects of inhomogeneous vertical reflectivity profiles, the potential role of wind drift (from Manila Bay to Metropolitan Manila), and also the hydrological processes which resulted from the rainfall event. Beyond, additional data for the region are available from a C-band weather radar located near Tagaytay City. However, these data were not considered in this study since the role of attenuation induced by heavy rainfall has yet to be determined. All these questions need to be addressed as soon as possible so that the equipment installed can allow for the most accurate analysis of extreme rain events that certainly will occur in the future. However, even with the current level of data processing, the recently installed Philippine radar network demonstrates a huge potential for high-resolution rainfall monitoring as well as for risk mitigation and management in the Philippines.

Acknowledgements

The radar data for this analysis were provided by the Philippine Atmospheric, Geophysical and Astronomical Services Administration (PAGASA, `http://pagasa.dost.gov.ph`). The rain gauge data were kindly provided by the Philippine government's Project NOAH (National Operational Assessment of Hazards, http://noah.dost.gov.ph). The study was also funded through Project NOAH, as well as by the German Ministry for Education and Research (BMBF) through the PROGRESS project (http://www.earth-in-progress), and through the GeoSim graduate research school (`http://www.geo-x.net/geosim`).

Supplemental material to the manuscript

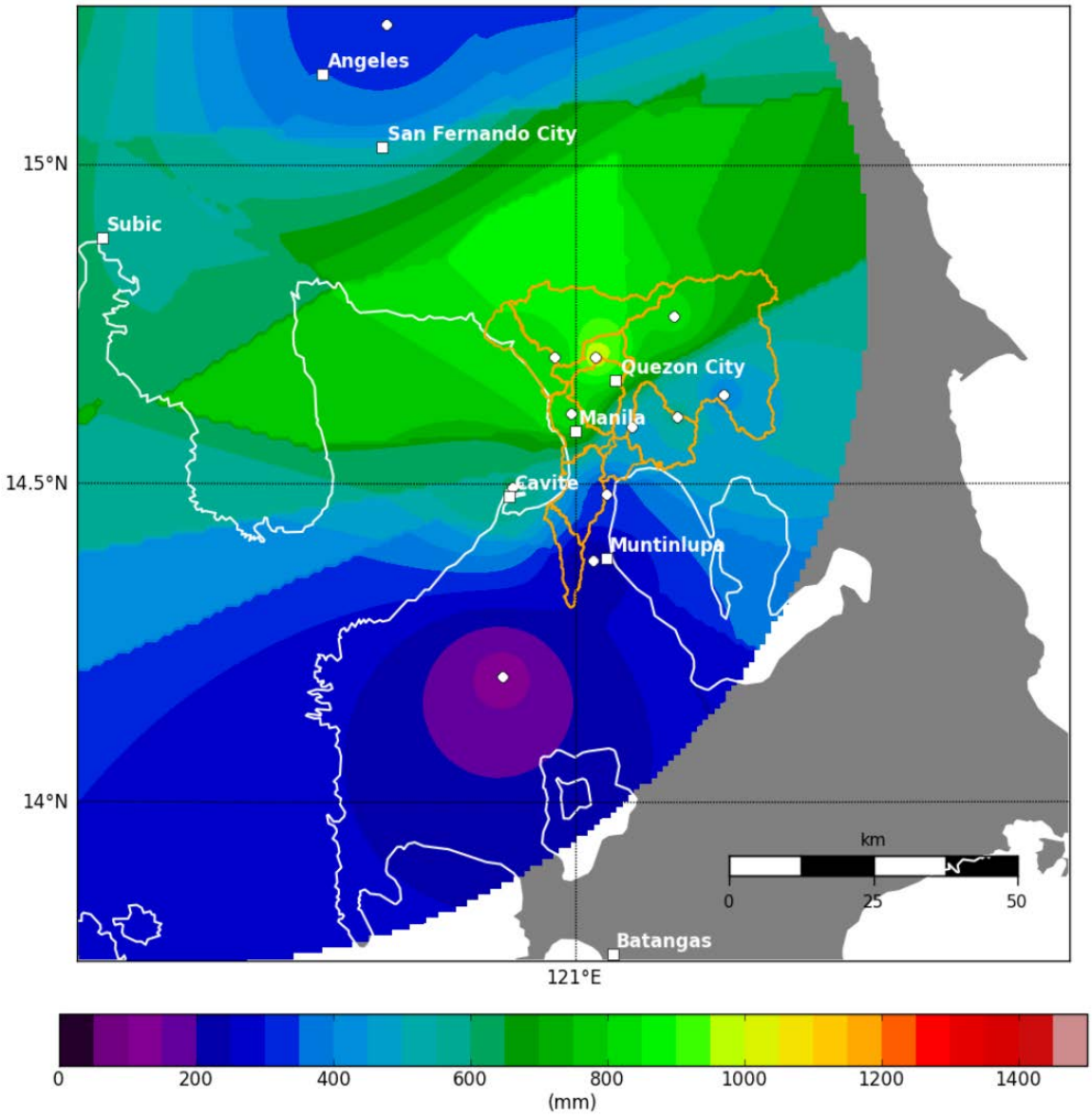

Figure 2.5: Accumulated rainfall as estimated from the interpolation of rain gauge observations using inverse distance weighting; accumulation period from Aug 6 (00:80 UTC) to Aug 9 (20:00 UTC). Basins draining to Metropolitan Manila are shown in orange, coastlines in white. Major cities are shown as white squares, while rain gages are represented as white circles.

Chapter 3

Enhancing the Consistency of Spaceborne and Ground-Based Radar Comparisons by Using Beam Blockage Fraction as a Quality Filter

This chapter is published as:

Crisologo, Irene, Robert A. Warren, Kai Mühlbauer, and Maik Heistermann. 2018. "Enhancing the Consistency of Spaceborne and Ground-Based Radar Comparisons by Using Beam Blockage Fraction as a Quality Filter." Atmospheric Measurement Techniques 11 (9): 5223–36. https://doi.org/10.5194/amt-11-5223-2018.

Abstract

We explore the potential of spaceborne radar (SR) observations from the Ku-band precipitation radars onboard the Tropical Rainfall Measuring Mission (TRMM) and Global Precipitation Measurement (GPM) satellites as a reference to quantify the ground radar (GR) reflectivity bias. To this end, the 3D volume-matching algorithm proposed by Schwaller and Morris (2011) is implemented and applied to 5 years (2012–2016) of observations. We further extend the procedure by a framework to take into account the data quality of each ground radar bin. Through these methods, we are able to assign a quality index to each matching SR–GR volume, and thus compute the GR calibration bias as a quality-weighted average of reflectivity differences in any sample of matching GR–SR volumes. We exemplify the idea of quality-weighted averaging by using the beam blockage fraction as the basis of a quality index. As a result, we can increase the consistency of SR and GR observations, and thus the precision of calibration bias estimates. The remaining scatter between GR and SR reflectivity, as well as the variability of bias estimates between overpass events indicate, however, that other error sources are not yet fully addressed. Still, our study provides a framework to introduce any other quality variables that are considered relevant in a specific context. The code that implements our analysis is based on the open-source software library *wradlib*, and is, together with the data, publicly available to monitor radar calibration, or to scrutinize long series of archived radar data back to December 1997, when TRMM became operational.

3.1 Introduction

Weather radars are essential tools in providing high-quality information about precipitation with high spatial and temporal resolution in three dimensions. However, several uncertainties deteriorate the accuracy of rainfall products, with calibration contributing the most amount (Houze et al., 2004), while also varying in time (Wang and Wolff, 2009). While adjusting ground radars (GR) by comparison with a network of rain gauges (also know as *gauge adjustment*) is a widely used method, it suffers from representativeness issues. Furthermore, gauge adjustment accumulates uncertainties along the entire rainfall estimation chain (e.g. including the uncertain transformation from reflectivity to rainfall rate), and thus does not provide a direct reference for the measurement of reflectivity. Relative calibration (defined as the assessment of bias between the reflectivity of two radars) has been steadily gaining popularity, in particular the comparison with spaceborne precipitation radars (SR) (such as the precipitation radar onboard the Tropical Rainfall Measuring Mission (TRMM; 1997–2014; Kummerow et al. (1998)) and the dual-frequency precipitation radar on

the subsequent Global Precipitation Measurement mission (GPM; 2014–present; Hou et al. (2013)). Several studies have shown that surface precipitation estimates from GRs can be reliably compared to precipitation estimates from SRs for both TRMM (Amitai et al., 2009; Joss et al., 2006; Kirstetter et al., 2012) and GPM (Gabella et al., 2017; Petracca et al., 2018; Speirs et al., 2017). In addition, a major advantage of relative calibration and gauge adjustment in contrast to the absolute calibration (i.e. minimizing the bias in measured power between an external or internal reference noise source and the radar at hand) is that they can be carried out *a posteriori*, and thus be applied to historical data.

Since both ground radars and spaceborne precipitation radars provide a volume-integrated measurement of reflectivity, a direct comparison of the observations can be done in three dimensions (Anagnostou et al., 2001; Gabella et al., 2006, 2011; Keenan et al., 2003; Warren et al., 2018). Moreover, as the spaceborne radars are and have been constantly monitored and validated (with their calibration accuracy proven to be consistently within 1 dB) (TRMM: Kawanishi et al. (2000); Takahashi et al. (2003); GPM: Furukawa et al. (2015); Kubota et al. (2014); Toyoshima et al. (2015)), they have been suggested as a suitable reference relative calibration of ground radars (Anagnostou et al., 2001; Islam et al., 2012; Liao et al., 2001; Schumacher and Houze Jr, 2003).

Relative calibration between SRs and GRs was originally suggested by Schumacher and Houze (2000), but the first method to match SR and GR reflectivity measurements was developed by Anagnostou et al. (2001). In their method, SR and GR measurements are resampled to a common 3-D grid. Liao et al. (2001) developed a similar resampling method. Such 3-D resampling methods have been used in comparing SR and GR for both SR validation and GR bias determination (Bringi et al., 2012; Gabella et al., 2006, 2011; Park et al., 2015; Wang and Wolff, 2009; Zhang et al., 2018; Zhong et al., 2017) Another method was suggested by Bolen and Chandrasekar (2003) and later on further developed by Schwaller and Morris (2011), where the SR–GR matching is based on the geometric intersection of SR and GR beams. This geometry matching algorithm confines the comparison to those locations where both instruments have actual observations, without interpolation or extrapolation. The method has also been used in a number of studies comparing SR and GR reflectivities (Chandrasekar et al., 2003; Chen and Chandrasekar, 2016; Islam et al., 2012; Kim et al., 2014; Wen et al., 2011). A sensitivity study by Morris and Schwaller (2011) found that method to give more precise estimates of relative calibration bias as compared to grid-based methods.

Due to different viewing geometries, ground radars and spaceborne radars are affected by different sources of uncertainty and error. Observational errors with regard to atmospheric properties such as reflectivity are, for example, caused by ground clutter or partial beam blocking. Persistent systematic errors in the observation of reflectivity by ground radars are particularly problematic: the intrinsic assumption of the bias estimation is that the only systematic source of error is radar calibration. It is therefore particularly important to address such systematic observation errors.

In this study, we demonstrate that requirement with the example of partial beam blocking. The analysis is entirely based on algorithms implemented in the open-source software library *wradlib* (Heistermann et al., 2013b), including a technique to infer partial beam blocking by simulating the interference of the radar beam with terrain surface based on a digital elevation model. Together, that approach might become a reference for weather services around the world who are struggling to create unbiased radar observations from many years of archived single-polarized radar data, or to consistently monitor the bias of their radar observations. We demonstrate the approach in a case study with 5 years of data from the single-polarized S-band radar near the city of Subic, Philippines, which had been shown in previous studies to suffer from substantial miscalibration (Abon et al., 2016; Heistermann et al., 2013a).

3.2 Data

3.2.1 Spaceborne precipitation radar

Precipitation radar data were gathered from TRMM 2A23 and 2A25 version 7 products (NASA, 2017) for overpass events intersecting with the Subic ground radar coverage from 1 June 2012 to 30 September 2014, and GPM 2AKu version 5A products (Iguchi et al., 2010) from 1 June 2014 to 31 December 2016. Ka-band observations have not been considered due to higher susceptibility to attenuation, and a limited validity of Rayleigh scattering in a substantial portion of rainfall cases (Baldini et al., 2012). From the collection of overpasses within these dates, only 183 TRMM overpasses and 103 GPM passes were within the radar coverage. The data were downloaded from NASA's Precipitation

Processing System (PPS) through the STORM web interface (https://storm.pps.eosdis.nasa.gov/storm/) on 15 February 2018 for TRMM and 14 June 2018 for GPM. The parameters of TRMM/GPM extracted for the analysis are the same as Warren et al. (2018; their Table 3).

It is important to note that, at the time of writing, changes in calibration parameters applied in the GPM Version 5 products resulted in an increase of +1.1 dB from the corresponding TRMM version 7 products (NASA, 2017).

3.2.2 Ground radar

The Philippine Atmospheric, Geophysical, and Astronomical Services Administration (PAGASA) maintains a nationwide network of 10 weather radars, 8 of which are single-polarization S-band radars and 2 are dual-polarization C-band radars. The Subic radar, which covers the greater Metropolitan Manila area, has the most extensive set of archived data. The radar coverage includes areas that receive some of the highest mean annual rainfall in the country.

The Subic radar sits on top of a hill at 532 m.a.s.l. in the municipality of Bataan, near the border with Zambales (location: 14.82 °N, 120.36 °E) (see Figure 3.1). To its south stands Mt. Natib (1253 m.a.s.l.) and to its north run the Zambales Mountains (the highest peak stands at 2037 m.a.s.l.). To the west is the Redondo Peninsula in the southern part of the Zambales province, where some mountains are also situated. Almost half of the coverage of the Subic radar is water, with Manila Bay to its south-east and the West Philippine Sea to the west. Technical specifications of the radar are summarized in Table 3.2.2. Data from April 2012 to December 2016 were obtained from PAGASA. Throughout the 5 years the scan strategy remained the same, except for 2015 when it was limited to only three elevation angles per volume due to hardware issues. The standard scanning strategy was re-implemented in 2016.

Table 3.1: Characteristics of the Subic radar and its volume scan strategy. The numbers in parentheses correspond to scans in 2015, where the scanning strategy was different due to hardware issues.

	Subic Radar
Polarization	Single-Pol
Position (lat/lon)	14.82° N 120.36 ° E
Altitude	532 m.a.s.l.
Maximum Range	120 km (150 km)
Azimuth resolution	1 °
Beam width	0.95 °
Gate length	500 m (250 m)
Number of elevation angles	14 (3)
Elevation angles	0.5, 1.5, 2.4, 3.4, 4.3, 5.3, 6.2, 7.5, 8.7, 10, 12, 14, 16.7, 19.5 (°) (0.0, 1.0, 2.0)
Volume cycle interval	9 minutes
Data available since	April 2012
Peak power	850 kW
Wavelength	10.7 cm

3.3 Method

3.3.1 Partial beam shielding and quality index based on beam blockage fraction

In an ideal situation, SR and GR should have the same measurements for the same volume of the atmosphere, as they are measuring the same target. However, observational differences may arise due to different view geometries, different operating frequencies, different environmental conditions of each instrument, and different processes along the propagation path of the beam. As pointed out before, we focus on beam blockage as an index of GR data quality.

In regions of complex topography, ground radars are typically affected by the effects of beam blockage, induced by the interaction of the beam with the terrain surface resulting in a weakening or even loss of the signal. To quantify that process within the Subic radar coverage, a beam blockage map is generated following the algorithm proposed by Bech et al. (2003). It assesses the extent of occultation using a digital elevation model (DEM). While Bech et al. (2003) used the GTOPO30 DEM at a resolution of around 1 km, higher DEM resolutions are expected to increase the accuracy of estimates of beam blockage fraction, as shown by Kucera et al. (2004), in particular the near range of the radar

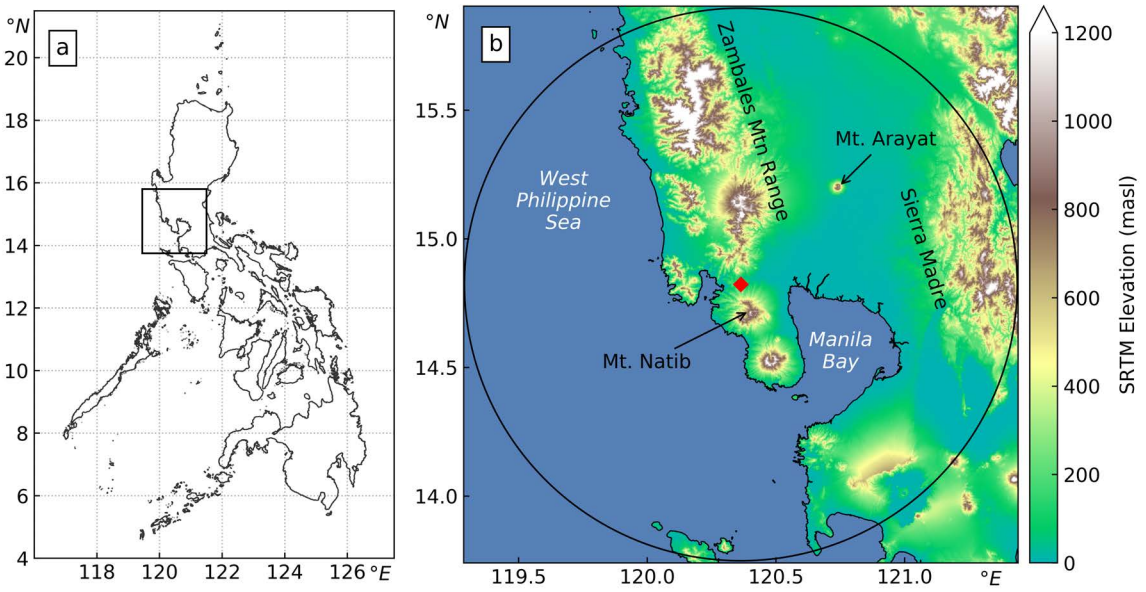

Figure 3.1: (a) Map of the Philippines showing the region of study and (b) the 120km coverage of the Subic radar (location marked with red diamond) with the SRTM digital elevation model of the surrounding area.

(Cremonini et al., 2016). The DEM used in this study is from the Shuttle Radar Topography Mission (SRTM) data, with 1 arc-second (approximately 30-meter) resolution. The DEM was resampled to the coordinates of the radar bin centroids, using spline interpolation, in order to match the polar resolution of the radar data (500 m in range and 1° in azimuth, extending to a maximum range of 120 km from the radar site; see Figure 3.1). A beam blockage map is generated for all available elevation angles.

The beam blockage fraction was calculated for each bin and each antenna pointing angle. The cumulative beam blockage was then calculated along each ray. A cumulative beam blockage fraction (BBF) of 1.0 corresponds to full occlusion, and a value of 0.0 to perfect visibility.

The quality index based on beam blockage fraction is then computed following Zhang et al. (2011) as

$$Q_{BBF}=\begin{cases}1 & BBF \leq 0.1\\ 1-\frac{BBF-0.1}{0.4} & 0.1 < BBF \leq 0.5\\ 0 & BBF > 0.5\end{cases} \quad (3.1)$$

A slightly different formulation to transform partial beam blockage to a quality index has been presented in other studies (Figueras i Ventura and Tabary, 2013; Fornasiero et al., 2005; Ośródka et al., 2014; Rinollo et al., 2013) where the quality is zero (0) if BBF is above a certain threshold, and then linearly increases to one (1) above that threshold. It should be noted that these approaches are equally valid and can be used in determining the quality index based on beam blockage.

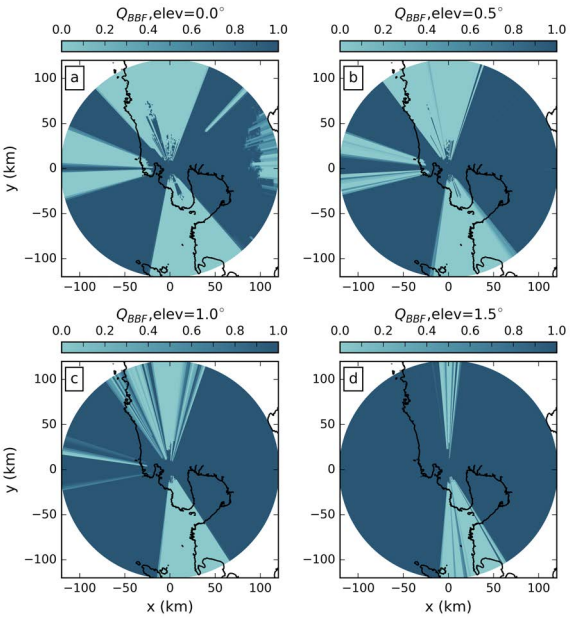

Figure 3.2: Quality index map of the beam blockage fraction for the Subic radar at (a) 0.0°, (b) 0.5°, (c) 1.0°, and (d) 1.5° elevation angles.

Figure 3.2 shows the beam blockage map for the two lowest elevation angles of each scanning strategy. Figure 3.2a and c are for 0.0° and 1.0°, which are the two lowest elevation angles in 2015, while Figure 3.2b and d are for 0.5° and 1.5°, which are the two lowest elevation angles for the rest of the dataset.

As expected, the degree of beam blockage decreases with increasing antenna elevation, yielding the most pronounced beam blockage at 0.0°. Each blocked sector can be explained by the topography (see Figure 3.1), with the Zambales Mountains causing blockage in the northern sector, Mt. Natib in the southern sector, and the Redondo peninsula mountains in the western sector. The Sierra Madre also causes some partial beam blocking in the far east, and a narrow partial blocking northeast of the station where Mt. Arayat is located. As the elevation angle increases, the beam blockage becomes less pronounced or even disappears. Substantial blockage persists, however, for the higher elevation angles in the northern and southern sectors.

3.3.2 SR–GR Volume Matching

SR and GR data were matched only for the wet period within each year, which is from June to December. Several meta-data parameters were extracted from the TRMM 2A23 and GPM 2AKu products for each SR gate, such as the corresponding ray's brightband height and width, gate coordinates in three dimensions (longitude and latitude of each ray's Earth intercept and range gate index), time of overpass, precipitation type (*stratiform*, *convective*, or *other*), and rain indicators (*rain certain* or *no-rain*). The parallax-corrected altitude (above mean sea level) and horizontal location (with respect to the GR) of each gate were determined as outlined in the appendix of Warren et al. (2018). From the brightband height/width and the altitude of each SR gate, the brightband membership of each gate was calculated by grouping all rays in an overpass and computing the mean brightband height and width. A ratio value of less than zero indicates that the gate is below the brightband, and greater than one indicates that the gate is above the brightband, and a value between zero and one means that the gate is within the brightband. Only gates below and above the brightband were considered in the comparison. Warren et al. (2018) found a positive bias in GR–SR reflectivity difference for volume-matched samples within the melting layer, compared to those above and below the melting layer. They speculated that this was due to underestimation of the Ku- to S-band frequency correction for melting snow. In addition, while usually the samples above the brightband are used in GPM validation, there are significantly more samples below the melting layer, especially in a tropical environment such as the Philippines. To ensure that there are sufficient bins with actual rain included in the comparison, overpasses with less than 100 gates flagged as rain certain were discarded.

For each SR overpass, the GR sweep with the scan time closest to the overpass time within a 10-min window (±5-min from overpass time) was selected. Both the SR and GR data were then geo-referenced into a common azimuthal equidistant projection centered on the location of the ground radar.

In order to minimize systematic differences in comparing the SR and GR reflectivities caused by the different measuring frequencies, the SR reflectivities were converted from Ku- to S-band following the formula:

$$Z(S) = Z(Ku) + \sum_{i=0}^{4} a_i [Z(Ku)]^i \qquad (3.2)$$

where the a_i are the coefficients for dry snow and dry hail, rain, and in between at varying melting stages (Table 1 of Cao et al. (2013)). We used the coefficients for snow in the reflectivity conversion above the brightband, following Warren et al. (2018).

The actual volume matching algorithm closely follows the work of Schwaller and Morris (2011), where SR reflectivity is spatially and temporally matched with GR reflectivity without interpolation. The general concept is highlighted by Figure 3.3: each matching sample consists of bins from only *one SR ray* and *one GR sweep*. From the SR ray, those bins were selected that intersect with the vertical extent of a specific GR sweep at the SR ray location. From each GR sweep, those bins were selected that intersect with the horizontal footprint of the SR ray at the corresponding altitude. The SR and GR reflectivity of each matched volume was computed as the average reflectivity of the intersecting SR and GR bins.

The nominal minimum sensitivity of both TRMM PR and GPM KuPR is 18 dBZ, so only values above this level were considered in the calculation of average SR reflectivity in the matched volume. In addition, the fraction of SR gates within a matched volume above that threshold was also recorded. On the other hand, all GR bins are included in the calculation of average GR reflectivity, after setting the bins with reflectivities below 0.0 dBZ to 0.0 dBZ, as suggested by Morris and Schwaller (2011). The filtering criteria applied in the workflow are summarized in Table 3.2.

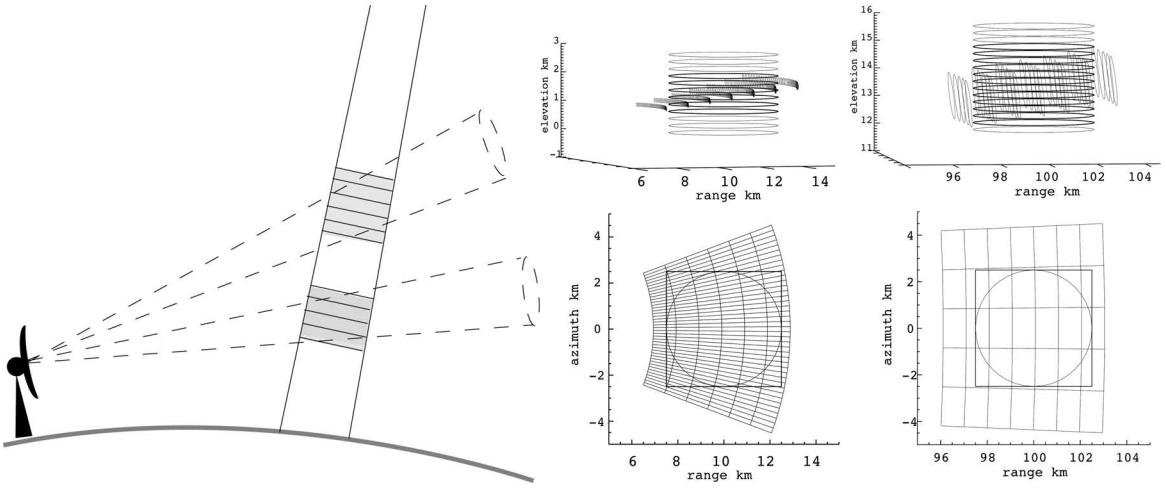

Figure 3.3: Diagram illustrating the geometric intersection. Left panel shows a single SR beam intersecting GR sweeps of two different elevation angles. The two top right panels illustrate the intersection of SR–GR sample volumes in the near and far ranges and the two bottom right panels show the projection of these intersections along an SR ray. From Schwaller and Morris (2011) ©American Meteorological Society. Used with permission.

Table 3.2: Filtering criteria for the matching workflow.

Criteria	Condition
Minimum number of pixels in overpass tagged as 'rain'	100
Brightband membership	below or above
GR range limits (min–max)	15 – 115 km
Minimum fraction of bins above minimum SR sensitivity	0.7
Minimum fraction of bins above minimum GR sensitivity	0.7
Maximum time difference between SR and GR	5 min
Minimum PR reflectivity	18 dBZ

3.3.3 Assessment of the average reflectivity bias

Beam blockage and the corresponding GR quality maps were computed for each GR bin (cf. Section 3.3.1). For each matched SR–GR volume, the data quality was then based on the minimum quality of the GR bins in that volume.

To analyze the effect of data quality on the estimation of GR calibration bias, we compared two estimation approaches: a simple mean bias that does not take into account beam blockage, and a weighted mean bias that considers the quality value of each sample as weights. The corresponding standard deviation and weighted standard deviation were calculated as well. The overall process is summarized in Figure 3.4. In this way, we provide an overview of the variability of our bias estimates over time.

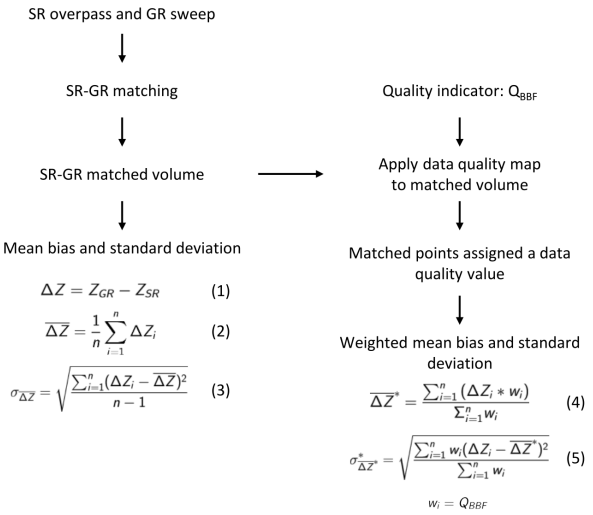

Figure 3.4: Flowchart describing the processing steps to calculate the mean bias and the weighted mean bias between ground radar data and satellite radar data. The results of each step are shown in Section 3.4.

3.3.4 Computational details

In order to promote transparency and reproducibility of this study, we mostly followed the guidelines provided by Irving (2016) which have also been implemented by a number of recent studies (Blumberg et al., 2017; Irving and Simmonds, 2016; Rasp et al., 2018).

The entire processing workflow is based on *wradlib* (Heistermann et al., 2013b), an extensively documented open-source software library for processing weather radar data. At the time of writing, we used version 1.0.0 released on 01 April 2018, based on Python 3.6. The main dependencies include Numerical Python (NumPy; Oliphant (2015)), Matplotlib (Hunter, 2007), Scientific Python (SciPy; Jones et al. (2014)), h5py (Collette, 2013), netCDF4 (Rew et al., 1989), and gdal (GDAL Development Team, 2017).

Reading the TRMM 2A23 and 2A25 version 7 data, GPM 2AKu version 5A data, and Subic ground radar data in the netCDF format converted through the EDGE software of EEC radars was done through the input-output module of wradlib. The beam blockage modelling is based on the Bech et al. (2003) method implemented as a function in wradlib's data quality module. The volume-matching procedure is built upon the georeferencing and zonal statistics modules, accompanied by Pandas (McKinney, 2010) for organizing and analysing the resulting database of matched bins. Visualization was carried out with the help of matplotlib (Hunter, 2007) and Py-ART (Helmus and Collis, 2016).

An accompanying GitHub repository that hosts the Jupyter notebooks of the workflow and sample data is made available at `https://github.com/wradlib/radargpm-beamblockage`.

3.4 Results and discussion

3.4.1 Single event comparison

From the 183 TRMM and 103 GPM overpasses that intersected with the 120 km Subic radar range, only 74 TRMM and 40 GPM overpasses were considered valid after applying the selection criteria listed in Table 3.2. In order to get a better idea about the overall workflow, we first exemplify the results for two specific overpass events—one for TRMM, and one for GPM.

Case 1: 08 November 2013

For the TRMM overpass event on November 8, 2013, the top row of Figure 3.5 shows SR (a) and GR (b) reflectivity as well as the resulting differences (c) for matching samples at an elevation angle of 0.5°. Each circle in the plots represents a matched volume. A corresponding map of Q_{BBF} is shown in (d) while (e) shows a scatter plot of GR versus SR reflectivities, with points coloured according to their Q_{BBF}. The reflectivity difference map and scatter plot indicate significant variability with absolute differences of up to and exceeding 10 dB. Large differences can be observed at the edges of the southern sector affected by beam blockage (cf. also Figure 3.2). Major parts of that sector did not receive any signal due to total beam blockage, highlighted in Figure 3.5a with black circles showing the bins where the GR did not obtain valid observations. At the edges, however, partial beam blockage caused substantially lower GR reflectivity values. As expected, large negative differences of Z_{GR}–Z_{SR} are characterized by low quality.

Consequently, the estimate of the calibration bias substantially depends on the consideration of partial beam blockage (or quality). Ignoring quality (simple mean) yields a bias estimate of -1.9 dB while the quality-weighted average yields a bias estimate of -1.2 dB. Accordingly, the standard deviation is reduced from 3.4 to 2.6 dB, indicating a more precise bias estimate.

This case demonstrates how partial beam blockage affects the estimation of GR calibration bias. At a low elevation angle, substantial parts of the sweep are affected by *total* beam blockage. The affected bins are either below the detection limit, or they do not exceed the GR threshold specified in Table 3.2. As a consequence, these bins will not be considered in the matched samples and will thus not influence the bias estimate, irrespective of using partial beam blockage as a quality filter. At a higher elevation angle, though, the same bins might not be affected by *total* beam blockage, but by *partial* beam blockage, as also becomes obvious from Figure 3.2. Considering these bins in the matched samples will cause a systematic error in the estimate of calibration bias, unless we use the partial beam blockage fraction as a quality filter by computing a quality-weighted average of reflectivity. As a consequence, the effect of quality-weighted averaging (with partial beam blockage fraction as a quality variable) can be most pronounced at "intermediate" elevation angles, depending on the specific topography and its location with respect to the ground.

The effect becomes obvious for the next elevation angle. Figure 3.6 is equivalent to Figure 3.5, but for an elevation angle of 1.5°: as the sector of total beam blockage shrinks at that elevation, the impact of partial beam blockage on the estimation of GR calibration bias increases. For an antenna elevation of 1.5°, some bins in areas of partial beam blockage have very large negative biases (over 20 dB). Ignoring beam blockage for this elevation angle yields a bias estimate of -2.1 dB (simple mean), while the quality-weighted average yields a bias of -1.4 dB. At the same time, considering quality

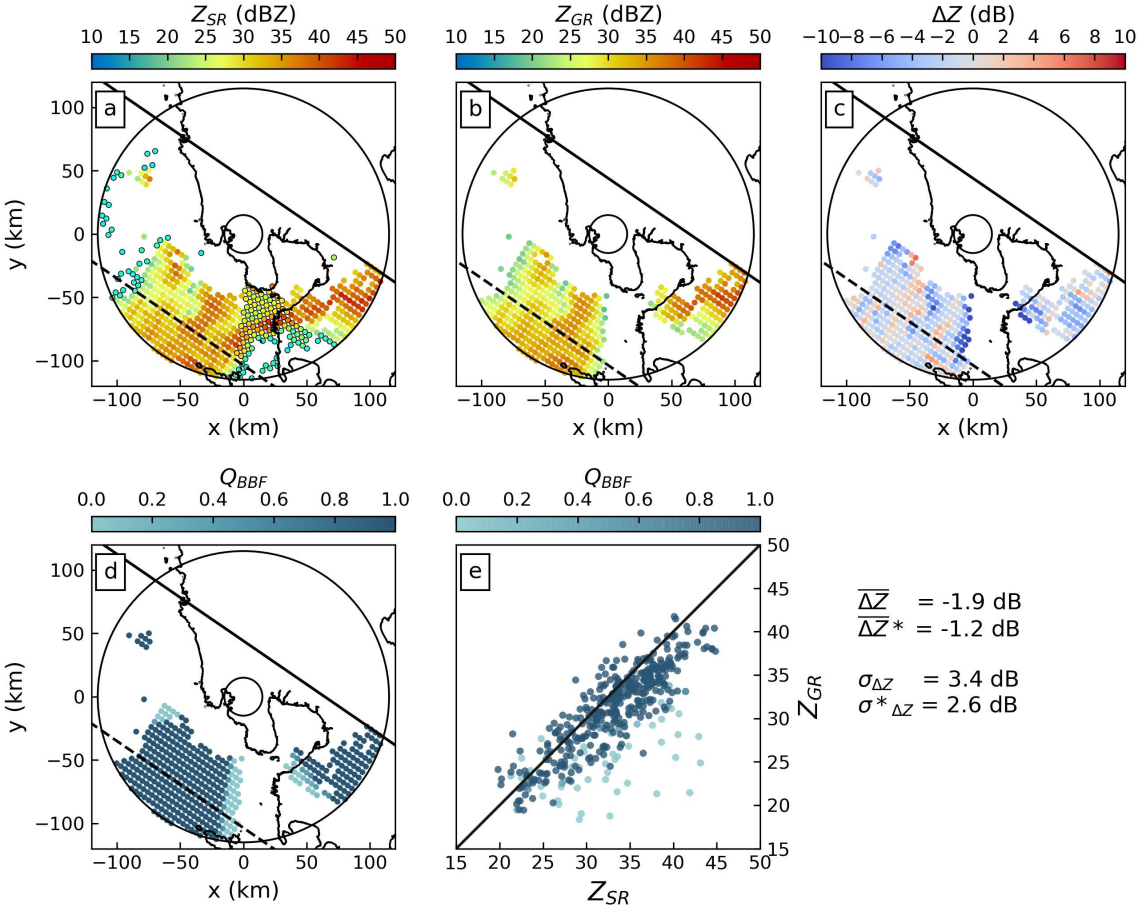

Figure 3.5: GR-centered maps of volume-matched samples from 8 November 2013 at 0.5° elevation angle of (a) SR reflectivity, (b) GR reflectivity, (c) difference between GR and SR reflectivities, and (d) Q_{BBF}. (e) Scatter plot of Z_{GR} versus Z_{SR} where each point is coloured based on the data quality (Q_{BBF}). The solid line in (a)–(d) is the edge of the SR swath, the other edge lies outside the figure. The dashed line denotes the central axis of the swath. The solid concentric circles demarcate the 15 km and 115 km ranges from the radar. In (a) observations that are present in the SR data but not detected by the GR are encircled in black. The mean brightband is at a height of 4685 meters.

substantially reduces the standard deviation from 3.4 dB to 2.1 dB.

Case 2: 01 October 2015

The second case confirms the findings in the previous section for a GPM overpass on October 1, 2015. That overpass captured an event in the northern and eastern part of the radar coverage where partial beam blockage is dominant, as well as a small part of the southern sector with partial and total beam blockage. Figure 3.7 shows the results of that overpass in analogy to the previous figures, for an antenna elevation of 0.0°. The figure shows a dramatic impact of partial beam blockage, with a dominant contribution from the northern part, but also clear effects from the eastern and southern sectors. The scatter plot of Z_{GR} over Z_{SR} in Figure 3.7e demonstrates how the consideration of partial beam blockage increases the consistency between GR and SR observations and allows for a more reliable estimation of the GR calibration bias: ignoring partial beam blockage (simple mean) yields a bias of -2.7 dB, while the quality-weighted average bias is -1.1 dB. Taking into account quality decreases the standard deviation from 3.8 dB to 2.7 dB.

3.4.2 Overall June–November comparison during the 5-year observation period

Finally, we applied both the simple and quality-weighted mean bias estimations to each of the TRMM and GPM

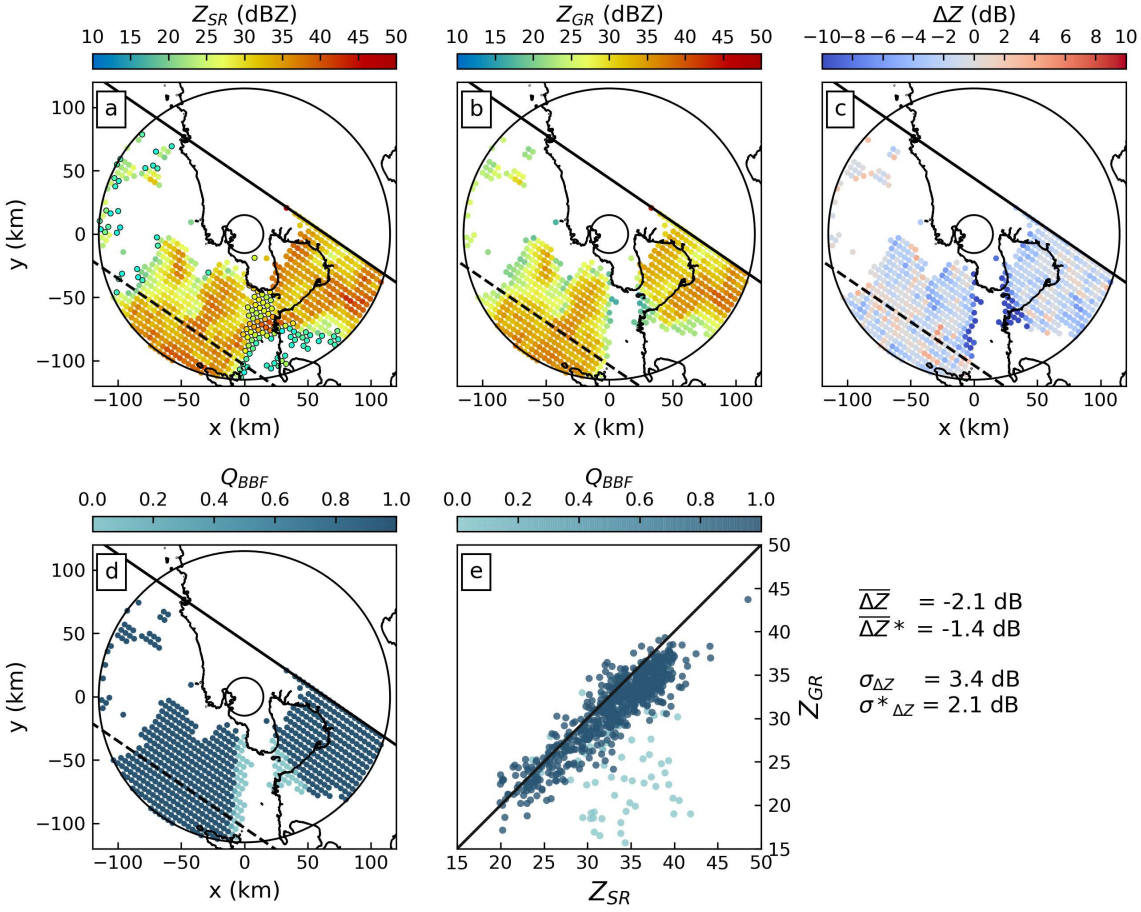

Figure 3.6: Same as in Figure 3.5 but for 1.5° elevation angle.

overpasses from 2012 to 2016 that met the criteria specified in Section 3.3.2, Table 3.2. As pointed out in Section 3.3.2, the matching procedure itself is carried out per GR sweep, i.e. separately for each antenna elevation angle.

As a result, we obtain a time series of bias estimates for GR calibration, as shown in Figure 3.8. In this figure, the calibration bias for each overpass is computed from the full GR volume, i.e. including matched samples from all available antenna elevations. In the upper panel (a), each marker represents the quality-weighted mean bias for a specific SR overpass (circles for GPM, triangles for TRMM). The centre panel (b) highlights the differences between the quality-weighted and simple mean approaches, by quantifying the effect of taking into account GR data quality (in this case, partial beam blockage). The bottom panel (c) shows the differences between the quality-weighted standard deviation and the simple standard deviation of differences, illustrating how taking into account GR quality affects the precision of the bias estimates.

The time series provide several important insights.

(1) **Effect of quality-weighting on bias estimation**. Figure 3.8b and c together illustrate the benefit of taking into account GR data quality (i.e. beam blockage) when we estimate GR calibration bias. It does not come as a surprise that the difference between ΔZ^* and ΔZ is mostly positive because the areas suffering from partial beam blockage register weaker signals (i.e. lower reflectivity) than expected, producing a lower mean bias. Giving the associated volume-matched samples low weights in the calculation of the mean bias brings the quality-weighted bias up. In the same vein, the beam-blocked bins introduce scatter, and assigning them low weights decreases the standard deviation. Figure 3.8c shows, as a consequence, that the quality-weighted bias estimates are consistently more precise: in the vast majority of overpasses, the quality-weighted standard deviation is substantially smaller than the simple standard deviation. That result is also consistent with the case study result shown above. It should be noted, though, that for some overpasses, the quality-weighting procedure (which is in effect a filtering) can

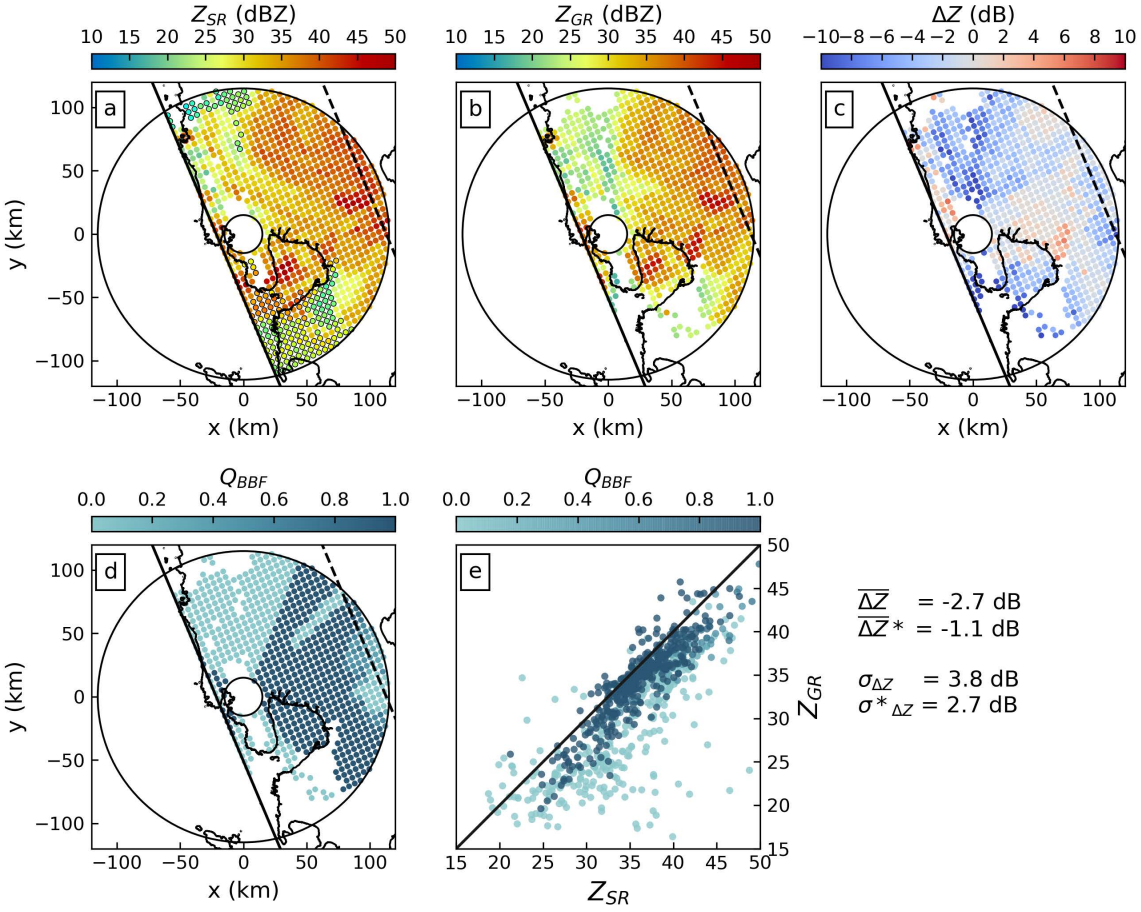

Figure 3.7: As in Figure 3.5 but for the overpass on 01 October 2015. The mean brightband level is found at 4719 meters for this case.

cause an increase in the bias estimate and/or the standard deviation of that estimate. That effect occurs for overpasses with particularly low numbers of matched samples, and, presumably, with rainfall in regions in which our estimated beam blockage fraction is subject to higher errors (caused by e.g. the inadequateness of the assumed Gaussian antenna pattern, variability of atmospheric refractivity, or errors related to the DEM, its resolution and its interpolation to ground radar bins). In total, however, the effect of decreasing standard deviation vastly dominates.

(2) **GPM and TRMM radars are consistent**. In 2014, both TRMM and GPM overpasses are available. That period of overlap shows that the GR calibration bias estimates that are based on both TRMM and GPM observations can be considered homogeneous. Using TRMM data, the average calibration bias for all 2014 overpasses amounts to 1.6 $\pm$ 1.3 dB, while using the GPM overpasses yields a bias of 1.8 $\pm$ 1.5 dB. The difference between TRMM version 7 and GPM version 5 reflectivities mentioned in Section 3.2.1 falls within the uncertainties in the annual estimated mean bias, which makes us confident that the substantial year-to-year changes in our bias estimates are based on changes in GR calibration.

(3) **Change in bias over time**: Despite the variability of bias estimates between the individual overpass events, the time series still provides us with a clear signal: the bias estimates appear to fluctuate around an average value that appears to be quite persistent over the duration of the corresponding wet seasons of the different years, i.e. over intervals of several months. Considering the average calibration bias over the different wet seasons (horizontal lines in Figure 3.8a), we can clearly observe changes in calibration bias over time. The bias was most pronounced in 2012 and 2013, with average bias estimates around -4.1 dB for 2012 and -2.5 dB for 2013. For 2014, the absolute calibration bias was much smaller, at a level of 1.4 dB, while for 2015 and 2016, the situation improved further, with an average bias of 0.0 dB in 2015 and 0.6 dB in 2016. It is important to note that these values were computed as the average bias and

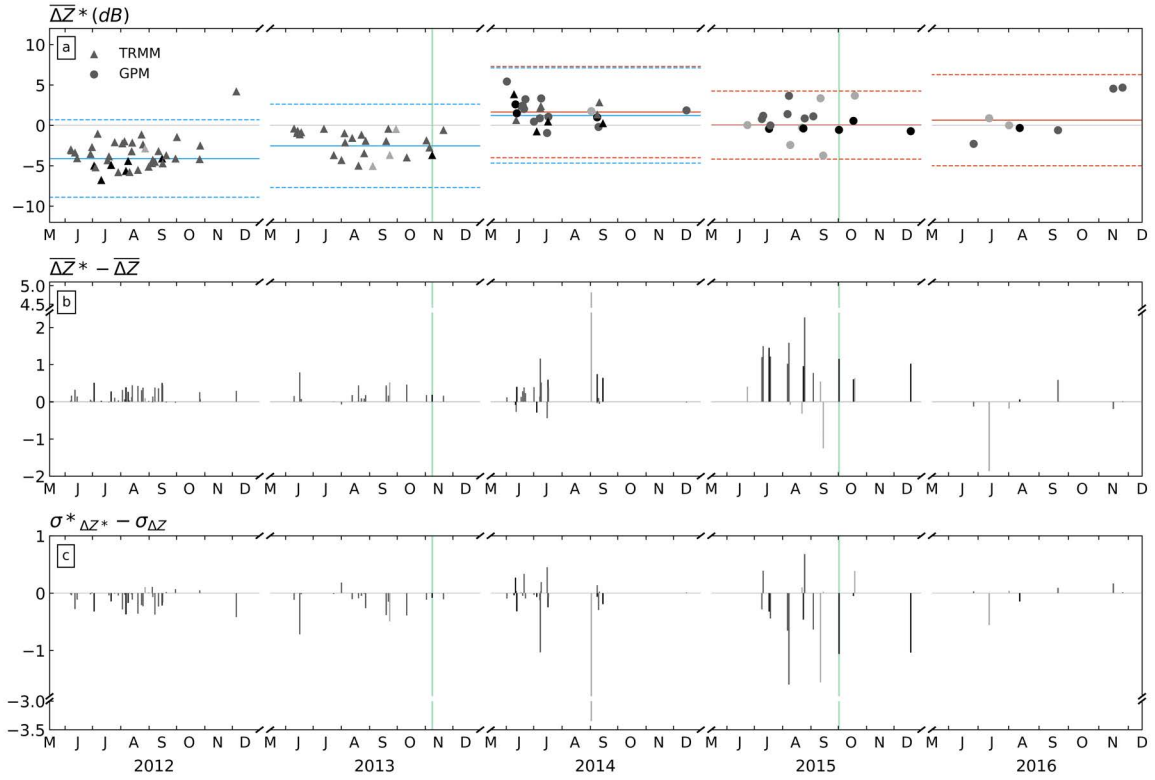

Figure 3.8: (a) Time series of the weighted mean bias (ΔZ^*) from 2012 to 2016. Analysis covers only the wet season from June to December. Triangle markers represent TRMM overpasses while circle markers are GPM overpasses. Symbols are coloured according to the number of volume-matched samples on a logarithmic scale: light grey: 10–99, medium grey: 100–999, and black: 1000+. Blue and orange solid (dashed) horizontal lines represent the weighted average (standard deviation) of *all* individual matched samples within the year for TRMM and GPM, respectively. (b) The difference between the weighted mean biases (ΔZ^*) and the simple mean biases (ΔZ). (c) The standard deviation of the weighted mean bias minus the standard deviation of the simple mean bias values. The green vertical lines indicate the dates of the two case studies.

its standard deviation across all matched volumes and not as the average of bias estimates across overpasses. Accordingly, the standard deviation (as indicated by the dashed lines) is quite high since it includes all the scatter from the individual overpasses. We have to assume that a fundamental issue with regard to calibration maintenance was addressed between 2013 and 2014 in the context of hardware changes (i.e. replacement of magnetron). Unfortunately, we were not able to retrieve detailed information on maintenance operations that might explain the changes in bias of the radar throughout the years.

(4) **Short-term variability of bias estimates between overpasses**. There is a strong variability of the estimated calibration bias between overpasses (Figure 3.8a) and spatially within each overpass (Figures 3.5 to 3.7). That variability is clearly not a desirable property, as we would not expect changes in calibration bias to occur at the observed frequency, amplitude, and apparent randomness. As a consequence, we have to assume that the variability is a cumulative result of various and dynamic sources of uncertainty along the entire process of observation, product generation, matching, and filtering. That assumption is well in line with many other studies (such as Anagnostou et al. (2001); Durden et al. (1998); Joss et al. (2006); Kim et al. (2014); Meneghini et al. (2000); Rose and Chandrasekar (2005); Schwaller and Morris (2011); Seto and Iguchi (2015); Wang and Wolff (2009); Warren et al. (2018), to name only a few) which discuss e.g. fundamental issues with the backscattering model for different wavelengths and sampling volumes; the uncertainty of beam propagation subject to fluctuations in atmospheric refractivity; residual errors in the geometric intersection of the volume samples; uncertainties in SR reflectivity subject to the effects of attenuation correction at Ku-band, non-uniform beam filling and undesirable synergies between the two; rapid dynamics in backscattering target during

the time interval between SR overpass and GR sweep; effects of non-meteorological echoes for both SR and GR; and, presumably, also short-term hardware instabilities. Considering these uncertainties, together with the fact that the quality-weighting in our case study explicitly accounts for beam blockage only, the short-term variability becomes plausible. However, it is beyond the scope of this study to disentangle the sources of this variability.

3.5 Conclusions

In 2011, Schwaller and Morris presented a new technique to match spaceborne radar (SR) and ground-based radar (GR) reflectivity observations, with the aim to determine the GR calibration bias. Our study extends that technique by an approach that takes into account the quality of the ground radar observations. Each GR bin was assigned a quality index between 0 and 1, which was used to assign a quality value to each matched volume of SR and GR observations. For any sample of matched volumes (e.g. all matched volumes of one overpass, or a combination of multiple overpasses), the calibration bias can then be computed as a quality-weighted average of the differences between GR and SR reflectivity in all samples. We exemplified that approach by applying a GR data quality index based on the beam blockage fraction, and we demonstrated the added value for both TRMM and GPM overpasses over the 115 km range of the Subic S-band radar in the Philippines for a 5-year period.

Although the variability of the calibration bias estimates between overpasses is high, we showed that taking into account partial beam blockage leads to more consistent and more precise estimates of GR calibration bias. Analyzing 5 years of archived data from the Subic S-band radar (2012–2016), we also demonstrated that the calibration standard of the Subic radar substantially improved over the years, from bias levels of around -4.1 dB in 2012 to bias levels of around 1.4 dB in 2014 and settling down to a bias of 0.6 dB in 2016. Of course, more recent comparisons with GPM are needed to verify that this level of accuracy has been maintained. Case studies for specific overpass events also showed that the necessity to account for partial beam blockage might even increase for higher antenna elevations. That applies when sectors with total beam blockage (in which no valid matched volumes are retrieved at all) turn into sectors with partial beam blockage at higher elevation angles.

Considering the scatter between SR and GR reflectivity in the matched volumes of one overpass (see case studies), as well as the variability of bias estimates between satellite overpasses (see time series), it is obvious that we do not yet account for various sources of uncertainties. Also, the simulation of beam blockage itself might still be prone to errors. Nevertheless, the idea of the quality-weighted estimation of calibration bias presents a consistent framework that allows for the integration of any quality variables that are considered important in a specific environment or setting. For example, if we consider C-band instead of S-band radars, path-integrated attenuation needs to be taken into account for the ground radar, and wet radome attenuation probably as well (Austin, 1987; Merceret and Ward, 2000; Villarini and Krajewski, 2010). The framework could also be extended by explicitly assigning a quality index to SR observations, too. In the context of this study, that was implicitly implemented by filtering the SR data, e.g. based on brightband membership. An alternative approach to filtering could be weighting the samples based on their proximity to the brightband, the level of path-integrated attenuation (as e.g. indicated by the GPM 2AKu variables *pathAtten* and the associated reliability flag (*reliabFlag*)) or the prominence of non-uniform beam filling (which could e.g. be estimated based on the variability of GR reflectivity within the SR footprint; see e.g. Han et al. (2018)).

In addition, with the significant effort devoted to weather radar data quality characterization in Europe (Michelson et al., 2005), and the number of approaches in determining an overall quality index based on different quality factors (Einfalt et al., 2010), it is straightforward to extend the approach beyond beam blockage fraction.

Despite the fact that there is still ample room for improvement, our tool that combines SR–GR volume matching and quality-weighted bias estimation is readily available for application or further scrutiny. In fact, our analysis is the first of its kind that is entirely based on open-source software, and is thus fully transparent, reproducible, and adjustable (see also Heistermann et al. (2014)). Therefore this study, for the first time, demonstrates the utilization of wradlib functions that have just recently been implemented to support the volume matching procedure and the simulation of partial beam blockage. We also make the complete workflow available together with the underlying ground and spaceborne radar data. Both code

and results can be accessed at the following repository `https://github.com/wradlib/radargpm-beamblockage` upon the publication of this paper.

Through these open-source resources, our methodology provides both research institutions and weather services with a valuable tool that can be applied to monitor radar calibration, and—perhaps more importantly—to quantify the calibration bias for long time series of archived radar observations, basically beginning with the availability of TRMM radar observations in December 1997.

Acknowledgements

The radar data for this analysis were provided by the Philippine Atmospheric, Geophysical and Astronomical Services Administration (PAGASA, http://pagasa.dost.gov.ph). The study was also funded by the German government through the German Academic Exchange Service (https://www.daad.de/en/). We would like to thank Daniel Michelson, Marco Gabella, and one anonymous referee for their valuable insights and comments that significantly improved the paper.

Chapter 4

Using ground radar overlaps to verify the retrieval of calibration bias estimates from spaceborne platforms

This chapter is submitted as:

Crisologo, I. and Heistermann, M.: Using ground radar overlaps to verify the retrieval of calibration bias estimates from spaceborne platforms, Atmospheric Measurement Techniques, submitted.

Abstract

Many institutions struggle to tap the potential of their large archives of radar reflectivity: these data are often affected by miscalibration, yet the bias is typically unknown and temporally volatile. Still, relative calibration techniques can be used to correct the measurements a posteriori. For that purpose, the usage of spaceborne reflectivity observations from the Tropical Rainfall Measuring Mission (TRMM) and Global Precipitation Measurement (GPM) platforms has become increasingly popular: the calibration bias of a ground radar is estimated from its average reflectivity difference to the spaceborne radar (SR). Recently, Crisologo et al. (2018) introduced a formal procedure to enhance the reliability of such estimates: each match between SR and GR observations is assigned a quality index, and the calibration bias is inferred as a quality-weighted average of the differences between SR and GR. The relevance of quality was exemplified for the Subic S-band radar in the Philippines which is much affected by partial beam blockage.

The present study extends the concept of quality-weighted averaging by accounting for path-integrated attenuation (PIA), in addition to beam blockage. This extension becomes vital for radars that operate at C- or X-band. Correspondingly, the study setup includes a C-band radar which substantially overlaps with the S-band radar. Based on the extended quality-weighting approach, we retrieve, for each of the two ground radars, a time series of calibration bias estimates from suitable SR overpasses. As a result of applying these estimates to correct the ground radar observations, the consistency between the ground radars in the region of overlap increased substantially. Furthermore, we investigated if the bias estimates can be interpolated in time, so that ground radar observations can be corrected even in the absence of prompt SR overpasses. We found that a moving average approach was most suitable for that purpose, although limited by the absence of explicit records of radar maintenance operations.

4.1 Introduction

Weather radar observations are the key to quantitative precipitation estimation (QPE) with large spatial coverage and at high resolution in space and time (in the order of $10^2 - 10^3$ meters, and $10^0 - 10^1$ minutes). Yet, the indirect nature of the precipitation retrieval paves the way for a multitude of systematic estimation and measurement errors. The *estimation errors* (in the retrieval of the precipitation rate R from the radar's prime observational target variable, the radar reflectivity factor Z) is caused mainly by the unknown microphysical properties of the target—let it be meteorological or non-meteorological. Before that, *measurement errors* affect the observation of Z through a multitude of mechanisms that can accumulate as the beam propagates through the atmosphere (such as beam blockage, or path-integrated attenuation). On top, the prominence of these measurement errors heavily depends on scenario-specific interaction of factors such as radar bandwidth, beam width, obstacles in the direct and

wider vicinity, topography in the radar coverage, atmospheric refractivity, or the microphysical properties of precipitation along the beam's propagation path. Much has been written about these sources of uncertainty, and much has been done to address them adequately (see Villarini and Krajewski (2010) for an extensive review).

Yet, the single-most contribution of uncertainty to radar-based QPE often comes, maybe surprising to some, from the (mis)calibration or (in)stability of the radar instrument itself (Houze et al., 2004) which can also vary in time (Wang and Wolff, 2009). Apart from the simple fact that miscalibration can easily deteriorate the accuracy of precipitation estimates by an order of magnitude, calibration issues become particularly annoying if weather radars are operated in a network where the consistency of calibration between radars is a prerequisite for high-quality radar mosaics (see e.g. Seo et al. (2014)).

There are various options to carry out and monitor the calibration of a radar instrument in an operational context through absolute calibration techniques (based on a well-defined reference noise source, see Doviak and Zrnić (2006) for an overview). Yet, to the reflectivity that is already measured and recorded, any changes to the instrument's calibration are irrelevant. In such a case, relative calibration techniques can be used to correct the measurements a posteriori. Many institutions have archived massive radar reflectivity records over the years, but they struggle to tap the potential of these data due to unknown and temporally volatile calibration biases. And while radar polarimetry offers new opportunities to address calibration issues, many archived data still originate from single-polarization radars.

As to relative calibration, the usage of rain gauge observations is typically not recommended, not only due to issues of representativeness in space and time, but also due to the fact that a comparison between R, as observed by rain gauges, and R, as retrieved from radar reflectivities, lumps over measurement *and* estimation uncertainties. As an alternative, the usage of spaceborne reflectivity observations from the Tropical Rainfall Measuring Mission (TRMM) and Global Precipitation Measurement (GPM) platforms has become increasingly popular over the recent years. Measurement accuracies of both TRMM and GPM are reported to have excellent calibration (within < 1dB) (Kawanishi et al., 2000; Hou et al., 2013), and thus can be used as a reference to calibrate reflectivity. Moreover, a major benefit of relative calibration is that it allows for a posteriori correction of historical data.

In a recent study for an S-band radar in the Philippines, Crisologo et al. (2018) adopted a technique to match ground radar (GR) and spaceborne radar (SR) observations. That technique was originally suggested by Bolen and Chandrasekar (2003), then further developed by Schumacher and Houze Jr (2003), and finally by Warren et al. (2018). The underlying idea of that technique is to match observations based on the geometric intersection of SR and GR beams. That way, the algorithm confines the comparison to locations where both instruments have valid observations, and avoids artefacts from interpolation or extrapolation. In that context, Crisologo et al. (2018) demonstrated that explicitly taking into account the quality of the GR observations is vital to enhance the consistency between SR and GR reflectivity measurements, and thus to estimate the calibration bias more reliably. The relevance of quality was exemplified by considering partial beam blockage: for each GR bin, a quality index between 0 and 1 was inferred from the beam blockage fraction. These quality indices were then used to compute a quality-weighted average of volume matched GR reflectivities.

The present study aims to extend the approach of Crisologo et al. (2018) in several respects:

1. We extend the framework to account for the quality of GR observations by introducing path integrated attenuation (PIA) as a quality variable, in addition to partial beam blockage. Instead of attempting to correct GR reflectivities for PIA, we explicitly acknowledge the uncertainty of any PIA estimate by assigning a low weight to any GR bins that are substantially affected by PIA. In order to investigate the role of PIA, we include a C-band weather radar in the present study, in addition to the S-band radar included by Crisologo et al. (2018).

2. We verify the ability to estimate the GR calibration bias from SR overpass data by evaluating the consistency of GR reflectivity measurements in a region of overlap, before and after bias correction.

3. We investigate whether estimates of GR calibration bias, as obtained from SR overpass data, can be interpolated in time in order to correct GR reflectivity observations for miscalibration, even for those times in which no suitable SR overpasses were available.

The latter item—the interpolation of bias estimates in time—would be a key requirement towards actually tapping the potential of the fundamental concept in research and applications: if we aim to use SR overpass data for monitoring GR calibration bias, and for a homogeneous correction of archived GR reflectivities, we have to assume that those bias estimates are, to some extent, representative in time. Crisologo et al. (2018) found that the bias estimates for the Subic S-band radar exhibited a substantial short-term temporal variability, and stated that they *"would not expect changes in calibration bias to occur at the observed frequency, amplitude, and apparent randomness."* By investigating whether such bias estimates can be interpolated in time, the present paper will investigate whether the apparently "volatile" behaviour of calibration bias is not a mere artefact of the estimation procedure, but a real property of the investigated radar systems.

Section 4.2 of the present paper will describe the study area and the underlying radar data sets; section 4.3 will outline the methodologies of matching GR and SR as well as GR and GR observations, the quantification of beam blockage and PIA, and the quality-based framework for bias estimation; in section 4.4, we will show and discuss the various inter-comparison results; and section 4.5 will conclude.

4.2 Data and Study Area

The Philippine Atmospheric, Geophysical, and Astronomical Services Administration (PAGASA), the country's weather agency, maintains a network of 10 ground radars all over the country, of which 8 are single-polarization S-Band radars and 2 are dual-polarization C-Band radars. Two of the longest running radars are Subic and Tagaytay. Between the two radars lies Manila Bay, bordered on the east by Metro Manila, the country's most densely populated area at approximately 13 Million inhabitants. This region of overlap regularly experiences torrential rains from monsoon and typhoons extending for several days (Heistermann et al., 2013a; Lagmay et al., 2015).

4.2.1 Subic radar (SUB)

The Subic radar is a single-polarization S-band radar situated on top of a hill at 532 m a.s.l. in the municipality of Bataan (location: 14.82°N, 120.36°E) (see Figure 4.1). To its north lies the Zambales Mountains (highest peak: 2037 m a.s.l.) and to its south stands Mt. Natib (1253 m a.s.l.). The Sierra Madre Mountains run along the eastern part of the Luzon Island, at the far-east end of the radar coverage. Technical specifications are available in Table 4.1. Please note that Subic sweeps at 1.5 and 2.4 degree elevation were excluded for the years 2013 and 2014, due to apparently erratic and inconsistent behaviour.

4.2.2 Tagaytay radar (TAG)

Located about 100 km across the Manila Bay from the Subic radar is the Tagaytay radar, a dual-polarized C-Band radar. It sits along the Taal Volcano caldera ridge at 752 m a.s.l. in the municipality of Batangas. The radar coverage also includes the southern part of the Sierra Madre Mountains. Technical specifications are available in Table 4.1.

Data during the rainy seasons of 2012–2014 and 2016 are used in this study. The scanning setup for Tagaytay was experimentally changed during 2015 and reverted back in 2016. In order to ensure homogeneity in the GR intercomparison, we excluded the year 2015 from the analysis.

4.2.3 Spaceborne precipitation radar

Spaceborne radar data were collected from TRMM 2A23 and 2A25 version 7 (NASA, 2017) for overpass events in 2012–2014, and GPM 2AKu version 5A products (Iguchi et al., 2010) from 2014–2016, during the rainy season of June to December. The data were downloaded from NASA's Precipitation Processing System (PPS) through the STORM web interface (https://storm.pps.eosdis.nasa.gov/storm/). The parameters of TRMM/GPM extracted for the analysis are the same as specified in Table 3 of Warren et al. (2018).

4.3 Methods

4.3.1 Overview

We facilitate the comparison of effectively three instruments: the two ground radars and the spaceborne radar (see 4.2). While throughout the study period, the available spaceborne radar platform changed from TRMM (2012–2014) to GPM (2014–2016), the consistency between the two for the year 2014 for the study area (Crisologo et al., 2018) allows us to consider the two rather as a single reference instrument. The comparison of the three platforms has two main components:

1. The SR–GR comparison is motivated by the **estimation of the GR calibration bias**. We define that bias as the mean difference ($\overline{\Delta Z}_{SR-SUB}$ or

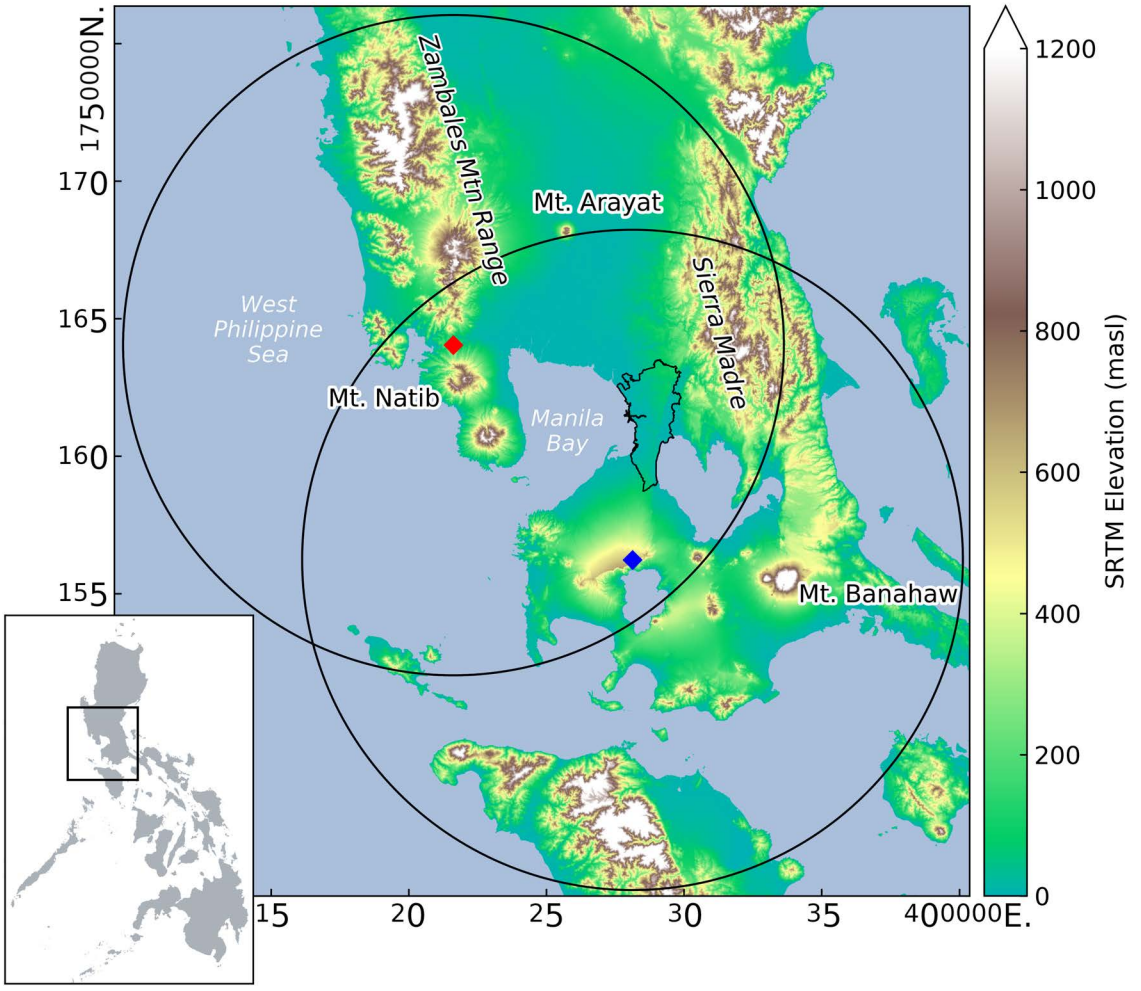

Figure 4.1: Locations of the Subic (red diamond) and Tagaytay (blue diamond) radars showing the 120 km range with the region of overlap. Metropolitan Manila is outlined in black beside Manila Bay. The relative location of the study area with respect to the Philippines is shown in the inset.

$\overline{\Delta Z}_{SR-TAG}$, in dBZ) between SR and GR, assuming SR to be a well-calibrated reference. As shown by Crisologo et al. (2018), we can improve the bias estimation if we give a lower weight to those matched samples which we assume to be affected by a systematic GR measurement error. Please note that we use the term c*alibration bias* throughout the paper, as it is more commonly used. Strictly speaking, though, it is rather an *"instrument bias"* that lumps over any systematic effects of calibration and instrument stability along the radar receiver chain.

2. The GR–GR comparison is motivated by the evaluation of the **consistency between the two ground radars**. For that purpose, we can consider the mean difference ($\overline{\Delta Z}_{TAG-SUB}$) between the two ground radars (in dBZ) and the standard deviation of the differences ($\sigma(\Delta Z_{TAG-SUB})$, in dBZ). The differences in the region of overlap of two error-free ground radars would have a mean and a standard deviation of zero. Different levels of miscalibration of the two ground radars would increase the absolute value of the mean difference (which, in turn, implies that the mean difference would be zero if both GR were affected by the same level of miscalibration). But what about systematic measurement errors that are spatially heterogeneous in the region of overlap (such as beam blockage or PIA)? Although they could also affect the mean difference, we expect them to particularly increase the standard deviation of the differences. Hence, a removal of spatially heterogeneous measurements errors from both GRs

Table 4.1: Technical specifications of Subic and Tagaytay Radar.

	Subic Radar	Tagaytay Radar
Bandwidth	S-Band	C-Band
Polarization	Single-pol	Dual-pol
Position (lat/lon)	14.822°N 120.363°E	14.123°N 120.974°E
Altitude	532 m a.s.l.	752 m a.s.l.
Maximum Range	120 km	
Azimuth Resolution	1 °	
Gate length	500 m	
Number of elevation angles	14	
Elevation angles	0.5°, 1.5°, 2.4°, 3.4°, 4.3°, 5.3°, 6.2°, 7.5°, 8.7°, 10°, 12°, 14°, 16.7°, 19.5°	
Volume cycle interval	8 minutes	15 minutes
Start of operation	2012	2012

would reduce $\sigma(\Delta Z_{TAG-SUB})$, while a correction of calibration bias of both GRs would reduce the absolute value of$(\overline{\Delta Z}_{TAG-SUB})$. And while we admit that neither $(\overline{\Delta Z}_{TAG-SUB})$ nor $\sigma(\Delta Z_{TAG-SUB})$ could be considered *imperative* measures of reliability of any of the two ground radars, we still assume that any decrease in their absolute values would raise our confidence in any of the two radars' reflectivity observations.

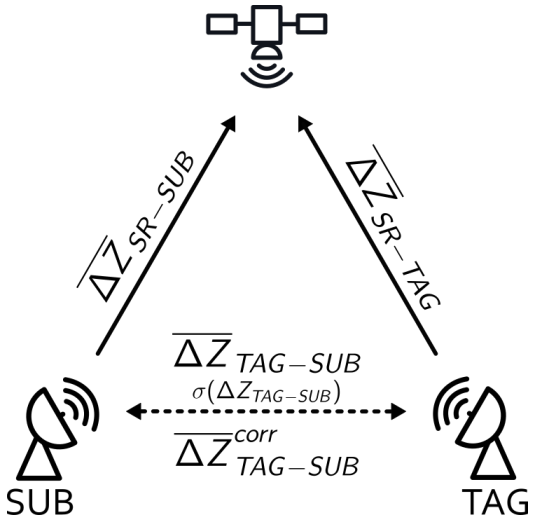

Figure 4.2: Schematic diagram of the SR–GR calibration bias estimation and GR–GR intercomparison. The SUB and TAG calibration biases ($\overline{\Delta Z}_{SR-SUB}$ and $\overline{\Delta Z}_{SR-TAG}$, respectively) are calculated with respect to SR, and used to correct the ground radar reflectivities. The mean difference between SUB and TAG radars are calculated before $(\overline{\Delta Z}_{TAG-SUB})$ and after bias correction $(\overline{\Delta Z}^{corr}_{TAG-SUB})$

4.3.2 SR–GR matching

To determine the calibration bias of each radar, we employ the relative calibration approach by using the spaceborne-radar (SR) as a reference. In order to avoid introducing errors by interpolation, we use a volume-matching procedure. The 3D geometric matching method proposed by Schwaller and Morris (2011), further developed by Warren et al. (2018), was used to match SR bins to GR bins. This method has been implemented with the Subic radar for the same time period by Crisologo et al. (2018). In this study, we extend it to the TAG radar. Since the two radars are operating under the same scanning strategy and spatial resolution, the thresholds applied in filtering the data are kept the same as in the SR–SUB comparison described in Section 3.2 Table 3 of Crisologo et al. (2018). Details of the SR data specifications and the matching procedure can be found in Crisologo et al. (2018).

4.3.3 GR–GR matching

We compare the reflectivities of both ground radars in the overlapping region to quantify the mean and the standard deviation of their differences, and thus the effectiveness of the quality-weighting and the relative calibration procedure. In order to compare reflectivities from different radars, the different viewing geometries must be carefully considered. The polar coordinates of each radar are transformed into azimuthal equidistant projection coordinates, centered on each radar. Each radar cartesian coordinate is then transformed into the other radar's spherical coordinate system, such that each of the radar bins of the TAG radar have coordinates with respect to the SUB radar, and vice versa.

For this purpose, we use the georeferencing module of the wradlib library (https://wradlib.org) which allows for transforming between any spherical and Cartesian reference systems. Bins of the TAG radar that are less than 120 km away from the SUB radar are chosen. The same is done for bins of the SUB radar. In order to match only bins of similar volume, Seo et al. (2014) suggested a matching zone of 3 km within the equidistant line between the two radars. We decided to make this requirement less strict in order to include more matches, and thus extended this range to 10 km. From the selected bins, each SUB bin is matched with the closest TAG bin, not exceeding 250 m in distance. The matching SUB and TAG bins are exemplarily shown in black in Figure 4.3 for the 0.5° elevation angle, such that each black bin in the SUB row corresponds with a black bin in the TAG row.

4.3.4 Estimation of path-integrated attenuation

Atmospheric attenuation depends on the radar's operating frequency (Holleman et al., 2006). For radar signals with wavelengths below 10 cm (such as C- and X-band radars), significant attenuation due to precipitation can occur (Vulpiani et al., 2006), depending on precipitation intensity (Holleman et al., 2006). In tropical areas such as the Philippines, where torrential rains and typhoons abound, C-band radars suffer from substantial PIA.

In this study, we require PIA estimates as a quality variable to assign different weights of GR reflectivity samples when computing quality-weighted averages of reflectivity (see section 4.3.6). For that purpose, PIA is estimated by using dual-pol moments observed by the TAG radar. The corresponding procedure includes the removal of non-meteorological echoes based on a fuzzy echo classification, and the reconstruction of the differential propagation phase from which PIA is finally estimated. The method is based on Vulpiani et al. (2012), and was comprehensively documented and verified for the TAG radar by Crisologo et al. (2014) which is why we only briefly outline it in the following.

The fuzzy classification of meteorological vs. non-meteorological echoes was based on the following decision variables: the Doppler velocity, the copolar cross-correlation, the textures (Gourley et al., 2007) of differential reflectivity, copolar cross-correlation, and differential propagation phase (Φ_{DP}), and a static clutter map. The parameters of the trapezoidal membership functions as well as the weights of the decision variables are specified in Table 2 of Crisologo et al. (2014). Bins classified as non-meteorological were removed from the beam profile and then filled in the subsequent processing step. In that step, a clean Φ_{DP} profile is reconstructed by removing the effects of wrapping, system offset and residual artifacts. The reconstruction consists of an iterative procedure in which K_{DP} is repeatedly estimated from Φ_{DP} using a convolutional filter, and Φ_{DP} again retrieved from K_{DP} via integration, after filtering spurious and physically implausible K_{DP} values.

According to Bringi et al. (1990), specific attenuation, α_{hh} (dB km^{-1}), is linearly related to K_{DP} by a coefficient γ_{hh} (dB deg^{-1}) which we assume to be constant in time and space with a value of $\gamma_{hh} = 0.08$ (Carey et al., 2000). Hence, the two-way path-integrated attenuation, A_{hh} (dB), can then be obtained from the integral of the specific attenuation along each beam—which is equivalent to our reconstructed Φ_{DP} from which the system offset ($\Phi_{DP}(r_0)$) was removed in the previous step.

$$A_{hh}(s) = 2\int_{r_0}^{r} \alpha_{hh}(s)ds \tag{4.1}$$

$$= 2\gamma_{hh}\int_{r_0}^{r} K_{DP}(s)ds \tag{4.2}$$

$$= \gamma_{hh}(\Phi_{DP}(r) - \Phi_{DP}(r_0)) \tag{4.3}$$

4.3.5 Beam Blockage

In regions of complex topography, the ground radar beam can be totally or partially blocked by topographic obstacles, resulting in weakening or loss of the signal. To simulate the extent of beam blockage for each ground radar, as introduced by topography, we used the algorithm proposed by Bech et al. (2003), together with the Shuttle Radar Topography Mission (SRTM) DEM with a 1 arc-second (approximately 30 m) resolution. The procedure has been documented in Crisologo et al. (2018) in more detail. In summary, the values of the DEM are resampled to the radar bin centroid coordinates to match the polar resolution of the radar data. Then, the algorithm computes the beam blockage fraction for each radar bin by comparing the elevation of the radar beam in that bin with the terrain elevation. Finally, the cumulative beam blockage fraction (BBF) is calculated for all the bins along each ray, where a value of 1.0 corresponds to total occlusion and a value of 0.0 to complete visibility.

4.3.6 Quality index and quality-weighted averaging

The quality index is a quantity used to describe data quality, represented by numbers ranging from 0 (poor quality) to 1 (excellent quality), with the objective of characterizing data quality independent of the source, hardware, and signal processing (Einfalt et al., 2010).

To calculate a quality index for the beam blockage fraction, the transformation function suggested by Zhang et al. (2011) is used:

$$Q_{BBF}=\begin{Bmatrix} 1 & BBF \leq 0.1 \\ 1-\frac{BBF-0.1}{0.4} & 0.1 < BBF \leq 0.5 \\ 0 & BBF > 0.5 \end{Bmatrix} \quad (4.4)$$

Figure 4.3 shows the beam blockage quality index (Q_{BBF}) maps of SUB and TAG for the lowest elevation angle. Subic is substantially affected by beam blockage in the northern and southern sector, due to the radar sitting between two mountains along a mountain range. The southern beam blockage sector of the Subic radar clearly affects the region of overlap with the Tagaytay radar. Meanwhile, TAG has a clearer view towards the north, with only a narrow sector to the east and partially in the south being affected by very high beam blockage. It is not shown in the figure, but the higher elevation angles of the TAG radar are not affected by any beam blockage.

For path-integrated attenuation, the values are transformed into a quality index as

$$Q_{PIA}=\begin{Bmatrix} 1 & \text{for} & K_{r,s} < K_{min} \\ 0 & \text{for} & K_{r,s} > K_{max} \\ \frac{K_{max}-K_{r,s}}{K_{max}-K_{min}} & \text{else,} & \end{Bmatrix} \quad (4.5)$$

following the function proposed by Friedrich et al. (2006), where K_{min} and K_{max} are the lower and upper attenuation thresholds. The values for K_{min} and K_{max} are chosen to be 1 dB and 10 dB.

Multiple quality indices from different quality variables can be combined in order to obtain a single index of total quality. Different combination approaches have been suggested, e.g. by addition or multiplication (Norman et al., 2010), or by weighted averaging (Michelson et al., 2005). We chose to combine Q_{BBF} and Q_{PIA} multiplicatively, in order to make sure that a low value of either of the two propagates to the total quality index ($Q_{GR} = Q_{GR,BBF} * Q_{GR,PIA}$), where Q_{GR} can either be Q_{SUB} or Q_{TAG}.

It should be noted that $Q_{SUB,PIA}$ is always considered to have a value of 1, as we consider attenuation negligible for S-band radars, so that effectively Q_{SUB} = $Q_{SUB,BBF}$.

Based on this quality index Q_{GR}, we follow the quality-weighting approach as outlined in Crisologo et al. (2018). For each match between SR and GR bins, the quality Q_{match} is obtained from the minimum Q_{GR} value of the GR bins in that match. We then compute the average and the standard deviation of the reflectivity differences between SR and GR by using the Qmatch values as linear weights (see Crisologo et al. (2018) for details). We basically follow the same approach when we compute the quality-weighted average and standard deviation of the differences between the two ground radars, SUB and TAG, in the region of overlap. Here, the quality Q_{match} of each match is computed as the product $Q_{SUB} * Q_{TAG}$ of the two matched GR bins.

It should be emphasized at this point that, in the region of overlap, the TAG radar is not affected by beam blockage. So while the computation of calibration bias for the TAG radar, based on SR overpasses, is affected by $Q_{TAG,BBF}$ (as it uses the full TAG domain), the comparison of SUB and TAG reflectivities is, in fact, only governed by $Q_{SUB,BBF}$ and $Q_{TAG,PIA}$.

4.3.7 Computational details

Following the guidelines for transparency and reproducibility in weather and climate sciences as suggested by Irving (2016), we have made the entire processing workflow and sample data available online at `https://github.com/IreneCrisologo/interradar`. The main components of that workflow are based on the open source software library for processing weather radar data called wradlib (Heistermann et al., 2013b), version 1.2 (released on 31.10.2018) based on Python 3.6. The main dependencies of wradlib include Numerical Python (NumPy; Oliphant (2015), Matplotlib (Hunter, 2007), Scientific Python (SciPy; Jones et al. (2014)), h5py (Collette, 2013), netCDF4 (Rew et al., 1989), gdal (GDAL Development Team, 2017), and pandas (McKinney, 2010).

4.4 Results and Discussion

The presentation and discussion of results falls into four parts.

1. In section 4.4.1, we demonstrate the effect of extending the framework of quality-weighting by path-integrated attenuation. This is done by

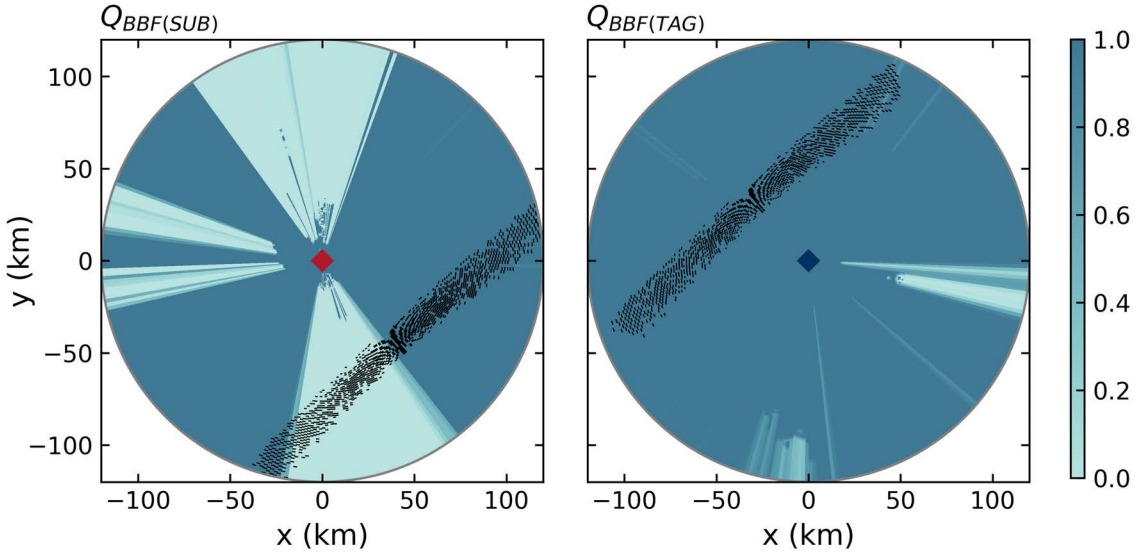

Figure 4.3: The beam blockage quality index (Q_{BBF}) for the two radars is shown in the background for each corresponding elevation angle. Black points show the locations of matched bins between SUB and TAG for each radar coverage, exemplarily for an elevation of 0.5 degree.

analysing the mean and the standard deviation of differences between the two ground radars, SUB and TAG, in different scenarios of quality filtering for a case in December 2014.

2. In section 4.4.2, we construct a time series of calibration bias estimates for the TAG C-band radar by using the extended quality-averaging framework together with spaceborne reflectivity observations from TRMM and GPM overpass events. This time series complements the calibration bias estimates we had already gathered for the SUB S-band radar in Crisologo et al. (2018).

3. In section 4.4.3, we use the calibration bias estimates for SUB and TAG in order to correct the GR reflectivity measurements, and investigate whether that correction is in fact able to reduce the absolute value of the mean difference $\overline{\Delta Z}_{TAG-SUB}$ between the two radars. This analysis is done for events in which we have both valid SR overpasses for both radars and a sufficient number of samples between the two ground radars in the region of overlap.

4. In section 4.4.4, finally, we evaluate different techniques to interpolate the sparse calibration bias estimates in time, attempting to correct ground radar reflectivity observations also for times in which no overpass data is available. The effect of different interpolation techniques is again quantified by the mean difference $\overline{\Delta Z}_{TAG-SUB}$ between the two ground radars.

4.4.1 The effect of extended quality filtering: the case of December 9, 2014

In this section, we demonstrate the effect of extending the quality framework by path-integrated attenuation. In Figure 4.3, we have already seen that the SUB radar is strongly affected by beam blockage in the region of overlap. Yet, as an S-band radar, it is not significantly affected by attenuation. For the TAG radar, it is vice versa: not much affected by beam blockage, yet it will be affected by atmospheric attenuation during intense rainfall. That setting provides an ideal environment to experiment with different scenarios of quality filtering. For such an experiment, we chose a heavy rainfall event on December 9, 2014, where there are sufficient radar bins with precipitation in the region of overlap. The scan times are 06:55:14 and 06:57:58 for the SUB and TAG radars, respectively.

Figure 4.4 shows scatter plots of matched reflectivities in the region of overlap, combining matched GR bins from all elevation angles. Note that in this region of overlap, Q_{SUB} is equivalent to Q_{BBF}, and Q_{TAG} is dominated by Q_{PIA}. To illustrate the individual effects

of the quality indices in the comparison, we simply refer to the dominating quality index instead of the associated radar (i.e. Q_{BBF} for SUB and Q_{PIA} for TAG). The points in the scatter plot are colored depending on the quality index of the corresponding matched sample: in Figure 4.4a, we can see that matches with a very low Q_{BBF} value (i.e. high beam blockage) are concentrated above the 1:1 line, since beam blockage causes the Subic radar to underestimate in comparison to the Tagaytay radar. If we consider each matched sample irrespective of data quality, the mean difference between the two radars is 1.7 dB, with a standard deviation of 8.1 dB. Taking Q_{BBF} into account changes the mean difference to -1.9 dB—which is higher in absolute terms—and decreases the standard deviation to 5.5 dB. Figure 4.4b demonstrates the effect of using only PIA for quality filtering: Points with low Q_{PIA} (i.e. high PIA) are concentrated below the 1:1 line, corresponding to an underestimation of the TAG radar as compared to the SUB radar. Considering only Q_{PIA} for quality-weighting increases the mean difference between TAG and SUB to a value of 3.5 dB, and decreases the standard deviation just slightly to a value of 7.5 dB. By combining the two quality factors, we can reduce the absolute value of $\overline{\Delta Z}_{TAG-SUB}$ from 1.7 dBZ to -0.7 dB, and, more notably, the standard deviation from 8.1 dBZ to 4.6 dBZ (Figure 4.4c). That effect also becomes apparent in Figure 4.4d in which we show how the multiplicative combination of quality factors not only pushes the mean of the differences towards zero, but also narrows down the distribution of differences dramatically.

Remembering item (2) from section 4.3.1, it is the reduction of standard deviation that we are most interested in at this point: it demonstrates that the two GR become more consistent if we filter systematic errors that are spatially heterogeneous in the region of overlap. The low absolute value of the mean difference is, for this case study, not a result of correcting for calibration bias—which is addressed in the following sections.

On the basis of these results, we will, in the following sections, only refer to values of mean and standard deviation of (SR–GR or GR–GR) differences that are computed by means of quality-weighting, with the quality of a matched sample quantified as Q_{match}.

4.4.2 Estimating the GR calibration bias from SR overpass events

In Figure 8a of Crisologo et al. (2018), we had already shown the time series of quality-averaged differences between the SUB ground radar and the SR platforms TRMM and GPM, using beam blockage as a quality variable. Extending the framework for quality-weighted averaging by PIA, we have now computed the corresponding time series of quality-weighted mean differences for the TAG radar. Figure 4.5 shows the time series of calibration biases, as estimated from quality-weighted mean differences, for both SUB and TAG radars for years 2012–2014 and 2016. The first panel corresponds to Figure 8a of Crisologo et al. (2018). For SUB, there is a total of 96 SR overpass events that fit the filtering criteria referred to in Section III.2, while for TAG, we only found 45 matches. Compared to the spaceborne radars, both SUB and TAG are dramatically underestimating at the beginning of operation in 2012, where the underestimation of the TAG radar is even more pronounced. From 2014, the calibration improves for both radars.

As pointed out in Crisologo et al. (2018), there is a strong variability of the estimated calibration biases between overpasses for SUB. This behaviour can be confirmed for the TAG radar, with particularly drastic cases in 2013. Potential causes for this short-term variability have been discussed in Crisologo et al. (2018), and could include, e.g., residual errors in the volume sample intersections, short-term hardware instability, rapid changes in precipitation during the time interval between GR sweep and SR overpass, and uncertainties in the estimation of PIA, to name a few.

4.4.3 The effect of bias correction on the GR consistency: case studies

In this and the following section, we evaluate the effect of using the calibration bias estimates obtained from SR overpasses to actually correct the GR reflectivity measurements. We start, in this section, by analysing events in which we have both: valid SR overpass events for SUB and TAG, as well as a sufficient number of matched GR samples in the region of overlap. That way, we can directly evaluate how an "instantaneous" estimate of the GR calibration bias estimates affects the GR consistency, as explained in item (2) of section 4.3.1. In contrast to section 4.4.1, in which we focused on the standard deviation of differences between the two ground radars, we now focus on the mean differences in order to capture the effect of bias correction.

The first case is a particularly illustrative example: an extreme precipitation event that took place right in the region of overlap at a time in which both radars, SUB and TAG, apparently were affected by massive miscalibration, according to Figure 4.6 the so-called

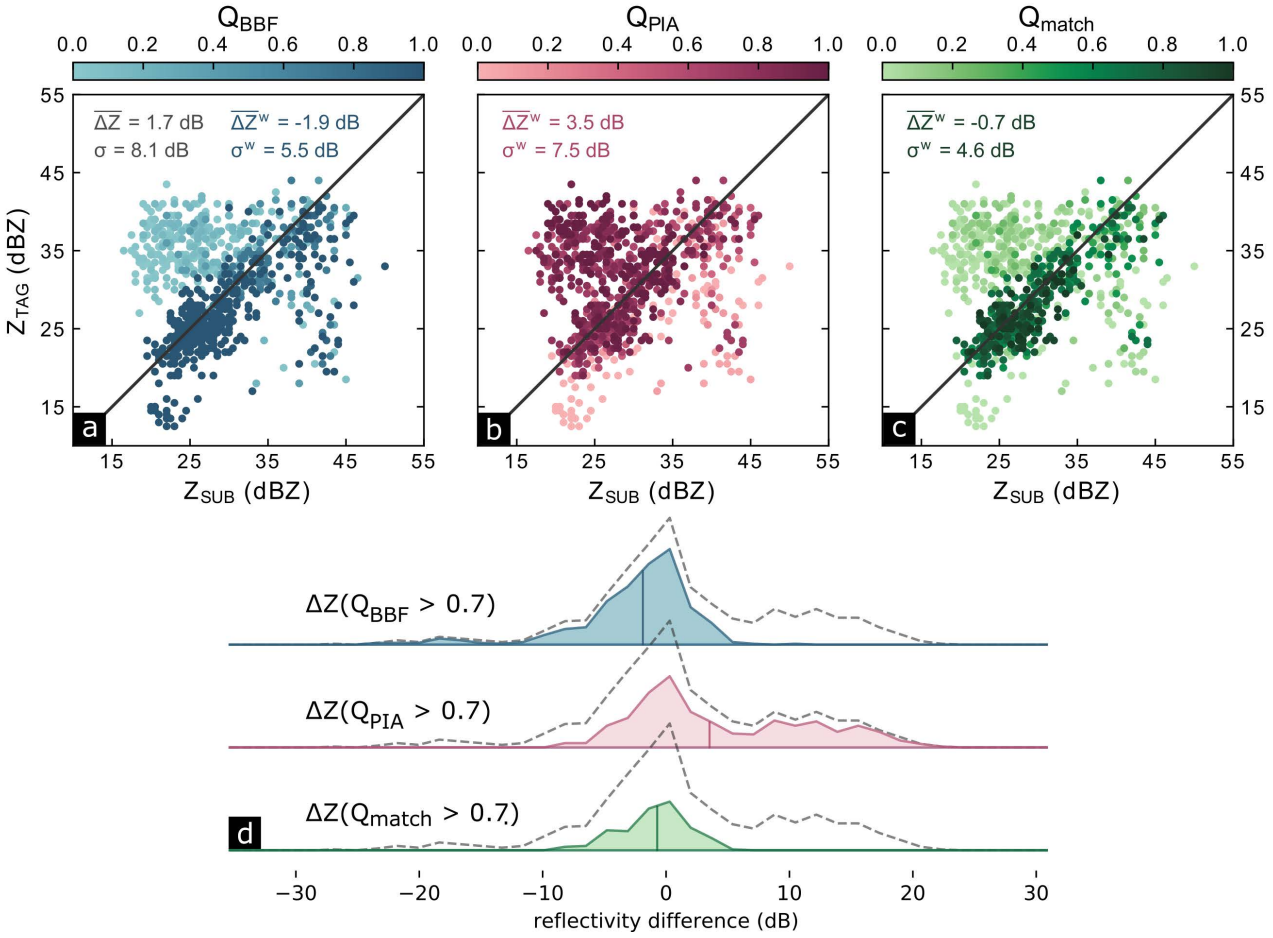

Figure 4.4: Scatter plot of reflectivity matches between Tagaytay and Subic radars. The marker color scale represents the data quality based on (a) beam blockage fraction (Q_{BBF}), (b) path-integrated attenuation (Q_{PIA}), and (c) the multiplicative combination of the two (Q_{match}), where the darker colors denote high data quality and lighter colors signify low data quality. The ridgeline plots (d) show the distribution of the reflectivity differences of the remaining points if we choose points only with high quality index (in this case, we select an arbitrary cutoff value of Q_{match} = 0.7). The mean is marked with the corresponding vertical line.

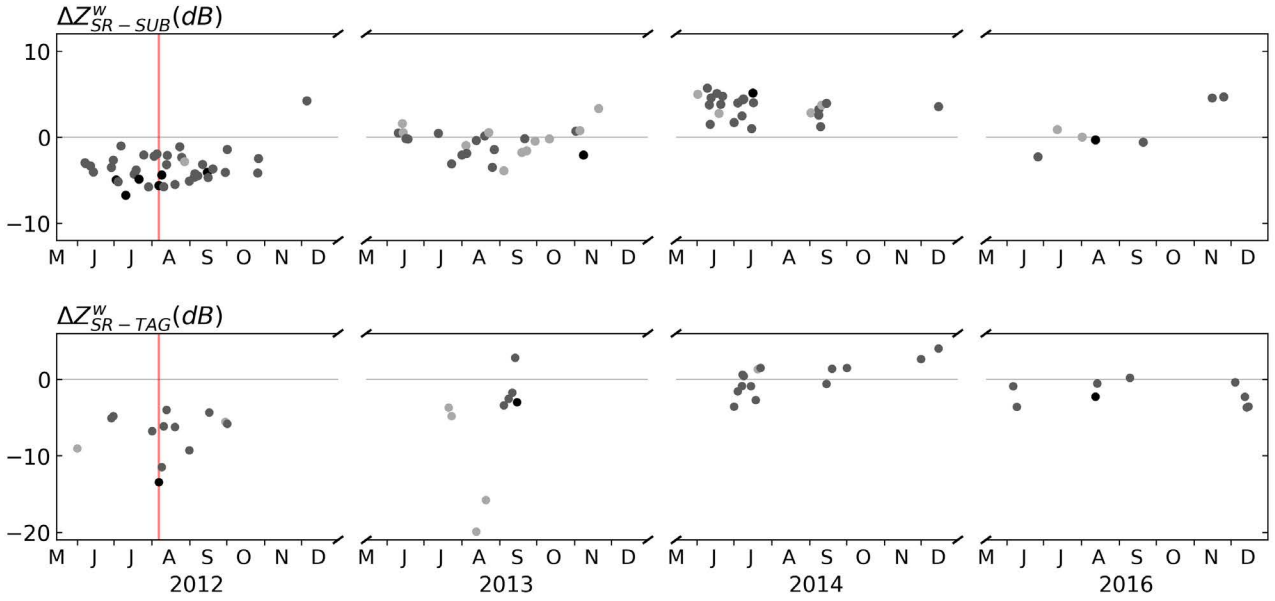

Figure 4.5: Calibration biases derived from comparison of GR with SR for SUB (a) and TAG (b) for the wet seasons (June to December) of the entire dataset. Symbols are coloured according to the number of matched samples: light grey: 10–99, medium grey: 100–999, and black: 1000+. The red line marks 06 August 2012 for the case study presented in Figure 6.

Habagat of 2012, an enhanced monsoon event that happened in August 2012 (Heistermann et al., 2013a).

Figure 4.6a and b illustrate the estimation of the calibration bias for the SUB and TAG radars from TRMM overpass data. The calibration bias estimates of -5.6 dB (for SUB) and -13.5 dB (for TAG) obtained from those scatter plots correspond to the dots intersecting the red line in the time series shown in Figure 4.5. Figure 4.6c shows the matching reflectivity samples of the two ground radars, SUB and TAG, in the region of overlap which have *not yet* been corrected for calibration bias. The quality-weighted mean difference of reflectivies amounts to -12.2 dB. Accordingly, Figure 4.6d shows the matches in the region of overlap, with both SUB and TAG reflectivities corrected for calibration bias, based on the values obtained from Figure 4.6a and b, respectively. The corresponding value of the mean difference amounts to -4.6 dB. These effects are further illustrated by Figure 4.6e which shows the distributions of SR–GR and GR–GR differences before and after bias correction.

The case clearly demonstrates how *massive* levels of miscalibration (-5.6 and -13.5 dB) can be reduced if an adequate SR overpass is available. That is proved by the massive reduction of the absolute value of mean difference between the two ground radars, or, inversely, the massive gain in GR consistency. Yet, the bias could not be entirely eliminated, which suggests that other systematic sources of error have not been successfully addressed for this case.

Table 4.2 summarizes our analysis of five additional events in which valid SR overpasses for both SUB and TAG coincided with a significant rainfall in the region of overlap between the two ground radars, most of which took place in 2012 (and one in 2016). Columns $\overline{\Delta Z}^{w}_{SR-SUB}$ and $\overline{\Delta Z}^{w}_{SR-TAG}$ show varying levels of calibration bias for SUB and TAG, quantified by the quality-weighted mean difference to the SR observations, together with varying levels of mismatch between the two ground radars, as shown by column $\overline{\Delta Z}^{nocorr}_{TAG-SUB}$. Using the calibration bias estimates for correcting the GR observations, we consistently reduce the quality-weighted mean difference between both ground radars, as expressed by column $\overline{\Delta Z}^{w,corr}_{TAG-SUB}$.

Altogether, the correction of GR reflectivities with calibration bias estimates of SR overpasses dramatically improves the consistency between the two ground radars which have shown largely incoherent observations *before* the correction. In all cases (including the *Habagat of 2012*), we were able to reduce the mean difference between the ground radars.

The question is now: Can we use these sparse calibration bias estimates also for points in time in which no adequate SR overpass data are available? Or, in other

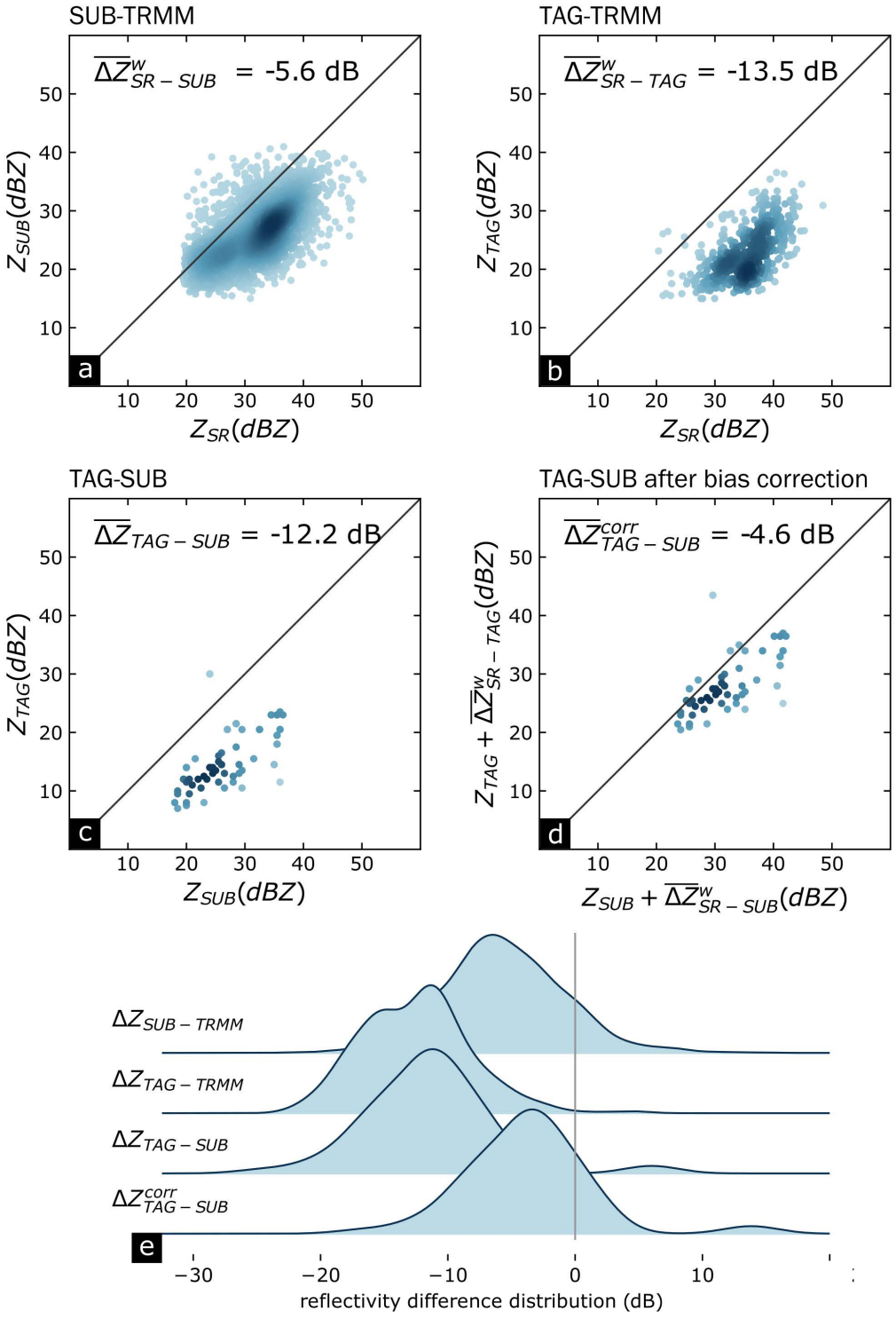

Figure 4.6: 3-way case study for 2012-08-06 17:15:47. (a) and (b): Scatter plots of SR–GR comparisons between TRMM and SUB and TAG radars for points where Q_{match}>0.7, where the darkness of the color represents the point density. The corresponding weighted biases are calculated for each radar. (c) and (d): GR–GR inter-radar consistencies before and after bias correction. (e) Distribution of the differences of the reflectivity pairs for each comparison scenario.

Table 4.2: Calibration biases and inter-radar consistencies for different bias calculation scenarios

	Npts	$\overline{\Delta Z}^{w}_{SR-SUB}$	$\overline{\Delta Z}^{w}_{SR-TAG}$	$\overline{\Delta Z}^{nocorr}_{TAG-SUB}$	$\overline{\Delta Z}^{w,corr}_{TAG-SUB}$
2012-06-11 21:37:41	528	-3.4	-6.3	-3.5	-0.2
2012-06-28 22:14:46	48	-3.5	-5.1	-1.3	-0.2
2012-07-02 20:09:47	1248	-5	-11.4	-7	-2.1
2012-08-06 17:17:23	1121	-5.6	-13.5	-12.3	-4.6
2012-08-31 13:44:31	34	-5.1	-9.3	-1.9	1.1
2016-08-12 11:40:28	1277	-0.3	-2.3	-5.7	-4.3

words, can we interpolate calibration bias estimates in time?

4.4.4 Can we interpolate calibration bias estimates in time?

The spaceborne radar platform (SR) rarely overpasses both GR radar domains in a way that significant rainfall sufficiently extends over both GR domains including the GR region of overlap. Hence, our previous demonstration of the effective correction of GR calibration bias yielded only few examples. From a more practical point of view, however, we are more interested in how we can use SR overpass data for those situations in which adequate SR coverage is unavailable—which is, obviously, rather the rule than the exception. An intuitive approach is to interpolate the calibration bias estimates from valid SR overpasses in time, and use the interpolated values to correct GR observations for any point in time. We can do such an interpolation independently for each ground radar, based on the set of valid SR overpasses available for each. In order to examine the effectiveness of such an interpolation, we again use the absolute value of the mean difference between the two ground radars as a measure of their (in-)consistency. Based on the reduction of that absolute value, as compared to uncorrected GR reflectivities, we benchmark the performance of three interpolation approaches:

1. *Linear interpolation* in time;
2. *Moving average*: we compute the calibration bias at any point in time based on calibration bias estimates in a 30-day window around that point, together with a triangular weighting function;
3. *Seasonal average*: For any point in time in the analyzed wet season of a year, we compute the calibration bias as the average of all calibration bias estimates available in that year.

This benchmark analysis is not considered to be comprehensive, but rather exemplary in terms of examined interpolation techniques. The three techniques illustrate different assumptions on the temporal representativeness of calibration bias estimates, as obtained from SR overpasses: a *seasonal average* reflects a rather low level of confidence in the temporal representativeness. The underlying assumption would be that we consider any short-term variability as "noise" which should be averaged out. The linear interpolation puts more confidence into each individual bias estimate, and assumes that we can actually interpolate between any two points in time. Obviously, a 30-day moving average is somewhere in between the two.

Table 4.3 provides an annual summary of the absolute mean differences in reflectivity between the two ground radars, without bias correction and with correction of bias obtained from different interpolation techniques. Firstly, the mean absolute difference between the radars is always lower *after* correction, irrespective of the year or the interpolation method. Hence, it is generally better to use calibration bias estimates to correct GR reflectivities even for those times in which no valid SR overpasses are available. The 30-day moving average appears to outperform the other two interpolation methods—on average, and for each year from 2012 to 2014. In 2016, neither interpolation method substantially reduces the mean absolute difference obtained for the uncorrected GR data.

The performance of the moving average suggests that it is possible for the calibration of radars to drift slowly in time, with variability stemming from sources which are difficult to disentangle. However, for periods of time when the radar is relatively well-calibrated and stable, the bias correction only offers a slight, if any, improvement in the consistency between two radars.

In order to better understand the variability "behind" the annual averages in Table 4.3, Figure 4.7 shows

Table 4.3: Mean absolute $\Delta Z_{TAG-SUB}$ for different correction scenarios and years

	Mean absolute $\Delta Z_{TAG-SUB}$ (dB)			
	No correction	Seasonal mean	Linear interpolation	Moving average
All years	4.9	4.0	3.0	2.7
2012	4.4	3.4	2.6	2.3
2013	8.6	7.1	4.5	4.1
2014	4.4	3.8	3.2	2.9
2016	1.8	1.8	1.7	1.7

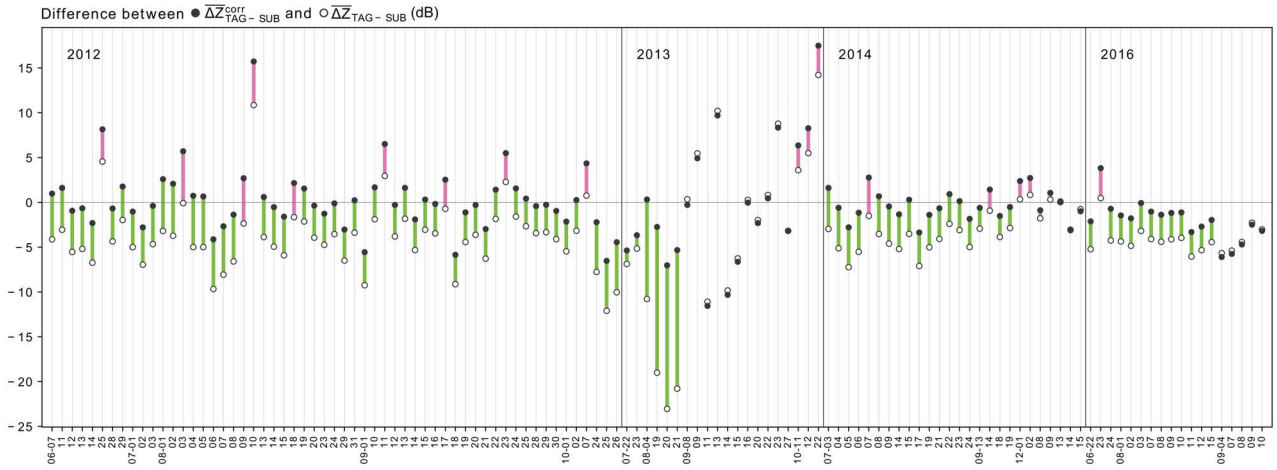

Figure 4.7: The differences between the inter-radar consistency before and after correcting for the ground radar calibration biases following a rolling window averaging for samples with significant number of matches. The hollow (filled) circles represent the daily mean before (after) correction. The line color represents an improvement (green) or a decline (pink) in the consistency between the two ground radars.

the effects of bias correction on a daily basis, exemplified for the moving average interpolation. The hollow circles represent the daily mean differences between the two ground radars before ($\overline{\Delta Z}_{TAG-SUB}$) correction, while the filled circles show the daily mean differences after ($\overline{\Delta Z}^{w,corr}_{TAG-SUB}$) correction. The length of the bar shows the magnitude of the change, while the color of the bar signifies a reduction of the absolute value of the mean difference (green, for improvement) or an increase in in the absolute value (pink, for a degradation of consistency between the two ground radars). In 83 out of 121 days, bias correction improves the consistency between the two ground radars by more than 1 dB. Inversely, though, this implies that in 17 out of 121 days, the use of interpolated bias estimates causes a degradation of consistency between the ground radars, expressed as an increase of more than 1 dB in the absolute mean differences. Furthermore, we can identify several days for which the bias correction decreases the absolute mean differences, but not to a level that could be considered as acceptable for quantitative precipitation estimation.

4.5 Conclusions

In 2011, Schwaller and Morris had presented a technique to match reflectivity observations from spaceborne radars (SR) and ground radars (GR). Crisologo et al. (2018) extended that technique by introducing the concept of quality-weighted averaging of reflectivity in order to retrieve the GR calibration bias from matching SR overpass data. They exemplified the concept of quality weighting by using beam blockage as a quality variable, and demonstrated the effectiveness of the approach for the Subic S-band radar in the Philippines.

The present study has extended the concept of quality-weighted averaging by accounting for path-integrated attenuation (PIA) as a quality variable, in addition to beam blockage. Accounting for PIA becomes vital for ground radars that operate at C- or X-band. In

addition to the Subic S-band radar, this study has included the Tagaytay C-band radar which substantially overlaps with the Subic radar.

In the first part of this study, we have demonstrated that only accounting for both, beam blockage and path-integrated attenuation, allows for a consistent comparison of observations from the two ground radars, Subic and Tagaytay: after transforming the quality variables "beam blockage fraction" and "path-integrated attenuation" into quality indices Q_{BBF} and Q_{PIA}, with values between zero and one, we computed the quality-weighted standard deviation of matching reflectivities in the region of overlap between the two ground radars for an event on December 9, 2014. Using a quality index based on the multiplicative combination of Q_{BBF} and Q_{PIA}, we were able to dramatically reduce the quality-weighted standard deviation from 8.1 dBZ to 4.6 dBZ, while using Q_{BBF} and Q_{PIA} alone would have only reduced the standard deviation to 5.5 or 7.5 dBZ, respectively. Based on that result, we have used, with confidence, the combined quality index throughout the rest of the study.

The next step involved the retrieval of the GR calibration bias from SR overpass data for the Tagaytay C-band radar (for the Subic S-band radar, that had already been done by Crisologo et al. (2018)). For each matched volume in the SR–GR intersection, the combined quality index was computed for the Tagaytay radar, and used as weights in calculating the calibration bias as a quality-weighted average of the differences between SR and GR reflectivities. We applied this approach throughout a 4-year period to come up with a time series of the historical calibration bias estimates of the TAG radar, and found the calibration of the TAG radar to be exceptionally poor and volatile in the years 2012 and 2013, with substantial improvements in 2014 and 2016.

In order to demonstrate the effectiveness of estimating and applying the GR calibration bias obtained from SR overpass data, we have compared, in the region of overlap, the corrected and uncorrected reflectivities of the Subic and Tagaytay radars, for six significant rainfall events in which all three instruments—TAG, SUB and the SR—had recorded a sufficient number of observations. We have shown that the independent bias correction is able to massively increase the consistency of the two ground radar observations, as expressed by a reduction of the absolute mean difference between the GR observations in the region of overlap, for each of the six events—in one case even by almost 7.7 dB. The main lesson from these cases is, that we can legitimately interpret the quality-weighted mean difference between SR and GR reflectivities as the instantaneous GR calibration bias, even if the magnitude of that bias varies substantially within short periods of time.

Yet, the question remains how to correct for calibration bias in the absence of useful SR overpasses. That question is particularly relevant for the reanalysis of archived measurements from single-pol weather radars. In this study, we have evaluated three different approaches to interpolate calibration bias estimates from SR overpass data in time: linear interpolation, a 30-day moving average, and a seasonal average. Each of these approaches illustrates different assumptions on the temporal representativeness of the calibration bias estimates. On average, any of these approaches produced calibration bias estimates that were able to reduce the mean absolute difference between the GR observations, which increases our confidence in the corrected GR observations. Of all interpolation approaches, the moving 30-day window outperformed the other two approaches. However, we also found that behind the average improvement of GR–GR consistency, there were also a number of cases in which the consistency between the ground radars was degraded, or in which high inconsistencies could not be significantly improved. Altogether, it still appears difficult to interpolate such a volatile behaviour, even if we consider the actual calibration bias estimates from the SR overpasses as quite reliable.

In that context, maintenance protocols of the affected ground radars would be very helpful in interpreting and interpolating time series of calibration bias estimates. Such records were unavailable for the present study, which made it hard to understand the observed variability of calibration bias estimates. Yet, this information will mostly be internally available at those institutions operating the weather radars. With the software code and sample data of our study being openly available (`https://github.com/IreneCrisologo/inter-radar`), such institutions are now enabled to carry out analyses as the present study themselves, while being able to benefit from cross-referencing the results with internal maintenance protocols.

The correction of GR calibration appeared particularly effective in periods with massive levels of miscalibration. For such cases, interpolated bias estimates allowed for an effective improvement of raw GR reflectivities. Yet, we need to continue disentangling different sources of uncertainty for both SR and GR observations in order to separate actual variations in instrument calibration and stability from measurement

errors that accumulate along the propagation path, and to better understand the requirements to robustly estimating these properties from limited samples. Progress on these ends should also improve the potential for interpolating calibration bias estimates in time, in order to tap the potential of historical radar archives for radar climatology, and to increase the homogeneity of composite products from heterogeneous weather radar networks.

Acknowledgements

The radar data for this analysis were provided by the Philippine Atmospheric, Geophysical and Astronomical Services Administration (PAGASA, http://pagasa.dost.gov.ph). The study was also funded by the German government through the German Academic Exchange Service (https://www.daad.de/en/).

Chapter 5

Discussion, Limitations, Outlook

Precipitation is the main driver of environmental and hydrological processes, and has a large impact in terms of natural hazards (through floods, debris flow, landslides, avalanches). Hence, there is an increasing need for more reliable precipitation estimates and forecasts at high temporal and spatial resolution. The recently-acquired Subic radar data allowed a first look at the capabilities and advantages it offers in weather monitoring in the Philippines. Radar data was used to reconstruct the enhanced southwest monsoon event of 2012 over Metro Manila. Torrential rainfall fell continuously over the course of four days, as the tail of Typhoon Haikui passing north of the Philippines pulled in even more moisture along with the already ongoing monsoon winds and rains. Radar-derived rainfall estimates underestimated by as much as 60% when compared with gauge measurements. Gauge-adjusted radar data reconstruction showed that while Metro Manila received the most rainfall over land, most of the rain actually fell over Manila Bay. This feature of the rainfall distribution would not have been identified from rain gauge interpolation alone, as demonstrated by the Supplemental figure of Chapter 2, as well as Figure 2a and c in a later study by (Abon et al., 2016). Additionally, the radar-based rainfall distribution map showed other localized areas (about 15–25 km wide) of high rainfall accumulation which were also missed in the rain gauge interpolation map (Supplemental figure of Chapter 2). These plume-like features re-appeared in the radar-based rainfall distribution map of a similar event (southwest monsoon enhanced by a north-passing typhoon) the following year, which were driven by the interaction of stratovolcanoes with the monsoon (Lagmay et al., 2015).

The archipelagic nature of the country's geography prohibits a dense and well-spaced network of rain gauges that can be used to effectively compare gauge measurements and radar rainfall-estimates. The highly convective characteristic of local rainfall produces strong thunderstorms that can be compact enough to travel in between rain gauges and be left undetected. With the sparseness of the gauges and the uncertainty that comes with the rainfall-rainrate transformation, as well as the lack of auxiliary calibrators such as disdrometers and radar profilers, we instead turned to relative calibration. Reflectivities from ground-based radars (GR) are compared with reflectivities from spaceborne radars (SR), namely TRMM (for data from 2012–2014) and GPM (for data from 2014–2016). A more common approach in comparing SR and GR is by reprojecting and interpolating the surface rainfall estimates onto either a common 2D cartesian grid on the Earth's surface or the volumetric rainfall estimates onto a common 3D cartesian grid. The 3D volume matching method of (Schwaller and Morris, 2011) used in this paper avoids uncertainties that could be introduced by interpolation by considering only the volumes of the SR beam and GR beam that intersect. In addition, directly comparing the primary measured quantity *reflectivity* circumvents the need to convert to rain rate, which is another potential source of uncertainties if rain gauges are used as a reference.

By avoiding these known potential additional sources of errors, this thesis was able to focus on the sources of systematic errors that could influence the comparison between SR and GR. The consideration of data quality started with the beam blockage fraction (BBF) for Chapter 3 and included path-integrated attenuation (PIA) for Chapter 4. These quality factors were then used as weights in taking the weighted-average of the differences between the SR and GR reflectivities for a single coincidence of an SR overpass and a GR sweep. The weighted-averaging approach allows low quality data resulting from BBF and PIA, sources of uncertainty that are *heterogeneous* in space, to be filtered out for a more consistent estimate of calibration bias, which is *homogeneous* in space.

In Chapters 3 and 4, it was shown that introducing a data quality framework in the comparison increases the consistency of bias estimates between two datasets. In a case study discussed in Section 3.4, reflectivity difference maps between SR overpass and GR sweep indicate that significant variability (with absolute differences up

to 10 dB) can be found at the edges of the blind sector, due to partial beam blockage. The locations of the large absolute differences are consistent with the locations of the low data quality. Assigning weights to beam blockage fraction (0 for the poorest data quality due to total beam blockage up to 1 for the best data quality without any topographic obstacles) in calculating the calibration bias reduces the scatter and consequently decreases the standard deviation of the differences between SR and GR reflectivity (Figure 3.6), which in turn increases the confidence in the bias estimation. The same reduction in standard deviation occurs as well in the vast majority of overpasses. The GR–GR comparison in Chapter 4 similarly demonstrates the benefits of considering BBF and PIA. The case study in Figure 4.4 shows that individually, using Q_{BBF} and Q_{PIA} as weights reduces the standard deviation of the differences between the reflectivities from the two ground radars, but considering both quality indices at the same time decreases the standard deviation by almost half, as opposed to considering all points equally. The combination of quality factors also dramatically narrows down the distribution of the reflectivity differences. These results demonstrate that BBF and PIA do not only affect Quantitative Precipitation Estimation (QPE), but also the comparability of two radars. The advantages of quality-weighting therefore applies to both SR–GR comparisons and GR–GR comparisons.

Being able to determine the calibration bias of one radar in Chapter 3 using the SR–GR matching approach and applying the method and correction to two overlapping radars in Chapter 4 tells us that SR and GR reflectivities are consistent enough (after filtering out low data quality) to allow for calibration bias estimates. This consistency presents the potential of calibrating multiple radars in a network against a single reference, using a uniform approach. In this study, this was demonstrated for at least two radars in the Philippine radar network. The increased agreement between the two ground radars after calibration demonstrates the feasibility of SR as a stable travelling reference. The method also allows for bias estimation at instantaneous points in time, as opposed to gauge calibration where errors are lumped over an hourly or daily timeframe. Due to its unobstructive nature, this relative calibration method can also be done continuously, so that calibration monitoring can be done even while the radars are operational.

Chapter 3 also discusses the consistency of TRMM and GPM with respect to each other. In the analysis of the bias time series for Subic radar, TRMM and GPM overpasses were both available for 2014. The period of overlap showed that GR calibration bias estimates based on both TRMM and GPM observations can be considered homogeneous. Based on this assessment, TRMM and GPM were lumped together as a continuous dataset when comparing SR and GR reflectivities for bias correction in Chapter 4.

It was discussed in the latter part of Chapter 3 (Section 3.4.2) that the bias fluctuates around an average value that varies year by year and appears to be quite persistent over the duration of the corresponding wet seasons from 2012–2016. The drastic change in bias between 2013 and 2014 for the Subic radar (Figure 3.8) has to be assumed to be due to calibration maintenance in terms of hardware changes (i.e. magnetron replacement). Unfortunately, similar information about the Tagaytay radar's maintenance history was not available. Detailed information regarding maintenance protocols would be useful in explaining the changes in bias of radars throughout the years as demonstrated in Warren et al. (2018). Chapter 4 (Section 4.4.4.) reaffirms us that there is substantial short-term variability. Even after identifying and addressing the effects of BBF and PIA, heavy fluctuations of bias persist. The causes of these fluctuations could not yet be disentangled. Yet, we were able to reduce the mean absolute difference *before* and *after* bias correction when using interpolated bias estimates. So irrespective of the actual causes of fluctuation, the variability exhibits some level of continuity, so that an interpolation of bias estimates in time contributes to an overall improvement.

Aside from internal calibration of the precipitation radars onboard TRMM/GPM, external monitoring is also carried out through comparison with selected well-calibrated ground radars. Several ground validation sites can be found in different locations around the world (Hou et al., 2013). Some of these sites are established primarily for this purpose, while some are part of existing radar networks whose calibration are deemed accurate enough to use as reference. The geometry matching method of Schwaller and Morris (2011) that was used in Chapters 3 and 4 was developed with this application in mind—to compare reflectivities between ground radars and spaceborne radars to check if they are consistent with each other. While ground validation sites are typically set up to have the least possible errors, the method can still be applied for a more extensive global approach in ground validation using radars not included in the validation radars list. The consistency of the ground radar observations with the spaceborne

radar observations in Chapter 3 also serves, albeit indirectly, as a validation of the SR estimates in the study region.

Limitations of the study

Beam blockage and path-integrated attenuation are only two of the possible sources of uncertainties that could affect data quality. Furthermore, attenuation was only considered for the ground radar, while the spaceborne radars may also experience attenuation. However, this has already been acknowledged and addressed by the corresponding SR data teams, by providing attenuation-corrected datasets. The SR data product used in the analysis are already attenuation-corrected and the values were taken as-is. To take this approach further, the framework of quality-weighted averaging could and should be extended to the SR data as well, including not only attenuation, but also the effects of non-uniform beam filling.

It should be noted that the approaches in calculating beam blockage and path-integrated attenuation are not absolute. In this thesis, they were calculated as part of the processing chain, and not as readily available quantities. Exploring these variables further are research topics in themselves, but a sufficient method had to be selected. For the beam blockage fraction calculation, the method presented by Bech et al. (2003) was used. The radar's field of view is simulated in their model using information on the scan geometry and the surrounding topography based on a digital elevation model. The implementation of this model assumes that there is no vertical gradient of refractivity, so in cases where super-refraction of the atmosphere may be possible, this method may not apply. As for the retrieval of the PIA, the specific differential phase (K_{DP}), which was used to calculate PIA following the algorithm proposed by Vulpiani et al. (2012). This method was already proven to work well with the dataset (Crisologo et al., 2014). While other K_{DP} retrieval methods exist (Bringi and Chandrasekar, 2001; Wang and Chandrasekar, 2009), it is beyond the scope of this thesis to explore their differences, but certainly, the philosopher's stone has not yet been found when it comes to the reliable reconstruction of Φ_{DP} and K_{DP}, and hence the retrieval of PIA.

Aside from the methodological, data limitations also exist. TRMM and its successor GPM was launched in 1997 and 2014, respectively, therefore the SR-GR method of bias estimation can only be done as far back as the start of the corresponding instrument. Additionally, with the study area close to the equator, the swath density is not as high as it is nearer the poles. There are at most two SR overpasses that go over the Philippines everyday, and they don't always intersect with the radars used in this study. Applying the methods to study areas with high swath overpass frequency could provide more samples to increase the reliability of the results.

Unfortunately, we were not able to gain access to the calibration and maintenance history of the Subic and Tagaytay radars as recorded by PAGASA, and manual cross-checking of the changes in radar calibration against the maintenance records was not possible. Determining the exact dates of maintenance events that could have changed the radar calibration and comparing them with the observed changes in the analysis would allow us to differentiate between the effects of deliberate calibration and those of instrument instability and system drift. The findings with respect to the annual calibration changes of the Subic radar were relayed to radar engineers in PAGASA, and they confirmed that some hardware changes (i.e. magnetron replacement) were performed in 2014, but no further details were given.

The observed variability of the calibration biases over time could result from cumulative effects of several sources of uncertainty along the entire data collection and generation process. Examples of such sources could be uncertainty of beam propagation due to fluctuations in atmospheric refractivity; non-uniform beam filling; residual errors in the geometric intersections of the volume samples; and rapid changes in precipitation during the time interval between the radars being compared, to name a few. Additionally, hardware instabilities owing to the effects of temperature, thermal expansion, and gradual degradation of the system, can also contribute to calibration drifts.

Outlook

There is still much to understand about radar calibration, and the myriad of factors that contribute to its stability and reliability. The quality-weighted framework developed in this thesis can be expanded to the spaceborne radar observations as well, by e.g. considering the clutter identification of the Dual-frequency Precipitation Radar of the GPM (Watters et al., 2018). The GPM 2a Ku dataset also includes other variables which could be related to data quality, such as the level of path-integrated attenuation, the quality of brightband detection, and estimation of ground clutter elevation (Iguchi

et al., 2010).

Furthermore, the quality-based method for bias estimation and correction can also be extended to the other radars in the Philippine radar network to ensure a consistent and reliable rainfall measurement throughout the country. The Philippine government program Nationwide Operational Assessment of Hazards (Project NOAH), which tackles disaster research and development, makes use of the weather radars together with the Himawari-8 satellite for monitoring and nowcasting rainfall probability in a web-based platform that delivers hazard-related information to the public in near-real-time (Lagmay et al., 2017). The project also conducts flood simulations for early warning using historical and real-time rainfall data based on rain gauges, which at the moment are more reliable in terms of accuracy and availability compared to radar data. With the potential increase in accuracy of radar rainfall estimates through careful bias estimation and calibration, and with the continuous efforts of PAGASA to improve the coverage and availability of the radar data, weather radar observations can be integrated to hydrological simulations for early warnings.

The improvement in the consistency between the Subic and Tagaytay radars after the bias correction of the individual radars signify a step towards better usability of archived data. Despite the remaining fluctuation, we have shown the possibility of increasing the homogeneity of reflectivity records by removing temporally variable calibration biases. Historical calibration of radar data archive could be useful for climatological studies and re-analysis of past events for better understanding of involved processes.

Chapter 6

Summary and Conclusion

Calibration and methods to improve calibration bias estimates serve as the main thread of the three papers comprising this thesis. This work tells the story of how the calibration bias was first noticed for the Subic radar, to the attempts at using spaceborne radars as reference for bias estimation for two overlapping radars (Subic and Tagaytay) experiencing different error sources, to investigating whether miscalibration of archived radar data can be corrected to a certain extent.

The first paper established the presence of miscalibration for the Subic radar, while also giving a first look at the unique rainfall distribution following an intense rainfall caused by typhoon-enhanced monsoon. In this chapter, we have shown that most of the rainfall during the Habagat 2012 actually precipitated over Manila Bay, and not in Quezon City, as the rain gauges recorded. The gap in the spatial distribution of the rain gauges was supplemented by the high-spatial resolution data of the radars.

An approach by Schwaller and Morris (2011) to compare spaceborne radars (SR) and ground radars (GR) for calibration bias estimation was extended in the second paper. A framework for data quality and quality-weighted averaging was introduced, where a quality index based on beam blockage fraction (where $Q_{BBF} = 0$ for total beam blockage and $Q_{BBF} = 1$ for absence of any beam blockage along the beam) was used as weights in calculating the weighted mean difference between SR and GR measurements. The use of quality-weighted averaging, as opposed to simple averaging, decreased the standard deviation of the mean differences between SR and GR reflectivities, thereby increasing the consistency between the two radars. This decrease in standard deviation means that the estimation of the bias is more reliable. Based on the map of the matched SR–GR bins and the scatter plot of the differences between SR and GR reflectivities colored based on Q_{BBF}, the points on the scatter plot lying far from the perfect match come from the areas affected by beam blockage.

We took this concept of quality-based calibration bias estimation further in the third paper and applied it to the neighboring Tagaytay radar (TAG) which overlaps with the Subic radar (SUB). For days when data for all three radars (SR, TAG, SUB) were present, we showed that the agreement of the reflectivity measurements in the overlapping area between the two ground radars increased after bias correction.

Furthermore, a moving average interpolation of the SR-derived biases was able to fill in the gaps in the radar calibration time series where no SR overpasses were available. We demonstrate that taking a moving average (therefore assuming that the bias drifts slowly in time) of the bias to correct for days without an SR overpass produces better results than simply taking the seasonal average and using that to correct all days within that season.

In support of reproducibility and transparency in the atmospheric sciences, all software used in this thesis are reported in the text, and workflow scripts and sample data are made available in publicly available Github repositories.

Chapter 7

Additional Publications

I also contributed to the following publications during the course of the doctoral research, aside from the manuscripts listed in Chapter 1.

Bronstert, Axel, Ankit Agarwal, Berry Boessenkool, **Irene Crisologo**, Madlen Fischer, Maik Heistermann, Lisei Köhn-Reich, et al. 2018. "Forensic Hydro-Meteorological Analysis of an Extreme Flash Flood: The 2016-05-29 Event in Braunsbach, SW Germany." Science of The Total Environment 630 (July): 977–91. https://doi.org/10.1016/j.scitotenv.2018.02.241.

Ozturk, Ugur, Dadiyorto Wendi, **Irene Crisologo**, Adrian Riemer, Ankit Agarwal, Kristin Vogel, José Andrés López-Tarazón, and Oliver Korup. 2018. "Rare Flash Floods and Debris Flows in Southern Germany." Science of The Total Environment 626 (June): 941–52. https://doi.org/10.1016/j.scitotenv.2018.01.172.

Bibliography

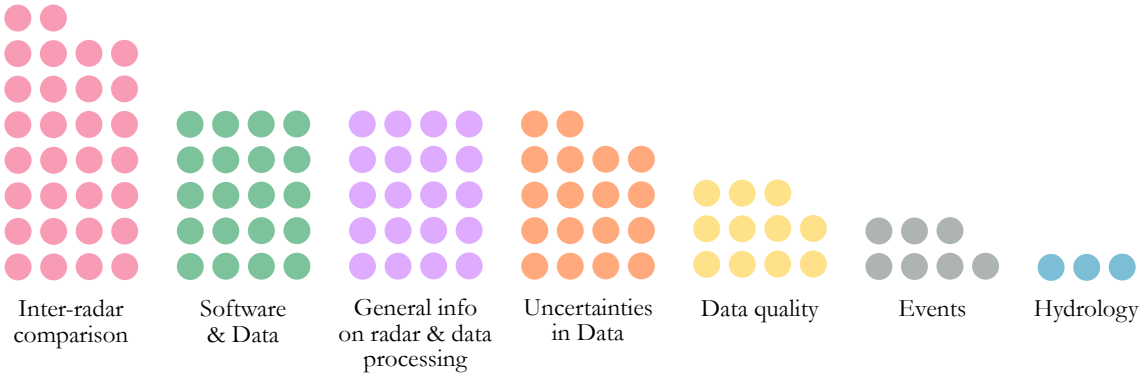

- Abon, C. C., David, C. P. C., and Pellejera, N. E. B. (2011). Reconstructing the Tropical Storm Ketsana flood event in Marikina River, Philippines. *Hydrology and Earth System Sciences*, 15(4):1283–1289. Event.
- Abon, C. C., Kneis, D., Crisologo, I., Bronstert, A., David, C. P. C., and Heistermann, M. (2016). Evaluating the potential of radar-based rainfall estimates for streamflow and flood simulations in the Philippines. *Geomatics, Natural Hazards and Risk*, 7(4):1390–1405. Hydrology.
- Amitai, E., Llort, X., and Sempere-Torres, D. (2009). Comparison of TRMM radar rainfall estimates with NOAA next-generation QPE. *Journal of the Meteorological Society of Japan*, 87(Sp. Iss. SI):109–118. interradar.
- Anagnostou, E. N., Morales, C. A., and Dinku, T. (2001). The use of TRMM precipitation radar observations in determining ground radar calibration biases. *Journal of Atmospheric and Oceanic Technology*, 18(4):616–628. interradar.
- Atlas, D. (2002). Radar calibration. *Bulletin of the American Meteorological Society*, 83(9):1313–1316. General.
- Austin, P. M. (1987). Relation between Measured Radar Reflectivity and Surface Rainfall. *Monthly Weather Review*, 115(5):1053–1070. Radar Uncertainty.
- Baldini, L., Chandrasekar, V., and Moisseev, D. (2012). Microwave radar signatures of precipitation from S-band to Ka-band: application to GPM mission. *European Journal of Remote Sensing*, 45(1):75–88. General.
- Bech, J., Codina, B., Lorente, J., and Bebbington, D. (2003). The sensitivity of single polarization weather radar beam blockage correction to variability in the vertical refractivity gradient. *Journal of Atmospheric and Oceanic Technology*, 20(6):845–855. Radar Uncertainty.
- Blumberg, W. G., Halbert, K. T., Supinie, T. A., Marsh, P. T., Thompson, R. L., and Hart, J. A. (2017). SHARPpy: An Open-Source Sounding Analysis Toolkit for the Atmospheric Sciences. *Bulletin of the American Meteorological Society*, 98(8):1625–1636. Software.
- Bolen, S. M. and Chandrasekar, V. (2003). Methodology for aligning and comparing spaceborne radar and ground-based radar observations. *Journal of Atmospheric and Oceanic Technology*, 20(5):647–659. interradar.

- Bringi, V. N. and Chandrasekar, V. (2001). *Polarimetric Doppler Weather Radar: Principles and Applications*. Cambridge University Press.
- Bringi, V. N., Chandrasekar, V., Balakrishnan, N., and Zrnić, D. S. (1990). An Examination of Propagation Effects in Rainfall on Radar Measurements at Microwave Frequencies. *Journal of Atmospheric and Oceanic Technology*, 7(6):829–840. Radar Uncertainty.
- Bringi, V. N., Huang, G.-J., Munchak, S. J., Kummerow, C. D., Marks, D. A., and Wolff, D. B. (2012). Comparison of Drop Size Distribution Parameter (D_0) and Rain Rate from S-Band Dual-Polarized Ground Radar, TRMM Precipitation Radar (PR), and Combined PR–TMI: Two Events from Kwajalein Atoll. *Journal of Atmospheric and Oceanic Technology*, 29(11):1603–1616. General.
- Cao, Q., Hong, Y., Qi, Y., Wen, Y., Zhang, J., Gourley, J. J., and Liao, L. (2013). Empirical conversion of the vertical profile of reflectivity from Ku-band to S-band frequency. *Journal of Geophysical Research: Atmospheres*, 118(4):1814–1825. General.
- Carey, L. D., Rutledge, S. A., Ahijevych, D. A., and Keenan, T. D. (2000). Correcting Propagation Effects in C-Band Polarimetric Radar Observations of Tropical Convection Using Differential Propagation Phase. *Journal of Applied Meteorology*, 39(9):1405–1433. Radar Uncertainty.
- Cayanan, E., Chen, T.-C., Argete, J., Yen, M.-C., and Nilo, P. (2011). The Effect of Tropical Cyclones on Southwest Monsoon Rainfall in the Philippines. *Journal of the Meteorological Society of Japan*, 89A:123–139. Event.
- Chandrasekar, V., Bolen, S., and Gorgucci, E. (2003). Microphysical cross validation of spaceborne radar and ground polarimetric radar. *IEEE Transactions on Geoscience and Remote Sensing*, 41(10):2153–2165. interradar.
- Chen, H. and Chandrasekar, V. (2016). Validation of NASA's Global Precipitation Measurement mission with a high-resolution ground radar network. In *URSI Asia-Pacific Radio Science Conference (URSI AP-RASC)*, pages 836–839. IEEE. interradar.
- Collette, A. (2013). *Python and HDF5*. O'Reilly. Software.
- Cremonini, R., Moisseev, D., and Chandrasekar, V. (2016). Airborne laser scan data: a valuable tool with which to infer weather radar partial beam blockage in urban environments. *Atmospheric Measurement Techniques*, 9(10):5063–5075. Data quality.
- Crisologo, I., Vulpiani, G., Abon, C. C., David, C. P. C., Bronstert, A., and Heistermann, M. (2014). Polarimetric rainfall retrieval from a C-Band weather radar in a tropical environment (The Philippines). *Asia-Pacific Journal of Atmospheric Sciences*, 50(S1):595–607. General.
- Crisologo, I., Warren, R. A., Mühlbauer, K., and Heistermann, M. (2018). Enhancing the consistency of spaceborne and ground-based radar comparisons by using beam blockage fraction as a quality filter. *Atmospheric Measurement Techniques*, 11(9):5223–5236. interradar.
- Doviak, R. J. and Zrnić, D. S. (2006). *Doppler radar and weather observations*. Academic Press, Mineola, N.Y., 2nd ed., dover ed. edition. General.
- DPWH-JICA (2003). Department of Public Works and Highways, DPWH Japan International Cooperation Agency, JICA: Manual on Flood Control Planning, Project for the Enhancement of Capabilities in Flood Control. Event.
- Droegemeier, K. K., Smith, J. D., Businger, S., Doswell, C., Doyle, J., Duffy, C., Foufoula-Georgiou, E., Graziano, T., James, L. D., Krajewski, V., LeMone, M., Lettenmaier, D., Mass, C., Pielke, R., Rutledge, S., Ray, P., Schaake, J., and Zipser, E. (2000). Hydrological Aspects of Weather Prediction and Flood Warnings: Report of the Ninth Prospectus Development Team of the U.S. Weather Research Program. *Bulletin of the American Meteorological Society*, 81(11):2665–2680. Hydrology.
- Durden, S. L., Haddad, Z. S., Kitiyakara, A., and Li, F. K. (1998). Effects of Nonuniform Beam Filling on Rainfall Retrieval for the TRMM Precipitation Radar. *Journal of Atmospheric and Oceanic Technology*, 15(3):635–646. Radar Uncertainty.

- Einfalt, T., Szturc, J., and Ośródka, K. (2010). The quality index for radar precipitation data: a tower of Babel? *Atmospheric Science Letters*, 11(2):139–144. Data quality.
- Fabry, F. (2015). *Radar Meteorology: Principles and Practice*. Cambridge University Press, Cambridge. General.
- Figueras i Ventura, J. and Tabary, P. (2013). The New French Operational Polarimetric Radar Rainfall Rate Product. *Journal of Applied Meteorology and Climatology*, 52(8):1817–1835. General.
- Fornasiero, A., Alberoni, P. P., Amorati, R., Ferraris, L., and Taramasso, A. C. (2005). Effects of propagation conditions on radar beam-ground interaction: impact on data quality. *Advances in Geosciences*, 2:201–208. Data quality.
- Friedrich, K., Hagen, M., and Einfalt, T. (2006). A quality control concept for radar reflectivity, polarimetric parameters, and Doppler velocity. *Journal of Atmospheric and Oceanic Technology*, 23(7):865–887. Data quality.
- Furukawa, K., Nio, T., Konishi, T., Oki, R., Masaki, T., Kubota, T., Iguchi, T., and Hanado, H. (2015). Current status of the dual-frequency precipitation radar on the global precipitation measurement core spacecraft. In *Sensors, Systems, and Next-Generation Satellites XIX*, volume 9639, page 96390G. International Society for Optics and Photonics. General.
- Gabella, M., Joss, J., Perona, G., and Michaelides, S. (2006). Range adjustment for ground-based radar, derived with the spaceborne TRMM precipitation radar. *IEEE Transactions on Geoscience and Remote Sensing*, 44(1):126–133. interradar.
- Gabella, M., Morin, E., and Notarpietro, R. (2011). Using TRMM spaceborne radar as a reference for compensating ground-based radar range degradation: Methodology verification based on rain gauges in Israel. *Journal of Geophysical Research*, 116(D2). interradar.
- Gabella, M. and Notarpietro, R. (2002). Ground clutter characterization and elimination in mountainous terrain. In *Proceedings of ERAD (2002)*, pages 305–311, Delft. Copernicus GmbH. Radar Uncertainty.
- Gabella, M., Speirs, P., Hamann, U., Germann, U., and Berne, A. (2017). Measurement of Precipitation in the Alps Using Dual-Polarization C-Band Ground-Based Radars, the GPM Spaceborne Ku-Band Radar, and Rain Gauges. *Remote Sensing*, 9(11):1147. interradar.
- GDAL Development Team (2017). GDAL - Geospatial Data Abstraction Library, Version 2.2.3. Software.
- Goudenhoofdt, E. and Delobbe, L. (2009). Evaluation of radar-gauge merging methods for quantitative precipitation estimates. *Hydrology and Earth System Sciences*, 13(2):195–203. General.
- Gourley, J. J., Tabary, P., and Parent du Chatelet, J. (2007). A Fuzzy Logic Algorithm for the Separation of Precipitating from Nonprecipitating Echoes Using Polarimetric Radar Observations. *Journal of Atmospheric and Oceanic Technology*, 24(8):1439–1451. Radar Uncertainty.
- Han, J., Chu, Z., Wang, Z., Xu, D., Li, N., Kou, L., Xu, F., and Zhu, Y. (2018). The establishment of optimal ground-based radar datasets by comparison and correlation analyses with space-borne radar data. *Meteorological Applications*, 25(1):161–170. interradar.
- Heistermann, M., Collis, S., Dixon, M. J., Giangrande, S., Helmus, J. J., Kelley, B., Koistinen, J., Michelson, D. B., Peura, M., Pfaff, T., and Wolff, D. B. (2014). The Emergence of Open-Source Software for the Weather Radar Community. *Bulletin of the American Meteorological Society*, 96(1):117–128. Software.
- Heistermann, M., Crisologo, I., Abon, C. C., Racoma, B. A., Jacobi, S., Servando, N. T., David, C. P. C., and Bronstert, A. (2013a). Brief communication "Using the new Philippine radar network to reconstruct the Habagat of August 2012 monsoon event around Metropolitan Manila". *Nat. Hazards Earth Syst. Sci.*, 13(3):653–657. Event.
- Heistermann, M., Jacobi, S., and Pfaff, T. (2013b). Technical Note: An open source library for processing weather radar data (wradlib). *Hydrology and Earth System Sciences*, 17(2):863–871. Software.

- Heistermann, M. and Kneis, D. (2011). Benchmarking quantitative precipitation estimation by conceptual rainfall-runoff modeling. *Water Resources Research*, 47(6). Hydrology.
- Helmus, J. and Collis, S. (2016). The Python ARM Radar Toolkit (Py-ART), a Library for Working with Weather Radar Data in the Python Programming Language. *Journal of Open Research Software*, 4(1). Software.
- Holleman, I., Michelson, D., Galli, G., Germann, U., and Peura, M. (2006). Quality information for radars and radar data. Data quality.
- Hong, Y. and Gourley, J. J. (2015). *Radar Hydrology: Principles, models, and applications*. CRC Press, Taylor & Francis Group. General.
- Hou, A. Y., Kakar, R. K., Neeck, S., Azarbarzin, A. A., Kummerow, C. D., Kojima, M., Oki, R., Nakamura, K., and Iguchi, T. (2013). The Global Precipitation Measurement Mission. *Bulletin of the American Meteorological Society*, 95(5):701–722. Software.
- Houze, Jr., R. A., Brodzik, S., Schumacher, C., Yuter, S. E., and Williams, C. R. (2004). Uncertainties in oceanic radar rain maps at Kwajalein and implications for satellite validation. *Journal of Applied Meteorology*, 43(8):1114–1132. Radar Uncertainty.
- Hunter, J. D. (2007). Matplotlib: A 2d Graphics Environment. *Computing in Science Engineering*, 9(3):90–95. Software.
- Iguchi, T., Seto, S., Meneghini, R., Yoshida, N., Awaka, J., and Kubota, T. (2010). GPM/DPR level-2 algorithm theoretical basis document. *NASA Goddard Space Flight Center, Greenbelt, MD, USA, Tech. Rep.* Software.
- Irving, D. (2016). A Minimum Standard for Publishing Computational Results in the Weather and Climate Sciences. *Bulletin of the American Meteorological Society*, 97(7):1149–1158. Software.
- Irving, D. and Simmonds, I. (2016). A New Method for Identifying the Pacific–South American Pattern and Its Influence on Regional Climate Variability. *Journal of Climate*, 29(17):6109–6125. Software.
- Islam, T., Rico-Ramirez, M. A., Han, D., Srivastava, P. K., and Ishak, A. M. (2012). Performance evaluation of the TRMM precipitation estimation using ground-based radars from the GPM validation network. *Journal of Atmospheric and Solar-Terrestrial Physics*, 77:194–208. interradar.
- Jones, E., Oliphant, T. E., and Peterson, P. (2014). SciPy: open source scientific tools for Python. Software.
- Joss, J., Gabella, M., Michaelides, S. C. h. r., and Perona, G. (2006). Variation of weather radar sensitivity at ground level and from space: case studies and possible causes. *Meteorologische Zeitschrift*, pages 485–496. interradar.
- Joss, J., Thams, J., and Waldvogel, A. (1968). The accuracy of daily rainfall measurements by radar. In *Proceedings of the 13th Radar Meteorology Conference*, pages 448–451, Montreal. American Meteorological Society. Radar Uncertainty.
- Kawanishi, T., Kuroiwa, H., Kojima, M., Oikawa, K., Kozu, T., Kumagai, H., Okamoto, K., Okumura, M., Nakatsuka, H., and Nishikawa, K. (2000). TRMM Precipitation Radar. *Advances in Space Research*, 25(5):969–972. Software.
- Keenan, T. D., Ebert, E., Chandrasekar, V., Bringi, V. N., and Whimpey, M. (2003). Comparison of TRMM Satellite-Based Rainfall with Surface Radar and Gauge Information. In *31st Conference on Radar Meteorology*, Seattle, Washington. American Meteorological Society. interradar.
- Kim, J.-H., Ou, M.-L., Park, J.-D., Morris, K. R., Schwaller, M. R., and Wolff, D. B. (2014). Global Precipitation Measurement (GPM) Ground Validation (GV) Prototype in the Korean Peninsula. *Journal of Atmospheric and Oceanic Technology*, 31(9):1902–1921. interradar.
- Kirstetter, P.-E., Hong, Y., Gourley, J. J., Schwaller, M., Petersen, W., and Zhang, J. (2012). Comparison of TRMM 2a25 Products, Version 6 and Version 7, with NOAA/NSSL Ground Radar–Based National Mosaic QPE. *Journal of Hydrometeorology*, 14(2):661–669. interradar.
- Kubota, T., Yoshida, N., Urita, S., Iguchi, T., Seto, S., Meneghini, R., Awaka, J., Hanado, H., Kida,

S., and Oki, R. (2014). Evaluation of Precipitation Estimates by at-Launch Codes of GPM/DPR Algorithms Using Synthetic Data from TRMM/PR Observations. *IEEE Journal of Selected Topics in Applied Earth Observations and Remote Sensing*, 7(9):3931–3944. Radar Uncertainty.

Kucera, P. A., Krajewski, W. F., and Young, C. B. (2004). Radar beam occultation studies using GIS and DEM technology: An example study of Guam. *Journal of Atmospheric and Oceanic Technology*, 21(7):995–1006. Radar Uncertainty.

Kummerow, C., Barnes, W., Kozu, T., Shiue, J., and Simpson, J. (1998). The Tropical Rainfall Measuring Mission (TRMM) Sensor Package. *Journal of Atmospheric and Oceanic Technology*, 15(3):809–817. Software.

Lagmay, A. M. F., Bagtasa, G., Crisologo, I. A., Racoma, B. A. B., and David, C. P. C. (2015). Volcanoes magnify Metro Manila's southwest monsoon rains and lethal floods. *Frontiers in Earth Science*, 2:36. Event.

Lagmay, A. M. F., Racoma, B. A., Aracan, K. A., Alconis-Ayco, J., and Saddi, I. L. (2017). Disseminating near-real-time hazards information and flood maps in the Philippines through Web-GIS. *Journal of Environmental Sciences*, 59:13–23. Software.

Lazo, J. K., Morss, R. E., and Demuth, J. L. (2009). 300 Billion Served: Sources, Perceptions, Uses, and Values of Weather Forecasts. *Bulletin of the American Meteorological Society*, 90(6):785–798. General.

Liao, L., Meneghini, R., and Iguchi, T. (2001). Comparisons of rain rate and reflectivity factor derived from the TRMM precipitation radar and the WSR-88d over the Melbourne, Florida, site. *Journal of Atmospheric and Oceanic Technology*, 18(12):1959–1974. interradar.

McKinney, W. (2010). Data structures for statistical computing in python. In *Proceedings of the 9th Python in Science Conference*, volume 445, pages 51–56. Austin, TX. Software.

Meneghini, R., Iguchi, T., Kozu, T., Liao, L., Okamoto, K., Jones, J. A., and Kwiatkowski, J. (2000). Use of the Surface Reference Technique for Path Attenuation Estimates from the TRMM Precipitation Radar. *Journal of Applied Meteorology*, 39(12):2053–2070. Radar Uncertainty.

Merceret, F. and Ward, J. G. (2000). Attenuation of Weather Radar Signals Due to Wetting of the Radome by Rainwater or Incomplete Filling of the Beam Volume. Technical report, NASA Center for AeroSpace Information. Radar Uncertainty.

Michelson, D., Einfalt, T., Holleman, I., Gjertsen, U., Friedrich, Katja, Haase, G., Lindskog, M., and Jurczyk, A. (2005). *Weather radar data quality in Europe quality control and characterisation*. Publications Office, Luxembourg. Data quality.

Morris, K. R. and Schwaller, M. (2011). Sensitivity of spaceborne and ground radar comparison results to data analysis methods and constraints. In *35th Conference on Radar Meteorology*, Pittsburgh, PA. American Meteorological Society. interradar.

Moser, H., Howard, K., Zhang, J., and Vasiloff, S. (2010). Improving QPE for Tropical Systems with Environmental Moisture Fields and Vertical Profiles of Reflectivity. In *Extended Abstract for the 24th Conf. on Hydrology. Amer. Meteor. Soc.* General.

NASA (2017). Precipitation Processing System Tropical Rainfall Measuring Mission File Specification for TRMM Products. Software.

NASA (2017). Release Notes for the PR Level 1 products. Software.

NDRRMC (2012). NDRRMC (National Disaster Risk Reduction and Management Council) Update: SitRep No. 20: re Effects of Southwest Monsoon Enhanced by Typhoon Haikui. Event.

Norman, K., Gaussiat, N., Harrison, D., Scovell, R., and Boscacci, M. (2010). A quality index for radar data. *OPERA deliverable OPERA_2010_03*. Data quality.

Oliphant, T. E. (2015). *Guide to NumPy*. CreateSpace Independent Publishing Platform, USA, 2nd edition. Software.

Ośródka, K., Szturc, J., and Jurczyk, A. (2014). Chain of data quality algorithms for 3-D single-polarization radar reflectivity (RADVOL-QC system). *Meteorological Applications*, 21(2):256–270.

Data quality.

- Park, S., Jung, S.-H., and Lee, G. (2015). Cross Validation of TRMM PR Reflectivity Profiles Using 3d Reflectivity Composite from the Ground-Based Radar Network over the Korean Peninsula. *Journal of Hydrometeorology*, 16(2):668–687. interradar.
- Petracca, M., D'Adderio, L. P., Porcù, F., Vulpiani, G., Sebastianelli, S., and Puca, S. (2018). Validation of GPM Dual-Frequency Precipitation Radar (DPR) Rainfall Products over Italy. *Journal of Hydrometeorology*, 19(5):907–925. interradar.
- Peura, M., Koistinen, J., and Hohti, H. (2006). Quality information in processing weather radar data for varying user needs. In *Proceedings of Fourth European Conference on Radar Meterology (ERAD06)*. Data quality.
- Rasp, S., Selz, T., and Craig, G. C. (2018). Variability and Clustering of Midlatitude Summertime Convection: Testing the Craig and Cohen Theory in a Convection-Permitting Ensemble with Stochastic Boundary Layer Perturbations. *Journal of the Atmospheric Sciences*, 75(2):691–706. General.
- Rew, R., Davis, G., Emmerson, S., Cormack, C., Caron, J., Pincus, R., Hartnett, E., Heimbigner, D., Lynton Appel, and Fisher, W. (1989). Unidata NetCDF. Software.
- Rinehart, R. (1991). *Radar for Meteorologists*. University of North Dakota, Office of the President. General.
- Rinollo, A., Vulpiani, G., Puca, S., Pagliara, P., Kaňák, J., Lábó, E., Okon, L., Roulin, E., Baguis, P., Cattani, E., Laviola, S., and Levizzani, V. (2013). Definition and impact of a quality index for radar-based reference measurements in the H-SAF precipitation product validation. *Natural Hazards and Earth System Science*, 13(10):2695–2705. Data quality.
- Rose, C. R. and Chandrasekar, V. (2005). A systems approach to GPM dual-frequency retrieval. *IEEE Transactions on Geoscience and Remote Sensing*, 43(8):1816–1826. General.
- Schumacher, C. and Houze, Jr., R. A. (2000). Comparison of Radar Data from the TRMM Satellite and Kwajalein Oceanic Validation Site. *Journal of Applied Meteorology*, 39:2151–2164. interradar.
- Schumacher, C. and Houze Jr, R. A. (2003). Stratiform rain in the tropics as seen by the TRMM precipitation radar. *Journal of Climate*, 16(11):1739–1756. General.
- Schwaller, M. R. and Morris, K. R. (2011). A Ground Validation Network for the Global Precipitation Measurement Mission. *Journal of Atmospheric and Oceanic Technology*, 28(3):301–319. interradar.
- Seo, B.-C., Krajewski, W. F., and Smith, J. A. (2014). Four-dimensional reflectivity data comparison between two ground-based radars: methodology and statistical analysis. *Hydrological Sciences Journal*, 59(7):1320–1334. interradar.
- Seto, S. and Iguchi, T. (2015). Intercomparison of Attenuation Correction Methods for the GPM Dual-Frequency Precipitation Radar. *Journal of Atmospheric and Oceanic Technology*, 32(5):915–926. interradar.
- Speirs, P., Gabella, M., and Berne, A. (2017). A comparison between the GPM dual-frequency precipitation radar and ground-based radar precipitation rate estimates in the Swiss Alps and Plateau. *Journal of Hydrometeorology*. interradar.
- Tabios III, G. (2009). Marikina River flood hydraulic simulation during typhoon Ondoy of 26 September 2009. Event.
- Takahashi, N., Kuroiwa, H., and Kawanishi, T. (2003). Four-year result of external calibration for Precipitation Radar (PR) of the Tropical Rainfall Measuring Mission (TRMM) satellite. *IEEE Transactions on Geoscience and Remote Sensing*, 41(10):2398–2403. General.
- Toyoshima, K., Masunaga, H., and Furuzawa, F. A. (2015). Early Evaluation of Ku- and Ka-Band Sensitivities for the Global Precipitation Measurement (GPM) Dual-Frequency Precipitation Radar (DPR). *SOLA*, 11(0):14–17. Radar Uncertainty.
- Ulbrich, C. and Lee, L. (1999). Rainfall Measurement Error by WSR-88d Radars due to Variations in Z R Law Parameters and the Radar Constant. *Journal of Atmospheric and Oceanic Technology*, 16(8):1017.

Radar Uncertainty.

- Villarini, G. and Krajewski, W. F. (2010). Review of the Different Sources of Uncertainty in Single Polarization Radar-Based Estimates of Rainfall. *Surveys in Geophysics*, 31(1):107–129. Radar Uncertainty.
- Vulpiani, G., Marzano, F. S., Chandrasekar, V., Berne, A., and Uijlenhoet, R. (2006). Rainfall rate retrieval in presence of path attenuation using C-band polarimetric weather radars. *Natural Hazards and Earth System Science*, 6(3):439–450. Radar Uncertainty.
- Vulpiani, G., Montopoli, M., Passeri, L. D., Gioia, A. G., Giordano, P., and Marzano, F. S. (2012). On the Use of Dual-Polarized C-Band Radar for Operational Rainfall Retrieval in Mountainous Areas. *Journal of Applied Meteorology and Climatology*, 51(2):405–425. Radar Uncertainty.
- Wang, J. and Wolff, D. B. (2009). Comparisons of Reflectivities from the TRMM Precipitation Radar and Ground-Based Radars. *Journal of Atmospheric and Oceanic Technology*, 26(5):857–875. interradar.
- Wang, Y. and Chandrasekar, V. (2009). Algorithm for Estimation of the Specific Differential Phase. *Journal of Atmospheric and Oceanic Technology*, 26(12):2565–2578.
- Warren, R. A., Protat, A., Siems, S. T., Ramsay, H. A., Louf, V., Manton, M. J., and Kane, T. A. (2018). Calibrating ground-based radars against TRMM and GPM. *Journal of Atmospheric and Oceanic Technology*. interradar.
- Watters, D., Battaglia, A., Mroz, K., and Tridon, F. (2018). Validation of the GPM Version-5 Surface Rainfall Products over Great Britain and Ireland. *Journal of Hydrometeorology*, 19(10):1617–1636.
- Wen, Y., Hong, Y., Zhang, G., Schuur, T. J., Gourley, J. J., Flamig, Z., Morris, K. R., and Cao, Q. (2011). Cross Validation of Spaceborne Radar and Ground Polarimetric Radar Aided by Polarimetric Echo Classification of Hydrometeor Types. *Journal of Applied Meteorology and Climatology*, 50(7):1389–1402. interradar.
- Zhang, J., Qi, Y., Howard, K., Langston, C., and Kaney, B. (2011). Radar quality index (RQI)—A combined measure of beam blockage and VPR effects in a national network. In *Proceedings, International Symposium on Weather Radar and Hydrology*. Data quality.
- Zhang, S., Zhu, Y., Wang, Z., and Wang, Y. (2018). Consistency analysis and correction of ground-based radar observations using space-borne radar. *Journal of Atmospheric and Solar-Terrestrial Physics*, 169:114–121. interradar.
- Zhong, L., Yang, R., Wen, Y., Chen, L., Gou, Y., Li, R., Zhou, Q., and Hong, Y. (2017). Cross-evaluation of reflectivity from the space-borne precipitation radar and multi-type ground-based weather radar network in China. *Atmospheric Research*, 196:200–210. interradar.